Max-Planck-Institut für Quantenoptik

Technische Universität München

Photon Blockade with Memory and Slow Light using a Single Atom in an Optical Cavity

Haytham Chibani

Vollständiger Abdruck der von der Fakultät für Physik der Technischen Universität München zur Erlangung des akademischen Grades eines

Doktors der Naturwissenschaften (Dr. rer. nat.)

genehmigten Dissertation.

Vorsitzender :		Univ.-Prof. Dr. W. Zwerger
Prüfer der Dissertation :	1.	Hon.-Prof. Dr. G. Rempe
	2.	Univ.-Prof. Dr. R. Gross

Die Dissertation wurde am 25.02.2016 bei der Technischen Universität München eingereicht und durch die Fakultät für Physik am 20.04.2016 angenommen.

Abstract

The realization of nonlinear systems able to mediate strong interactions between light fields at the few photon level in an environment with minimal absorption represents a cornerstone for future developments of quantum information science and photonic quantum technologies. One approach to reach this goal is via strong coupling of single emitters to optical cavities as provided by cavity quantum electrodynamics (QED). The other one is via electromagnetically induced transparency (EIT) with single atoms or with atomic ensembles.

This thesis reports on a system which merges both single-atom cavity QED in the strong coupling regime and EIT. First, we characterize this system theoretically and show that its energy eigenstates are very similar to the well known Jaynes-Cummings ladder of eigenstates. However, here, the eigenstates are optically controllable via the control field Rabi frequency provided by EIT. We show that increasing the control field Rabi frequency enhances the normal-mode splitting, and therefore the effective light-matter coupling. Moreover, with this system we are able to observe photon blockade and a two-photon gateway for the same input probe field and to tune the behavior of the second-order correlation function optically. Thanks to the long coherence times of EIT, photon blockade can be prolonged in time for longer times than the decay rates of the system. We refer to this effect as photon blockade with memory.

Next, we verify our theoretical findings experimentally. By performing spectroscopy measurements on the single-atom cavity EIT system, we show an unprecedented EIT on/off contrast of about 80 % thanks to our strong atom-cavity coupling rate. Later, we show experimentally, the ability to generate both, photon blockade and a two-photon gateway, for the same input field by just varying the control field Rabi frequency. Finally, by performing time-dependent second-order correlations we observe strong oscillations in the correlations which are a result of the creation of a new light field in the cavity which beats with the impinging probe laser. We show experimentally that this new field has a coherence time longer than the decay rates of the system, confirming its EIT origin.

In a final experiment, we take advantage of the strong atom-cavity coupling achieved to induce a group delay on probing pulses. Delays up to approximately 200 ns are measured. This is the first time a group delay is observed with a single atom as the delaying medium.

Contents

1. Introduction

1.1. Cavity quantum electrodynamics

Human understanding of the nature of light and its interaction with matter has changed dramatically over human history. Nearly one thousand years ago, Ibn Al-Haytham, interrogated in his *Book of Optics* [1] the theories of light put forward by Plato and Euclid, who argued that the way we see objects is by shining light out of our eyes onto them. Ibn Al-Haytham argued instead, that an object being viewed emits rays of light from every point on the object which travel to the viewer's eye. This understanding remained unchanged through time and is at the origin of the Lorentz model developed in the 19^{th} century. The Lorentz model was the first to describe light-matter interaction at the fundamental level where atoms are modeled as oscillating dipoles interacting according to Newton's and Maxwell's laws with electromagnetic light waves.
By the beginning of the 20^{th} century, quantum mechanics refined our understanding of light-matter interaction. In the context of black-body radiation [2], Planck was the first to heuristically introduce the quantization of the energy exchange. Few years later, Einstein extended Planck's quantum hypothesis and was able to describe the photoelectric effect [3]. In 1926, Schrödinger, in his semi-classical theory [4], treated only the atomic structure quantum mechanically while the light field was treated classically. The interpretation of electrodynamical processes between matter and light was formalized by Dirac, Pauli, Heisenberg, Feynman, Tomonaga and others leading to the sophisticated theory known as quantum electrodynamics (QED) [5]. QED has enabled the calculation of spontaneous emission [6] and of Lamb shifts [7, 8]. However, those predictions were made exclusively in a perturbative way, and exact calculations remained difficult since an infinity of modes of the electromagnetic field have to be taken into account.
This led Jaynes and Cummings to consider the simplest possible model of light-matter interaction: a single two-level atom interacting with a single mode of the electromagnetic field [9]. This system became a model system for the fundamental study of QED. Although first considered as a Gedankenexperiment, it was experimentally realized in the field of cavity QED by placing a single two-level atom in a small mode volume cavity. By exploiting the modified mode density between the cavity mirrors, the atom-light interaction can be resonantly enhanced. In the so-called *strong-coupling regime*, the interaction strength surpasses both the spontaneous emission rate of the atom and the

decay rate of the cavity. Strong-coupling can be demonstrated by either the observation of normal-mode splitting, or by the observation of the vacuum Rabi oscillations showing the coherent exchange of energy between the atom and the cavity [10]. Experimentally, these phenomena have been observed in both the optical and microwave domain. Experiments using Rydberg atoms coupled to microwave cavities [11, 12] or to microwave resonators [13] have shown signatures of strong-coupling. More recently, systems based on superconducting qubits coupled to microwave stripline resonators were used to achieve strong-coupling [14, 15, 16, 17]. In the optical regime, signatures of strong-coupling were observed in systems using alkali atoms coupled to Fabry-Perot cavities [18, 19, 20, 21], to microtoroidal resonators [22] , or to bottle resonators [23]. Also quantum dots coupled to microcavities [24, 25, 26, 27] or photonic crystal cavities [28] showed similar behavior.
Reaching the strong-coupling regime of cavity QED has paved the way for the realization of various effects and experiments. These include quantum non-demolition measurements [29, 30, 31, 32, 33], quantum feedback [34, 35], quantum gates [36, 37, 38], Observation of squeezed light from one atom [39] and new cooling techniques for atoms [40, 41, 42, 43, 44] just to cite a few examples.
This thesis studies a system which is based on a single atom coupled to a cavity mode in the strong coupling regime, however, contrary to previous related works, the cavity mode is strongly coupled to an open transition of the atom, opening a way for the phenomenon of electromagnetically induced transparency (EIT) to be incorporated in the strong coupling regime of cavity QED.

1.2. Electromagnetically induced transparency

EIT is a technique for making a normally opaque medium transparent by means of quantum interference [45]. Under certain conditions, EIT can be accompanied by a large change in the group velocity of the signal field traveling through the EIT medium, making the generation of slow and fast light possible. Although closely related to some early studies on laser-induced coherent phenomena in three-level atoms [46, 47, 48], the experimental observation of EIT was only achieved in 1991 [49, 50]. Since then, EIT has been the building block for many proposals predicting large optical nonlinearities and photon-photon interactions [51, 52, 53, 54, 55, 56, 57], which were later partially experimentally implemented for few photon all-optical switching [58, 59]. Moreover, it was realized that EIT can be used to map the properties of Rydberg atoms onto light fields [60], opening the path for the realization of deterministic quantum gates based on Rydberg blockade in EIT media [61, 62, 63, 64] and strongly correlated states of light [65, 66]. It was also realized that EIT could have a

potential for cooling the atomic motion to the ground state [67, 68]. By appropriately designing the absorption profile of the atoms using EIT, the cooling transitions induced by a cooling laser could be enhanced while heating by resonant absorption is suppressed. This technique was successfully used to cool the motional modes in an ion chain [69], the motion of a neutral atom to its motional ground state [70] and more recently has enabled single-site imaging of fermions in a quantum-gas microscope [71].
As already mentioned earlier, EIT can be used to reduce the group velocity of a propagating field due to the large normal dispersion of the EIT medium. Experiments have shown a slow down of optical pulses up to seven orders of magnitude [72, 73]. Demonstration of EIT-based slow light was not only limited to atomic physics but has also been realized in optomechanical systems both in the optical domain [74] and later in the microwave domain [75]. This slowdown of light can serve as a basis for a quantum memory. In fact, a light pulse resonant with the EIT window can be slowed down to zero velocity if the control field is switched off in the appropriate way. The light excitation can therefore be *transformed* into an atomic excitation and be stored in the medium thanks to the long coherence times of the two ground states of the EIT medium. When the pulse needs to be retrieved, the control field is turned back on, allowing the light pulse to resume its propagation. Quantum memories based on EIT have been experimentally demonstrated for coherent pulses [76, 77] and also for squeezed vacuum states [78, 79, 80, 81].
Most of the experiments mentioned above were carried out with systems involving large atomic ensembles with only few exceptions [82, 83, 84] where EIT was demonstrated for a single emitter but the strong coupling condition of cavity QED was lacking.

1.3. This work: Merging cavity QED with EIT

This thesis studies a system which merges single-atom cavity QED in the strong-coupling regime with EIT. The considered system has been predicted to improve the photon blockade effect [85] compared to the *standard* cavity QED system with a two-level atom. Furthermore, EIT gives the possibility of optically tuning the eigenstates of the system [86]. Measurements of second-order correlation functions are a powerful tool to study the quantum dynamics of the system from the photon stream emitted from the cavity. Previously, measurements of the second-order intensity correlation function have been used to investigate the dynamics of atomic ensembles [87] or single atoms [85, 88, 22, 89, 90, 91, 92] coupled to optical cavities. In contrast to these previous experiments, we investigate the possibility of coherently controlling the quantum dynamics of the system profiting from the optical control provided by the EIT control field. We verify experimentally our theoretical predictions

in reference [86], and observe a transition from a photon blockade behavior [85] to a two-photon gateway behavior [88] by only changing the control field Rabi frequency and keeping the input field parameters unchanged. Moreover, EIT, with its quantum memory potential, enables us to engineer non-classical states of light which can last for long times, beyond the decay rates of our system. By measuring time-dependent second-order correlation functions, we show that the timescale on which our system blocks subsequent photons could in principal be extended in time thanks to the long coherence times of the two ground states of the atom.
Finally, we conclude by performing slow light experiments using a single atom in the cavity. As mentioned above, an EIT medium can induce a reduction in the group velocity of traveling pulses. Using our single-atom-cavity system as the EIT medium we observe delay times up to about 200 ns. This is to our knowledge the first time slow light is generated from a medium composed of a single emitter.
The content of this thesis is organized as follows. **Chapter 2** briefly describes the theoretical concepts of a cavity QED system composed of a single two-level atom coupled to a single mode of an optical cavity. **Chapter 3** describes theoretically and in detail a single three-level atom strongly-coupled to a single mode of an optical cavity in an EIT configuration. We calculate the eigenstates of the system and show their dependence on the control field Rabi frequency. We show the implications of this dependence on the transmission spectrum of the system and perform numerical simulations of the equal-time second-order correlation function $g^{(2)}(0)$. By comparing the $g^{(2)}(0)$ in the cavity EIT case with the *standard* cavity QED case comprising a two-level atom, we show that EIT enhances the photon blockade effect and enables the optical tuning of $g^{(2)}(0)$ from a strongly antibunched and sub-Poissonian field to a bunched super-Poissonian field for the same input probe field. Finally, numerical simulations of the time-dependent second-order correlation function $g^{(2)}(\tau)$ reveal the generation of a new field inside the cavity with a long coherence time. This new field helps to extend the non-classical behavior of $g^{(2)}(\tau)$ in time, beyond the decoherence time of the system. **Chapter 4** briefly describes the experimental apparatus and the experimental implementation of the single-atom cavity EIT setup. **Chapter 5** shows the experimental realization of the theoretical proposal discussed in Chapter 3. Transmission spectra along with correlation measurements show a good agreement with our theoretical predictions. Moreover the *memory* effect on the behavior of $g^{(2)}(\tau)$ is clearly visible in the experiment. **Chapter 6** shows results of slow light with the single-atom cavity EIT system. Also, results from theoretical simulations are discussed. We conclude with a summary of this work and an outlook on future directions in **Chapter 7**.

2. Cavity Quantum Electrodynamics

2.1. Introduction

The ideal cavity quantum electrodynamics (QED) system is essentially composed of two components: a single two-level atom which is coupled to a single mode of a high finesse resonator (Fig. 2.1).This system allows research of light matter interaction at the fundamental level and has offered different applications over the last years such as cooling of the atomic motion, generation of non-classical fields and quantum networks [93, 94, 95, 96, 97] .
In this chapter we briefly review the quantum model which describes this system. We first derive the energy-level structure of the closed system, and then we discuss its interaction with the environment by including the driving and the dissipation. For a more careful treatment of this topic, the reader could check the following references [98, 99, 100, 10].

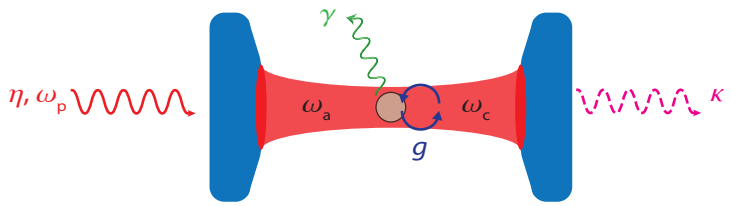

Figure 2.1.: Schematic of a single-atom cavity QED system. A two-level atom (resonance frequency ω_a) is strongly coupled to a single mode of the electromagnetic field of a Fabry-Perot cavity (resonance frequency ω_c) with a coupling strength g. The system is coherently driven by an impinging probe laser with a frequency ω_p and a driving strength η. Photons can escape from the system either through the cavity, with a decay rate κ, or through the atom, with a decay rate γ.

2.2. Quantum theory of the atom-cavity system

2.2.1. Hamiltonian

A two-level atom (with ground state, $|g\rangle$, and excited state, $|e\rangle$) interacting with a single mode of the electromagnetic field (with Fock states, $|n\rangle$, $n \in \mathbb{N}_{\geq 0}$) without losses, in the dipole and rotating wave approximations, is given by the Jaynes-Cummings Hamiltonian [9]:

$$H_{JC} = \hbar\omega_a \sigma^+\sigma^- + \hbar\omega_c a^\dagger a + \hbar g(a^\dagger\sigma^- + \sigma^+ a). \tag{2.1}$$

where $a^\dagger$, a are the creation and the annihilation operators of a photon in the cavity mode, respectively. σ^+ and σ^- are the creation and the annihilation operators for an atomic excitation respectively. The resonance frequencies of the cavity and the atom are ω_c and ω_a respectively (Fig. 2.1). The exchange of one quantum of excitation between the atom and the cavity mode is described by the third term of the Hamiltonian (Eq. 2.1). The coupling constant g_0 determines the exchange rate of the excitation between the atom and the cavity mode:

$$g = \sqrt{\frac{\omega_c}{2\epsilon_0 V\hbar}} d_{ge} \tag{2.2}$$

where d_{ge} is the atomic dipole matrix element of the atomic transition, V is the cavity mode volume and ϵ_0 is the vacuum permittivity.

2.2.2. The dressed states

The eigenstates of the Jaynes-Cummings Hamiltonian can be calculated analytically. The ground state $|0, g\rangle$, which is an eigenstate of the system, remains unchanged. The other eigenstates $|n, \pm\rangle$, which are called the dressed states, are arranged in doublets and are superpositions of the states $|n, g\rangle$ (with the atom in the ground state and n photons in the cavity) and $|n-1, e\rangle$ (with the atom in the excited state and $n-1$ photons in the cavity):

$$|n, +\rangle = \cos\theta\,|n-1, e\rangle + \sin\theta\,|n, g\rangle \tag{2.3}$$

$$|n, -\rangle = -\sin\theta\,|n-1, e\rangle + \cos\theta\,|n, g\rangle\,, \tag{2.4}$$

with θ the mixing angle:

$$\tan(\theta) = \frac{2g\sqrt{n}}{(\omega_a - \omega_c) + \sqrt{4g^2 n + (\omega_a - \omega_c)^2}}. \tag{2.5}$$

The energy eigenvalues of the system are given by:

$$E_{n,+} = n\hbar\omega_c + \frac{\hbar(\omega_a - \omega_c)}{2} + \frac{\hbar}{2}\sqrt{(\omega_a - \omega_c)^2 + 4g^2 n} \tag{2.6}$$

$$E_{n,-} = n\hbar\omega_c + \frac{\hbar(\omega_a - \omega_c)}{2} - \frac{\hbar}{2}\sqrt{(\omega_a - \omega_c)^2 + 4g^2 n} \tag{2.7}$$

and the energy splitting of the doublets is:

$$E_{n,+} - E_{n,-} = \hbar\sqrt{(\omega_a - \omega_c)^2 + 4g^2 n} \tag{2.8}$$

When the atom is on resonance with the cavity (i.e. $\omega_a = \omega_c$), the splitting increases with the square root of the number of excitations, see Fig. 2.2.

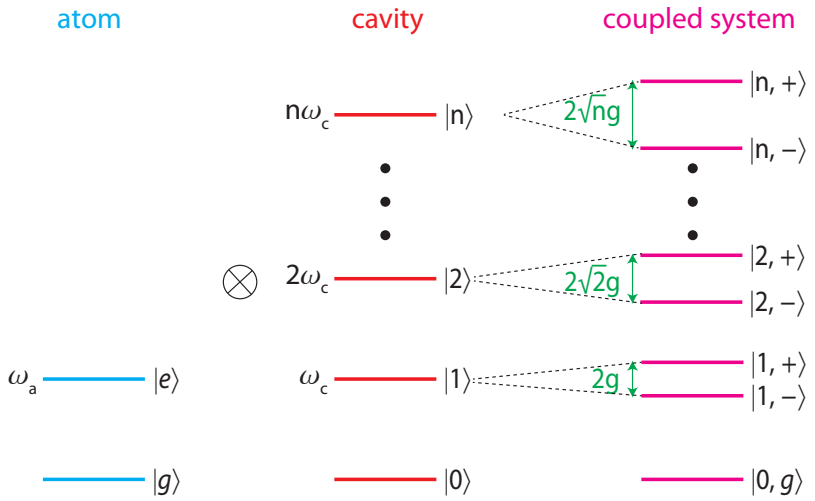

Figure 2.2.: The Jaynes-Cummings ladder of eigenvalues. A single two-level atom is coupled to a cavity mode which is resonant to the atomic transition ($\omega_a = \omega_c$). The cavity electromagnetic field is represented by a harmonic oscillator with an infinite number of equally spaced levels. The coupled system forms a ladder of energy levels which are arranged in doublets and with the splitting between the doublets increasing with the square root of the principal quantum number of the mode n.

2.2.3. Open quantum system

Driving and dissipation

So far we have presented the Jaynes-Cummings Hamiltonian which describes a closed system without losses. This simple model has allowed us to understand the basic concepts of a coupled atom-cavity system. However, in real experimental situations the interaction of the system with its environment has to be taken into account. This requires namely two steps: (a) coupling to modes other than the cavity mode to describe the decay of the atomic excitation and of the cavity mode and (b) including a pump term in order to drive the system

and to compensate for the losses. The pump term, which describes the excitation of the cavity mode by a coherent near-resonant probe field of frequency ω_p, is added in the following form to the Jaynes-Cummings Hamiltonian:

$$H_P = \hbar\eta(ae^{i\omega_p t} + a^\dagger e^{-i\omega_p t}) \tag{2.9}$$

where η is the driving strength which is proportional to the amplitude of the probe laser. The time dependence of the Hamiltonian reflects that the energy of the system is not conserved. This is expected since photons are exchanged with the probe laser.
Moreover, the system couples dissipatively to its environment which allows for the observation of its dynamics. This interaction gives rise to spontaneous emission of photons from the atom with the atomic polarization decay rate γ, or from the cavity with the cavity field decay rate κ (Fig. 2.1). Both decay channels have to be included in the theoretical model as loss processes. The strong-coupling condition is met when the internal dynamics of the atom-cavity system predominates over the losses which corresponds to:

$$g > \gamma, \kappa \tag{2.10}$$

Master equation

In quantum optics, different approaches exist to describe the time dependence of an open system and its interaction with the environment [101, 102, 103]. Here we briefly present a method based on the derivation of a master equation which describes the time evolution of the system's density matrix. For a detailed description the reader could check references [104, 99].
The density matrix ρ_{tot} includes all degrees of freedom and describes the system and its environment. It contains vectors from the combined Hilbert space $\mathcal{H}_{tot} = \mathcal{H}_S \otimes \mathcal{H}_R$, with $\mathcal{H}_S$ the Hilbert space of the system and $\mathcal{H}_R$ the Hilbert space of the environment. The von-Neumann equation for the density operator ρ_{tot} gives the time evolution of the total system:

$$\dot{\rho_{tot}} = -\frac{i}{\hbar}[H_{tot}, \rho_{tot}] \tag{2.11}$$

where H_{tot} is the total Hamiltonian consisting of the system and environment Hamiltonians H_S and H_R plus the Hamiltonian H_{int} which describes their interaction:

$$H_{tot} = H_S + H_R + H_{int} \tag{2.12}$$

We assume that the environment is not influenced by the system and that it remains in thermal equilibrium. Then, since only the system's density matrix ρ_S is of interest, it can be obtained by partially tracing over the eigenstates of the reservoir

$$\rho_S(t) = Tr_R(\rho_{tot}(t)) \tag{2.13}$$

Applying the Born and Markov approximations [99] yields the master equation for the reduced density operator of the system $\rho_S \equiv \rho$:

$$\dot{\rho} = -\frac{i}{\hbar}[H_S, \rho] + \kappa(2a\rho a^\dagger - a^\dagger a\rho - \rho a^\dagger a) + \gamma(2\sigma^-\rho\sigma^+ - \sigma^+\sigma^-\rho - \rho\sigma^+\sigma^-) \quad (2.14)$$

with the second term describing the cavity field decay and the third term describing the spontaneous emission of the atom. The master equation 2.14 can also be expressed in terms of the Liouville super operator $\mathcal{L}$:

$$\dot{\rho} = \mathcal{L}\rho \quad (2.15)$$

The time evolution of the expectation value of any system operator $\hat{o}$ can then be calculated via:

$$\langle\dot{\hat{o}}\rangle = Tr[\hat{o}\dot{\rho}] = Tr[\hat{o}(\mathcal{L}\rho)] \quad (2.16)$$

2.3. Observation and characterization

We saw previously that the system exchanges energy with its environment via mainly two channels: the atomic decay and the cavity decay.
Experimentally we only have access to the photons escaping from the cavity to get information about the system's dynamics. We characterize the photon stream emitted from the cavity by photon counting techniques. Moreover, by evaluating second-order correlation functions we gain information about the photon statistics of the transmitted field.
In the following, we briefly discuss the two methods and present some key features of a strongly coupled atom-cavity system.

2.3.1. Photon counting

All experiments performed through this thesis were carried out by driving the atom-cavity system with weak coherent fields which contain less than one photon on average per cavity lifetime. Using single photon counting modules (SPCM), we measure the mean photon number of the intracavity field $\langle a^\dagger a\rangle$ via photon counting of the output cavity field. Photons are emitted from the cavity at a rate 2κ, and the photon flux at the output cavity mirror is given by:

$$I = 2\kappa\eta_{out}\hbar\omega\langle a^\dagger a\rangle \quad (2.17)$$

where η_{out} is the outcoupling efficiency which takes into account that photons can be lost in the mirror substrates or transmitted through the input mirror. By monitoring the transmission of a weak probe beam as a function of

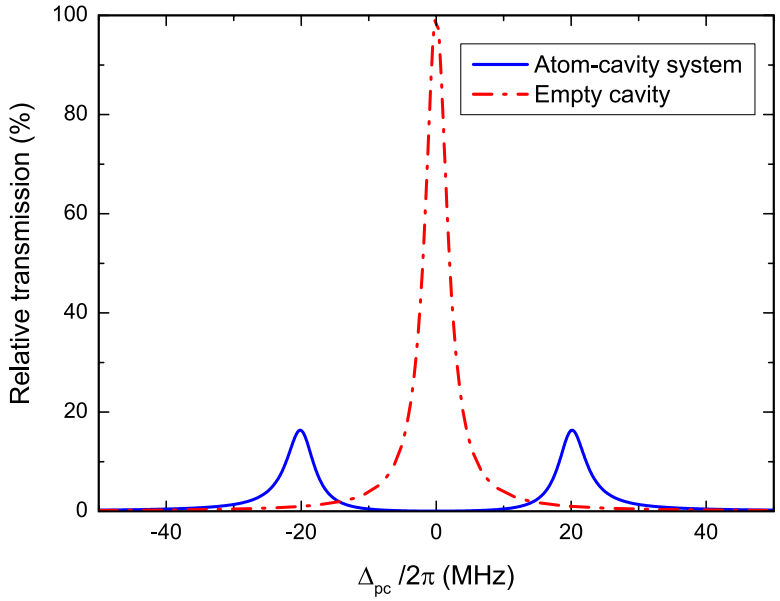

Figure 2.3.: A normal-mode spectrum showing the minimal splitting of $2g$ for the symmetric case $\omega_a = \omega_c$. Parameters are $\{g, \kappa, \gamma\}/2\pi = \{20,\ 2,\ 3\}$ MHz, and a driving strength of $\eta = 0.1\ \kappa$. The dashed red line is the relative transmission of the probe beam for an empty cavity for the same driving strength and as a function of the probe-cavity detuning $\Delta_{pc}/2\pi = (\omega_p - \omega_c)/2\pi$.

its frequency a spectrum showing the normal-mode splitting can be obtained confirming that the system is in the strong coupling regime as shown in a numerical simulation in Fig. 2.3 [19, 20].

2.3.2. Photon-photon correlations

The second-order correlation function is a powerful tool to study and observe the quantum dynamics of the atom-cavity system. It shows the temporal evolution of the mean intracavity photon number $\langle a^\dagger a \rangle$ after a photon has been detected. The quantum regression theorem [105, 99] enables the calculation of correlation function of system operators based on the solution of the master equation. The normally ordered [106] second-order correlation function can then be calculated via:

$$\langle a^\dagger a^\dagger(\tau) a(\tau) a \rangle = Tr\{a^\dagger a e^{\mathcal{L}\tau}[a \rho_S a^\dagger]\} \tag{2.18}$$

which can be understood in the following way:
the system starts in the steady state ρ_S, and the detection of the first photon projects the system into $a\rho_S a^\dagger$. The term $e^{\mathcal{L}\tau}[a\rho_S a^\dagger]$ reflects the time evolution of the mean photon number back to the steady-state expectation value.
In the experiments performed through this thesis, we measure the normalized

second-order correlation function defined by:

$$g^{(2)}(\tau) = \frac{\langle a^\dagger a^\dagger(\tau) a(\tau) a \rangle}{\langle a^\dagger a \rangle^2} \tag{2.19}$$

For a coherent laser beam with Poissonian photon statistics, $g^{(2)}(\tau)$ is independent of the delay time and $g^{(2)}(\tau) = 1$ for all τ. Thus photons arrive randomly. Thermal light on the other hand, shows super-Poissonian photon statistics with $g^{(2)}(0) = 2$ and photon bunching with $g^{(2)}(0) > g^{(2)}(\tau)$. Photon bunching is the tendency of photons to distribute themselves preferentially in bunches rather than at random [107]. Photon antibunching is the opposite effect. It is characterized by $g^{(2)}(0) < g^{(2)}(\tau)$, which means that fewer photon pairs are detected close together than further apart. Antibunching is a quantum effect which cannot be predicted using a classical analysis [98]. While it was first observed in a resonance fluorescence experiment [108], photon antibunching is also expected for a strongly-coupled single-atom-cavity system as shown in Fig. 2.4.

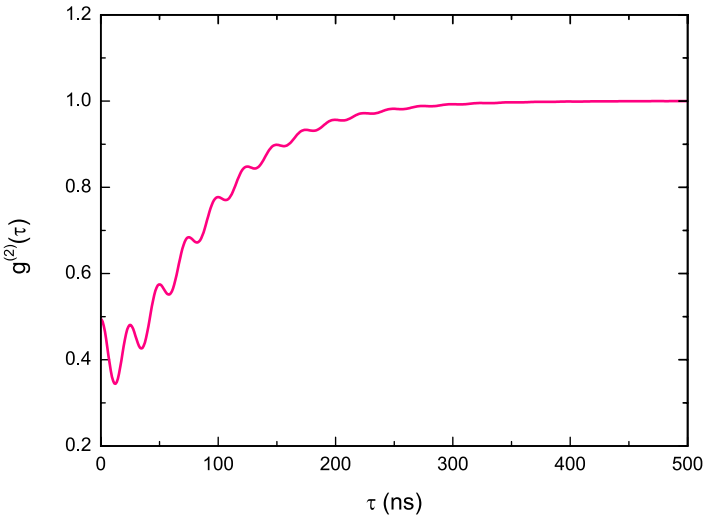

Figure 2.4.: A numerical simulation of $g^{(2)}(\tau)$ showing the photon blockade effect with $g^{(2)}(0) \approx 0.5 < g^{(2)}(\tau)$. Parameters are $\{g, \kappa, \gamma\}/2\pi = \{20, 2, 3\}$MHz, a driving strength of $\eta = 0.22\ \kappa$ and a probe-cavity detuning of $\Delta_{pc}/2\pi = -20$ MHz.

The underlying mechanism originates from the anharmonicity of the Jaynes-Cummings ladder. Tuning the probe beam frequency to the first manifold eigenstates $|1, \pm\rangle$ blocks the absorption of a second photon at the same frequency because transitions to $|2, \pm\rangle$ are detuned from resonance, resulting in the so-called photon blockade effect [85]. When the atom-cavity coupling g increases the detuning of the second photon to the second dressed states $|2, \pm\rangle$, given by: $\delta = 2(g - \sqrt{2}/2g)$, also increases which enhances the photon blockade effect and makes the $g^{(2)}(0)$ go to smaller values. Another interesting aspect in

measuring the second-order correlation function $g^{(2)}(\tau)$ in cavity QED is that it reveals internal quantum dynamics of the atom-cavity system [92]. In Fig. 2.4, we clearly see the vacuum-Rabi oscillations with a period of $2\pi/2g$ which is a result of the coherent exchange of a single excitation between the atom and the cavity. As explained in reference [109], even if the probe beam frequency is resonant with the first manifold eigenstates $|1,\pm\rangle$, there will always be some off-resonant excitation to the second manifold eigenstates $|2,\pm\rangle$. Moreover, since we are observing the behavior of the second-order correlation function $g^{(2)}(\tau)$, which is a two-photon measurement, only the states $|2,\pm\rangle$ can give rise to a two-photon emission in the weak driving regime. It is therefore reasonable to assume that the behavior of $g^{(2)}(\tau)$ is dominated by the steady-state population of the states $|2,\pm\rangle$. The $g^{(2)}(\tau)$ measurement is triggered by a detection of a photon at time $\tau = 0$ which is equal to applying the annihilation operator a to the states $|2,\pm\rangle$. This projects $|2,\pm\rangle$ into the states $(\sqrt{2}|1,g\rangle \pm |0,e\rangle)/\sqrt{3}$ which are more absorptive states than emitting since the amplitude of $|1,g\rangle$, a state where the atom is in the ground state, is larger than the amplitude of $|0,e\rangle$, a state where the atom is in the excited state. This explains the fact that $g^{(2)}(0)$ represents a local maximum for short times ($\tau < 20$ ns in Fig. 2.4) which is due to a higher absorption probability of a cavity photon by the atom after a photon has been detected at $\tau = 0$.

3. Merging cavity QED with EIT

It is a well known fact that photons traveling through a vacuum do not interact with each other. On the other hand, light fields can interact inside nonlinear optical media, although the nonlinearity remains weak in conventional materials specially at the few photon level [110]. Achieving strong interaction between individual photons in an environment with minimal absorption represents a cornerstone for future developments of quantum information science and photonic quantum technologies [111, 112, 53, 57, 113]. One way to reach this goal is via electromagnetically induced transparency (EIT) [114, 49] either with single atoms [83, 82, 84], or with atomic ensembles [115, 116]. In the previous chapter, we reported on some fundamental characteristics of the elementary cavity QED system, namely a single-atom coupled to a single cavity mode. This chapter theoretically describes a system which combines single-atom cavity QED in the strong coupling regime with EIT. It is shown that using such a system it is possible to convert an incoming laser beam into an outgoing light field with photon number fluctuations above or below the shot-noise level. Moreover, it enables the generation of multiple non classical states of light and to optically control their characteristics.
The content of this chapter has partially been published in [86]:

J. A. Souza, E. Figueroa, H. Chibani, C. J. Villas-Boas, and G. Rempe, "*Coherent Control of Quantum Fluctuations Using Cavity Electromagnetically Induced Transparency*", Physical Review Letters **111**, 113602 (2013).

3.1. Electromagnetically induced transparency

Electromagnetically induced transparency is a technique for making a resonant opaque medium transparent by means of quantum interference [117, 49, 115]. To illustrate how EIT works, let us consider a medium composed of three level atoms as in Fig. 3.1, with each atom having two long-lived ground states $|1\rangle$ and $|2\rangle$, in a Λ configuration. One could cancel the absorption of a resonant "signal" field which couples the ground state $|1\rangle$ to the excited state $|3\rangle$, by applying another "control" field driving the transition $|2\rangle \rightarrow |3\rangle$. The combination of the two fields stimulates the atoms into a dark superposition of the two ground states $|1\rangle$ and $|2\rangle$ which is a result of the two absorptive pathways (the direct pathway $|1\rangle \rightarrow |3\rangle$ or the indirect one $|1\rangle \rightarrow |3\rangle \rightarrow |2\rangle \rightarrow |3\rangle$) interfering

destructively with each other. The atoms are said to be in a "dark state" where none of them can be promoted to the excited state, resulting in a vanishing light absorption [118]. This transparency window in the spectrum of the atomic medium, is dependent on the control field parameters. Precisely, the transparency window position in the spectrum depends on the control field frequency, whereas its amplitude and width depend on the control field strength. This results in an optical tunability of the optical properties of the medium which can be seen in the dependence of the linear susceptibility of the EIT medium given by [117]:

$$\chi(\omega) = g^2 N \frac{\gamma_{12} + i\omega}{(\gamma_{13} + i\omega)(\gamma_{12} + i\omega) + \mid \Omega_c \mid^2} \tag{3.1}$$

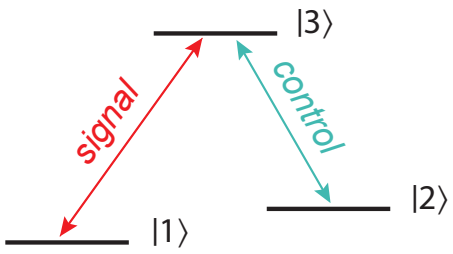

Figure 3.1.: Prototype atomic system for EIT. $|1\rangle$ and $|2\rangle$, two long-lived ground states, $|3\rangle$, the excited state.

where γ_{ij} corresponds to the coherence decay rates of the $i \rightarrow j$ coherence, Ω_c is the Rabi frequency of the control field, N is the total number of atoms in the medium, g is the atom-field coupling constant and ω is the detuning between the signal field frequency and the frequency of the atomic transition $|1\rangle \rightarrow |3\rangle$ (with $\omega = 0$ corresponding to the atom and signal field being on resonance). The absorptive properties of the medium is described by the imaginary part of the susceptibility, with the intensity transmission through the EIT medium given by:

$$T(\omega) = \exp(Im\chi(\omega)k_s L) \tag{3.2}$$

with $\lambda = 2\pi/k_s$ the wavelength of the signal field and L the length of the medium.
The EIT phenomenon has been used in different experimental works and has resulted in the observation of different effects. Examples include storage and controlled read-out of light pulses [119, 120, 121, 122, 123], observation of slow light [72, 124] and optical switching of light fields [116, 125, 58, 59]. Moreover, different theoretical works have emphasized the potential of single atom EIT for nonlinear optics and quantum information processing [126, 127, 55, 128, 56, 53].

3.2. Cavity EIT

Here, we show how a cavity EIT system [129, 130, 131] with a single atom provides the optical tunability offered by EIT and at the same time preserves the main characteristics of a cavity QED system.

3.2.1. Hamiltonian

We consider a three-level atom in a Λ configuration positioned inside an optical cavity as shown in Figure 3.2. The cavity mode of frequency ω_{cav} couples to the atomic transition $|1\rangle \rightarrow |3\rangle$ with a coupling strength g. A probe field of frequency ω_p and strength η drives the cavity. A classical coherent field with a frequency ω_c drives the atomic transition $|2\rangle \rightarrow |3\rangle$ with a Rabi frequency Ω_c. This field is the control field.
The time-independent Hamiltonian which describes this system in the electric dipole and rotating-wave approximations reads:

$$H_{CEIT} = \hbar\{\Delta_1\sigma_{33} + (\Delta_1 - \Delta_2)\sigma_{22} + \Delta\sigma_{11} - \Delta a^\dagger a + \eta(a^\dagger + a) + g(a^\dagger\sigma_{13} + \sigma_{31}a) + \Omega_c(\sigma_{23} + \sigma_{32})\} \quad (3.3)$$

where a, $a^\dagger$ are photon annihilation and creation operators, $\sigma_{ij} = |i\rangle\langle j|, i, j = 1, 2, 3$ are the atomic raising and lowering operators for $i \neq j$, and atomic energy-level population operators for $i = j$. The detunings are given by $\Delta = \omega_p - \omega_{cav}$, $\Delta_1 = \omega_{31} - \omega_{cav}$, and $\Delta_2 = \omega_{32} - \omega_c$. Similar to the two-

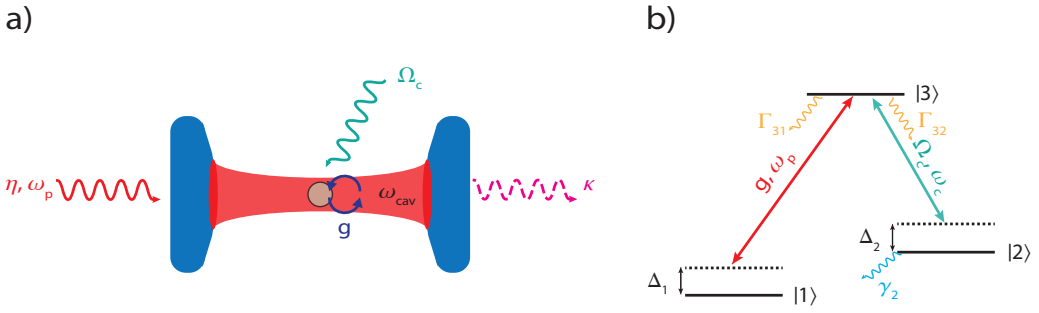

Figure 3.2.: a) Schematic of a single-atom cavity EIT system. b) The three-level atom in Λ configuration, with the transition $|1\rangle \rightarrow |3\rangle$ coupled to the cavity field of frequency ω_{cav} with a coupling strength g, and the transition $|2\rangle \rightarrow |3\rangle$ coupled to the control field of frequency ω_c and Rabi frequency Ω_c. $\Delta_{1,2}$ are the relevant detunings. Γ_{ij} radiative decay rates from state $|i\rangle$ to state $|j\rangle$. γ_2 the dephasing rate of state $|2\rangle$.

level atom case presented in the last chapter, the dynamics of the system is obtained numerically by solving the master equation for the atom-cavity density operator:

$$\dot{\rho} = -\frac{i}{\hbar}[H_{CEIT}, \rho] + \kappa(2a\rho a^\dagger - a^\dagger a\rho - \rho a^\dagger a) + \sum_{m=1,2} \Gamma_{3m}(2\sigma_{m3}\rho\sigma_{3m} - \sigma_{33}\rho - \rho\sigma_{33}) + \sum_{j=2,3} \gamma_j(2\sigma_{jj}\rho\sigma_{jj} - \sigma_{jj}\rho - \rho\sigma_{jj}) \quad (3.4)$$

where κ is the cavity-field decay rate, Γ_{3m} the polarization decay rates of the excited level $|3\rangle$ to the ground states $|m\rangle$ $(m = 1, 2)$ and γ_j the atomic dephasing rate of the state $|j\rangle$ $(j = 2, 3)$.
We solve for the steady state of ρ by truncating the Fock basis of the cavity field according to the probe strength following the method presented in [132].

3.2.2. The dressed states

The eigenstates of the single-atom cavity EIT system can be calculated analytically. For simplicity, we assume that the atom is on resonance with both the cavity and the control field, i.e., $\Delta_1 = \Delta_2 = 0$. With this assumption the system's Hamiltonian becomes:

$$H_{CEIT} = \hbar\{\Delta\sigma_{11} - \Delta a^\dagger a + \eta(a^\dagger + a) + g(a^\dagger\sigma_{13} + \sigma_{31}a) + \Omega_c(\sigma_{23} + \sigma_{32})\} \quad (3.5)$$

If we assume that $\eta = \Delta = 0$, this Hamiltonian can be rewritten in a new atomic basis $\{|1\rangle, |+\rangle, |-\rangle\}$, with $|\pm\rangle = (|2\rangle \pm |3\rangle)/\sqrt{2}$, in the following matrix form:

$$H_{CEIT} = \begin{pmatrix} 0 & g\sqrt{n/2} & -g\sqrt{n/2} \\ g\sqrt{n/2} & \Omega_c & 0 \\ -g\sqrt{n/2} & 0 & -\Omega_c \end{pmatrix} \quad (3.6)$$

with n the number of excitations in the system and with the following eigenvalues:

$$\lambda_n^{(0)} = 0 \quad (3.7)$$

$$\lambda_n^{(\pm)} = \pm\beta_n = \pm\sqrt{\Omega_c^2 + g^2 n} \quad (3.8)$$

and their respective eigenstates:

$$\left|\Psi_n^{(0)}\right\rangle = N_n^{(0)}\left[|1, n\rangle - \frac{g\sqrt{n}}{\Omega_c}\left(\frac{|+, n-1\rangle + |-, n-1\rangle}{\sqrt{2}}\right)\right] \quad (3.9)$$

$$\left|\Psi_n^{(\pm)}\right\rangle = N_n^{(\pm)}\left[|1,n\rangle + \frac{g\sqrt{n/2}}{\pm\beta_n - \Omega_c}|+,n-1\rangle - \frac{g\sqrt{n/2}}{\pm\beta_n + \Omega_c}|-,n-1\rangle\right] \quad (3.10)$$

where $N_n^{(0)}$ and $N_n^{(\pm)}$ are normalization factors. The eigenstates $\left|\Psi_n^{(0)}\right\rangle, n = 0,1,2,...$ or any combination of them with eigenvalues $\lambda_n^{(0)}$ are the intracavity dark states of the cavity EIT system, causing an empty-cavity-like transmission. Additionally, the dressed states $\left|\Psi_n^{\pm}\right\rangle$ with eigenvalues $\lambda_n^{(\pm)}$, represent a single-atom cavity EIT system sharing n excitations.

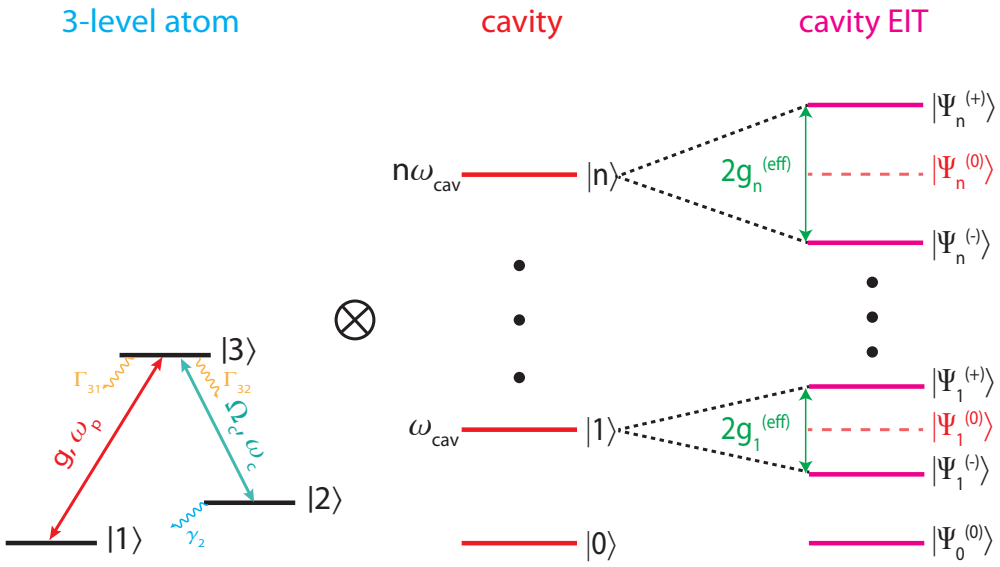

Figure 3.3.: The cavity EIT ladder of eigenvalues. A single three-level atom is coupled to a cavity mode which is resonant to the atomic transition ($\omega_{31} = \omega_{cav}$). A control field drives the other atomic transition ω_{32} with a Rabi frequency Ω_c. Γ_{ij} radiative decay rates from state $|i\rangle$ to state $|j\rangle$. γ_2 the dephasing rate of state $|2\rangle$. The cavity electromagnetic field is represented by a harmonic oscillator with an infinite number of equally spaced levels. The combined system forms a ladder of energy levels which are arranged in doublets, with the splitting between the doublets depending on the principal quantum number of the mode n and on the control field Rabi frequency: $2g_n^{(eff)} = 2\sqrt{ng^2 + \Omega_c^2}$. The states $\left|\Psi_n^{(0)}\right\rangle$ which lie between the doublets are the intracavity dark states of the cavity EIT system.

Similar to the usual cavity QED system with a two-level atom presented in the previous chapter, the dressed states of the cavity EIT system compose an anharmonic ladder structure. However, in the cavity EIT case, the energy-level splitting between the states depends on the control field Rabi frequency

Ω_c, with $2g_n^{(eff)} = 2\sqrt{ng^2 + \Omega_c^2}$ as shown in Fig. 3.3. This dependence of the splitting on the control field Rabi frequency gives an optical tuning knob on the energy eigenstates of the system. This will have important consequences on the dynamics of the system as we will see in the next paragraphs.

3.3. Cavity QED vs cavity EIT: a comparison

3.3.1. Transmission spectra

Before studying the optical control and quantum dynamics offered by the considered cavity EIT system, it is instructive to emphasize the main differences between a cavity EIT system and the standard two-level cavity QED configuration. Considering perfect cavity and control field resonance ($\Delta_1 = \Delta_2 = 0$), we calculate the relative transmission spectrum for both cases vs the normalized probe-cavity detuning Δ/κ. We consider both systems to be in the strong-coupling regime with $g \gg (\kappa, \Gamma_{32}, \Gamma_{31})$ and we set the driving strength of the probe field to $\eta = 1.0\ \kappa$, enough to sufficiently populate the energy levels associated with multiphoton transitions [133]. For the cavity QED sys-

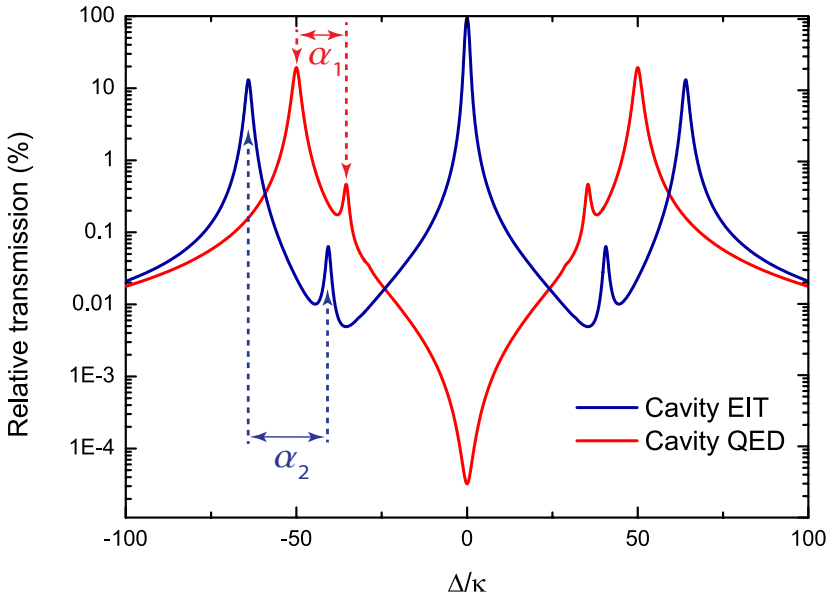

Figure 3.4.: Transmission spectra (on a logarithmic scale) vs normalized probe-cavity detuning Δ/κ for the two-level system (Cavity QED, solid red line) using the parameters: $g = 50\ \kappa$, $\eta = 1.0\ \kappa$, $\gamma = 0.1\ \kappa$. For the cavity EIT case (solid blue line) the parameters are: $g = 50\ \kappa$, $\eta = 1.0\ \kappa$, $\Gamma_{31} = \Gamma_{32} = 0.1\ \kappa$, and $\Omega_c = 40\ \kappa$. α_1 and α_2 are the frequency differences between the first and second doublets for the cavity EIT and cavity QED case, respectively.

tem (Fig 3.4, solid red line), we observe a pronounced vacuum Rabi splitting

with side peaks at smaller detunings corresponding to two-photon transitions $|0,g\rangle \rightarrow |2,\pm\rangle$, [133] between two different Jaynes-Cummings manifolds. All these transitions occur at different frequencies due to the anharmonic energy-level splitting, $2\sqrt{n}g$, $n = 1, 2, ...$[134].
The solid blue line of Fig. 3.4 shows the transmission spectrum for the cavity EIT case for similar parameters and with a control Rabi frequency of $\Omega_c = 40\kappa$. We directly distinguish the larger vacuum Rabi-splitting (corresponding to $\pm\sqrt{g^2+\Omega_c^2}$) and a second resonance corresponding to the first multiphoton transition $\left|\Psi_0^{(0)}\right\rangle \rightarrow \left|\Psi_2^{(\pm)}\right\rangle$. In addition, we see a narrow transmission window at zero detuning referred to as the intracavity dark state [83, 130, 131]. Moreover, we notice that the frequency difference between the first and second doublets $|1,-\rangle(\left|\Psi_1^{(-)}\right\rangle)$ and $|2,-\rangle(\left|\Psi_2^{(-)}\right\rangle)$ for the cavity EIT case is always larger than its cavity QED counter part, as $\alpha_1 = g(1-1/\sqrt{2}) < \alpha_2 = \sqrt{g^2+\Omega_c^2} - \sqrt{2g^2+\Omega_c^2}/2$ for any $\Omega_c \neq 0$.
Therefore, thanks to the dressing of the atom by the control field, cavity EIT helps to resolve the eigenstates of the system better than the usual two-level cavity QED system. This will induce important consequences on the photon-photon correlations as will be shown in the next paragraph.

3.3.2. Equal-time photon-photon correlations

To characterize the quantum nature of the cavity EIT system, we evaluate the equal-time photon-photon correlation function: $g^{(2)}(0) = \langle a^\dagger a^\dagger a a\rangle / \langle a^\dagger a\rangle^2$, which we calculate numerically for the steady state $\dot{\rho} = 0$ of the system's density operator.

In Fig. 3.5 (a) we compare between the equal time photon-photon correlation $g^{(2)}(0)$ behavior in the cavity QED (solid red line) and the cavity EIT (solid blue line) cases. We show the $g^{(2)}(0)$ correlation in both cases as a function of the normalized probe-cavity detuning Δ/κ. The minima in $g^{(2)}(0)$ for the cavity EIT case are associated with the one photon transitions A(1), A(3) and the two-photon transitions E(1), E(3) (see Fig. 3.6). This is similar to our previous observations in the transmission spectrum which we saw is also sensitive to these transitions. The photon-photon correlation, however, also shows signatures of other transitions. For example, the maxima are associated with the one photon transitions C(1), C(3), B(1), D(2) and the multiphoton transition $\left|\Psi_0^{(0)}\right\rangle \rightarrow \left|\Psi_3^{(\pm)}\right\rangle$ (marked with asterisks in Fig. 3.5 (a)). Another key aspect of the cavity EIT system is the presence of a coherent field ($g^{(2)}(0) = 1$) at $\Delta = 0$ (dashed line in Fig. 3.5 (a)) and photon bunching around $\Delta = \pm 80\kappa$. This is in stark contrast to the strong photon-bunching behavior ($g^{(2)}(0) \gg 1$) [135] and an almost coherent field for the respective detunings in the cavity QED case. The behavior of $g^{(2)}(0)$ is strongly correlated to the maxima in the frequency spectrum of the eigenstates populations (shown in Fig. 3.5 (b); see vertical dashed lines). A prominent feature is the improvement of the

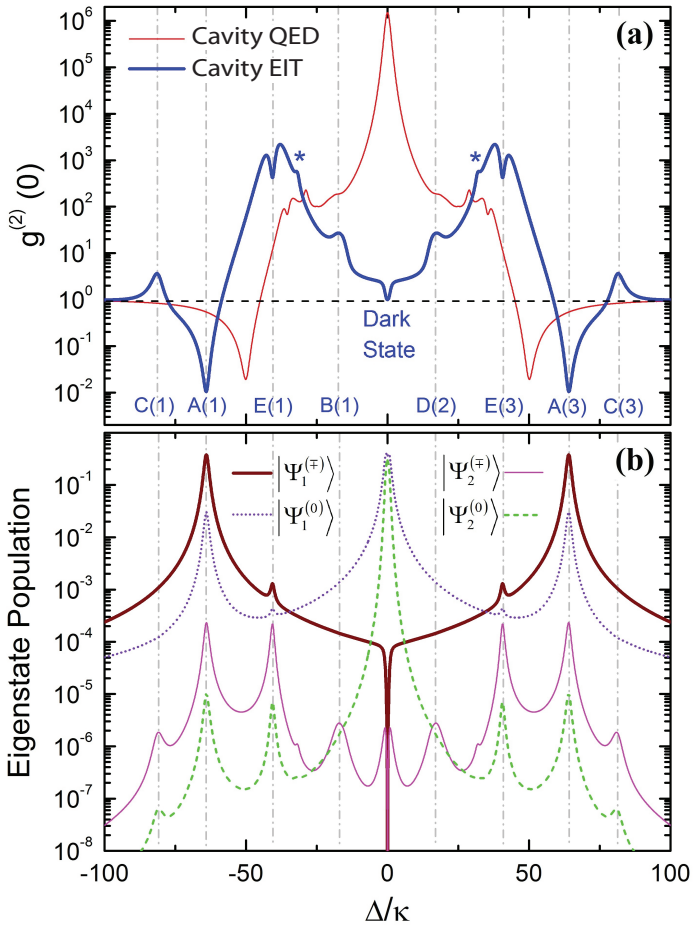

Figure 3.5.: (a) $g^{(2)}(0)$ correlation vs normalized probe-cavity detuning Δ/κ for the cavity QED case with $g = 50\ \kappa$,$\eta = 1\ \kappa$, and $\gamma = 0.2\ \kappa$ (red line) and for the cavity EIT configuration for the same g and η, $\Gamma_{31} = \Gamma_{32} = 0.1\ \kappa$ and $\Omega_c = 40\ \kappa$. (b) Population of the cavity EIT eigenstates $\left|\Psi_{1,2}^{(-)}\right\rangle$ for $\Delta < 0$, $\left|\Psi_{1,2}^{(+)}\right\rangle$ for $\Delta > 0$, and respective darks states $\left|\Psi_{1,2}^{(0)}\right\rangle$. The vertical dashed-dotted lines connect the maxima and minima in the $g^{(2)}(0)$ correlation with the populations of the relevant eigenstates.

maximum achievable photon antibunching (photon blockade) in the cavity EIT case compared to the cavity QED case. This is due to the larger frequency difference between the first and second doublets offered by the cavity EIT system, which results in a decreased probability of exciting the second manifold compared to the situation in the cavity QED system.

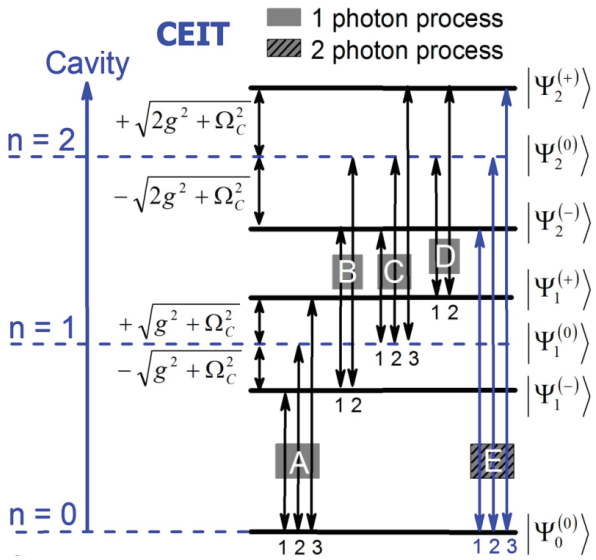

Figure 3.6.: Diagram of the eigenstates of the cavity EIT system with the relevant one-photon and two-photon transitions.

3.4. Coherent control of photon statistics using cavity EIT

We have shown in the last paragraph that it is possible to tune the photon statistics of the outgoing field by varying the frequency of the input field. In order to design a quantum control device, this possibility has to be provided by an external control field. We use the fact that in a cavity EIT system the eigenstates can be optically "moved" in the spectrum via the control field Rabi frequency to achieve this goal.

3.4.1. Optical switching from photon blockade to a two-photon gateway

In Fig. 3.7(a), we show how the equal-time photon-photon correlation $g^{(2)}(0)$ changes when we tune the control Rabi frequency Ω_c for different probe-cavity detunings. By keeping Δ constant and varying Ω_c, we probe the system over regions in which sub-Poissonian ($g^{(2)}(0) < 1$) and super-Poissonian ($g^{(2)}(0) > 1$) light is created. This is the first time optical control of photon statistics is predicted, a unique feature provided by the strongly coupled single-atom cavity EIT system. Similar to our analysis of Fig. 3.5(a), the first (left-most) super-Poissonian peak seen in Fig. 3.7(a) for each detuning Δ is associated with a local maximum in the population of the second dark state $\left|\Psi_2^{(0)}\right\rangle$ and the multiphoton state $\left|\Psi_2^{(+)}\right\rangle$, corresponding to the transition C(3), as depicted

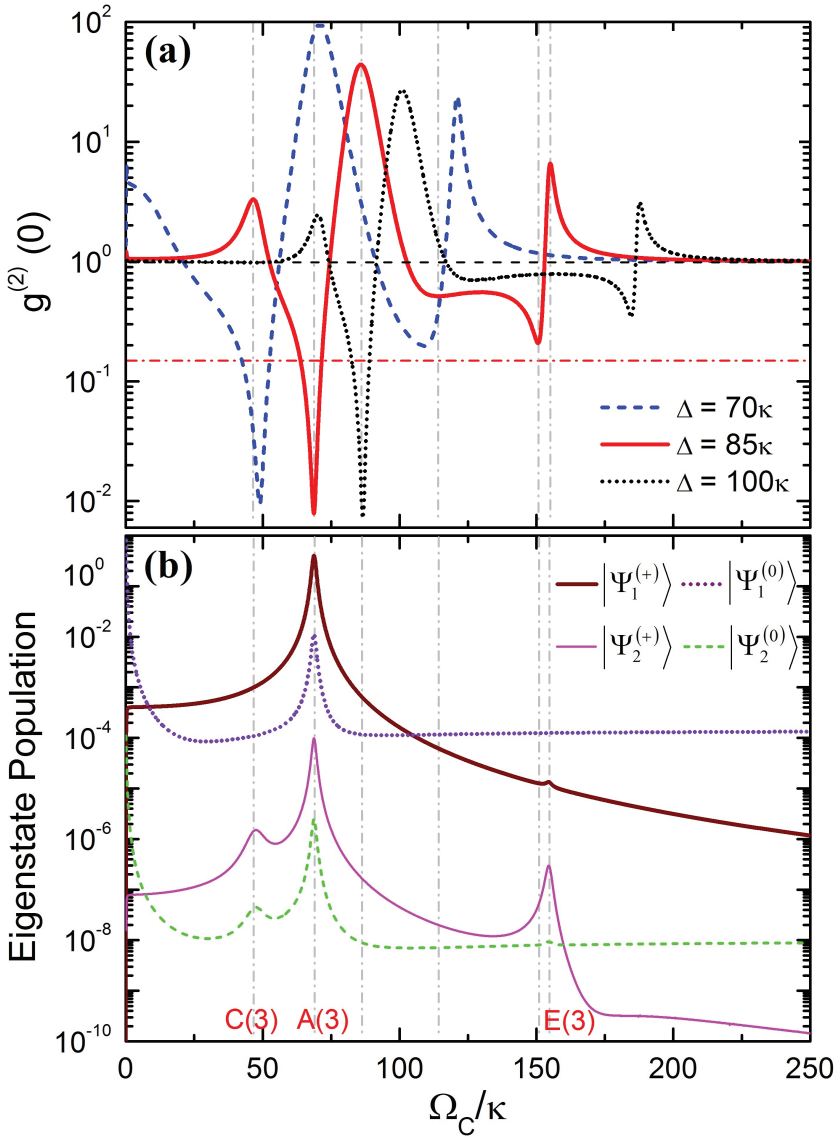

Figure 3.7.: (a) $g^{(2)}(0)$ correlation vs normalized Rabi frequency Ω_c/κ of the control field for the cavity EIT system for different probe-cavity detunings Δ using the same parameters as in Figure 3.5. (b) Population of the cavity EIT eigenstates $|\Psi_{1,2}^{(+)}\rangle$ and respective dark-states $|\Psi_{1,2}^{(0)}\rangle$ for $\Delta = 85\ \kappa$. The vertical dashed dotted lines connect the features in the $g^{(2)}(0)$ correlation with the populations of the relevant eigenstates.

in the eigenstate population (Fig. 3.7(b)) for $\Delta = 85\ \kappa$.
When further increasing Ω_c the first and most pronounced minimum of $g^{(2)}(0)$ is obtained when the transition A(3), $|\Psi_0^{(0)}\rangle \rightarrow |\Psi_1^{(+)}\rangle$, is resonantly driven by the probe field, resulting in sub-Poissonian light as a consequence of photon

blockade [85]. Once this resonance condition is violated for some larger Ω_c, a super-Poissonian field is generated [135]. We emphasize that in contrast to the first super-Poissonian peak discussed before, no maxima are observed in any of the eigenstate populations. A similar scenario occurs when the control Rabi frequency is increased to a value $\Omega_c = 150\kappa$ (for $\Delta = 85\kappa$). Here a pronounced sub-Poissonian minimum is observed with $g^{(2)}(0) = 0.2$, without any maxima in the eigenstate populations. The situation changes drastically when Ω_c is slightly increased so that the two-photon transition E(3), $\left|\Psi_0^{(0)}\right\rangle \rightarrow \left|\Psi_2^{(+)}\right\rangle$, is resonantly driven. This induces an increase in the population of state $\left|\Psi_2^{(+)}\right\rangle$ and therefore a higher two-photon emission probability or a two-photon gateway [133, 88]. However, contrary to what happens on the single-photon resonance A(3), $\left|\Psi_0^{(0)}\right\rangle \rightarrow \left|\Psi_1^{(+)}\right\rangle$, we now observe super-Poissonian photon statistics. Note that if only two-photon transition would be allowed, the light would exhibit sub-Poissonian statistics. The observed super-Poissonian statistics on the two-photon resonance results from the presence of single-photon transitions in both, the excitation and deexcitation of the system.
Another remarkable characteristic of our system is the presence of a broad region with $g^{(2)}(0) < 1$, independently of Ω_c. The width of this plateau region can be extended by increasing the probe-cavity detuning Δ, although at the expense of a less pronounced sub-Poissonian statistics.

3.4.2. Quantum dynamics of the single-atom cavity EIT system

Further insight into the studied cavity EIT system can be gained by studying the time-dependent second-order correlation function $g^{(2)}(\tau)$ of the emitted field. Figure 3.8 shows numerical simulations of $g^{(2)}(\tau)$ for different control field Rabi frequencies Ω_c. The control field is set to be on resonance with the atom (i.e. $\Delta_2 = 0$) and the probe field is being close to resonance with the state $\left|\Psi_1^{(-)}\right\rangle$ of the first manifold (i.e. $\Delta \approx -g_1^{(eff)}$).
As a general first remark, we notice that independently of the control field Rabi frequency Ω_c, the behavior of $g^{(2)}(\tau)$ is dominated by a strong oscillation at the probe-cavity detuning frequency Δ. This oscillation is due to a new field being generated at the empty cavity frequency: $\omega_{newfield} = \omega_p - \Delta = \omega_{cav}$, via a four-wave mixing process based on EIT [136, 137]. The fourth field involved in the process is generated at a frequency $\omega_c + \Delta$ and is not detected. This new EIT field interferes with the impinging probe field inducing the interference pattern at frequency Δ observed in the $g^{(2)}(\tau)$ behavior. Also, we notice that the oscillation lives for a longer duration than the decay rates of the system, Γ_{31}, Γ_{32} and κ. This is in stark contrast with the behavior observed in a cavity QED system with a two-level atom, where $g^{(2)}(\tau)$ reaches the steady state after a duration of $\tau = 2/(\gamma + \kappa)$ [85].

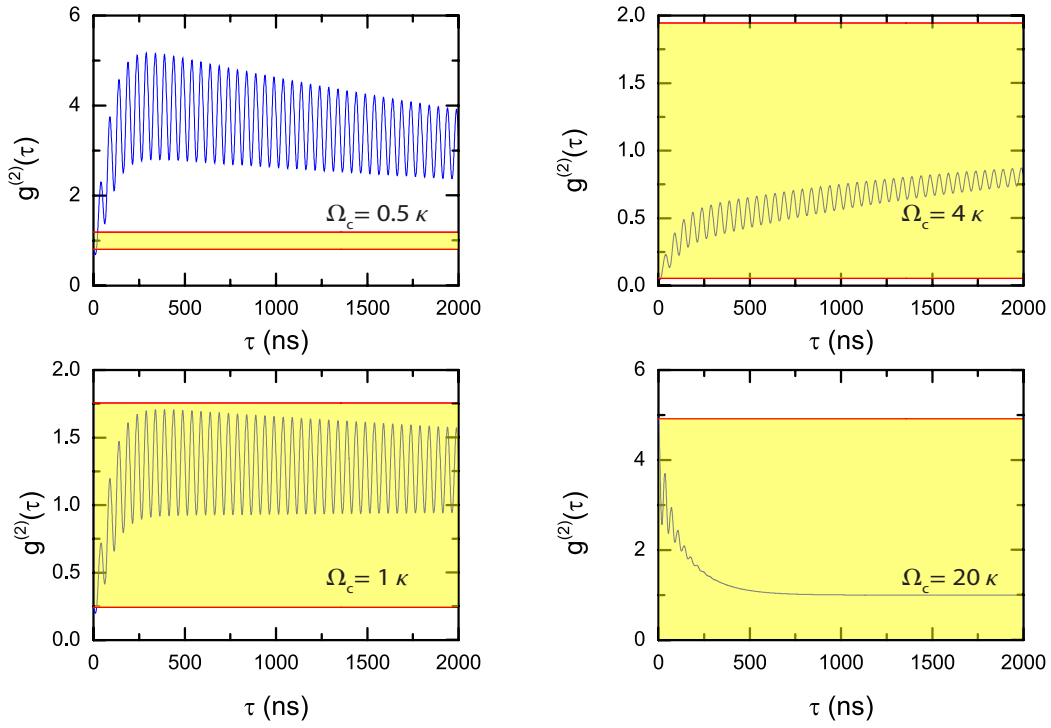

Figure 3.8.: Second-order intensity correlation functions vs. time delay for different values of the control field Rabi frequency Ω_c and for $g = 20\ \kappa$, $\Gamma_{31} = \Gamma_{32} = 2\ \kappa$ and $\eta = 1\ \kappa$. The control field is set to be on resonance with the atom (i.e. $\Delta_2 = 0$) and the probe field is being close to resonance with the state $\left|\Psi_1^{(-)}\right\rangle$ of the first manifold (i.e. $\Delta \approx -g_1^{(eff)}$). Shaded areas denote classically allowed values, calculated from Equation 3.13.

In order to understand these observations, it is useful to remember that $g^{(2)}(\tau)$ is a two-photon measurement, and in the weak driving regime only the states $\left|\Psi_2^{(0)}\right\rangle$ and $\left|\Psi_2^{(\pm)}\right\rangle$ can give rise to a two-photon emission. However, since in Fig. 3.8 the probe field is set to be close to resonance with the state $\left|\Psi_1^{(-)}\right\rangle$, it is reasonable to assume that the behavior of $g^{(2)}(\tau)$ will be dominated by the steady-state population of the state $\left|\Psi_2^{(-)}\right\rangle$. The $g^{(2)}(\tau)$ measurement is triggered by a detection of a photon at time $\tau = 0$ which is equivalent to applying the annihilation operator a to the state $\left|\Psi_2^{(-)}\right\rangle$. The obtained state is not an eigenstate of the system, therefore, at $\tau = 0$, the system will be in a coherent superposition of all the states in the first manifold of the cavity EIT ladder, $\left|\Psi_1^{(0)}\right\rangle$ and $\left|\Psi_1^{(\pm)}\right\rangle$. Using Fermi's golden rule, we can calculate the

decay rates of all those states:

$$\begin{aligned}\Gamma_{|\Psi_1^{(\pm)}\rangle} &= \kappa \cdot \left|\left\langle \Psi_0^{(0)}\right|a\left|\Psi_1^{(\pm)}\right\rangle\right|^2 + \Gamma_{31} \cdot \left|\left\langle \Psi_0^{(0)}\right|\sigma_{13}\left|\Psi_1^{(\pm)}\right\rangle\right|^2 + \Gamma_{32} \cdot \left|\left\langle \Psi_0^{(0)}\right|\sigma_{23}\left|\Psi_1^{(\pm)}\right\rangle\right|^2 \\ &= \frac{1}{2} \cdot \left[\frac{g^2\kappa}{g^2+\Omega_c^2} + \Gamma_{31}\right]\end{aligned} \tag{3.11}$$

and

$$\begin{aligned}\Gamma_{|\Psi_1^{(0)}\rangle} &= \kappa \cdot \left|\left\langle \Psi_0^{(0)}\right|a\left|\Psi_1^{(0)}\right\rangle\right|^2 \\ &= \frac{\kappa\Omega_c^2}{\Omega_c^2+g^2}\end{aligned} \tag{3.12}$$

We clearly see that the decay rates of the eigenstates of the single-atom cavity EIT system are dependent on both the control field Rabi frequency Ω_c and the coupling strength g, unlike the decay rates of the eigenstates of a cavity QED system with a two-level atom which are only dependent on the decay rates of the system. Since for the parameters used in Fig. 3.8 we have $\Gamma_{\left|\Psi_1^{(\pm)}\right\rangle} > \Gamma_{\left|\Psi_1^{(0)}\right\rangle}$, the EIT state $\left|\Psi_1^{(0)}\right\rangle$ will live for a longer time than the dressed states $\left|\Psi_1^{(\pm)}\right\rangle$. This explains why the oscillation observed in $g^{(2)}(\tau)$ is at the probe-cavity detuning frequency Δ since the state $\left|\Psi_1^{(0)}\right\rangle$ is generated at the empty cavity frequency. Moreover, increasing the control field Rabi frequency Ω_c increases the decay rate of the EIT state $\Gamma_{|\Psi_1^{(0)}\rangle}$, which explains the damping of the $g^{(2)}(\tau)$ oscillation in Fig. 3.8 for large values of Ω_c.
Another interesting aspect is the fact that for a certain control Rabi frequency Ω_c, the $g^{(2)}(\tau)$ can show a non-classical behavior as in Fig. 3.8 (a) where it clearly violates the Cauchy-Schwartz inequality, given by:

$$\mid g^{(2)}(\tau) - 1 \mid \leq \mid g^{(2)}(0) - 1 \mid \tag{3.13}$$

and which holds for classical fields [138, 139]. Values above those allowed classically are called overshoots, while values below are called undershoots. Overshoots have been observed in a cavity QED system with two-level atoms [140], however only for short times, typically below the cavity decay time $1/\kappa$ and the atomic decay time $1/\gamma$. Figure 3.8 (a) shows that overshoots can be prolonged in time using a single-atom cavity EIT system for a longer period, therefore introducing a memory effect on the non-classicality of the $g^{(2)}(\tau)$. This also holds for the photon blockade, shown in Fig. 3.8 (b), where $g^{(2)}(\tau)$ stays below one for $\tau \gg \frac{2}{\kappa+\Gamma_{31}}$, much longer than in the standard cavity QED case.

3.5. Conclusion and outlook

To conclude, we theoretically demonstrated that by means of a single three-level atom in a high-finesse cavity it is possible to optically control the quantum fluctuations of a probe beam via a fruitful combination of single-atom cavity QED in the strong coupling regime and EIT. By studying the equal-time photon-photon correlation $g^{(2)}(0)$, we showed that photon blockade can be enhanced in a single-atom cavity EIT system compared to the standard single-atom cavity QED system with a two-level atom. Moreover, we showed that the photon blockade could be changed optically to a two-photon gateway only by tuning the control field Rabi frequency Ω_c, and this for the same input field frequency.
The ability to produce sub-Poissonian and super-Poissonian outgoing light fields for the same Poissonian input field could be used in a network of cascaded atom-cavity systems, with the goal to control the predicted phase transition of light into an ordered Mott-insulator-like state of photons [141, 142, 143].
Our analysis of the time-dependent second-order correlation function $g^{(2)}(\tau)$ revealed a memory effect on the photon statistics of the emitted fields [144]. This memory is an EIT based memory [145, 146], since it is due to most of the atomic population being in a superposition between the two ground states. Furthermore, we showed that a single-atom cavity EIT system in the strong coupling regime could be used to engineer a plethora of non-classical fields with a longer lifetime than any decay rate of the system. This feature could open new possibilities for new quantum information protocols, where the photon statistics of the emitted field could be preserved by turning off the control and probe fields simultaneously and turning them back on later in time to recover the $g^{(2)}(\tau)$ behavior.
Finally, future avenues include extending our analysis to configurations in which both the probe and the control fields are quantized, thus, providing optical control using single photons as gate fields. This might allow the realization of photonic quantum gates in which the interaction between photons is controlled with single atoms.

4. Experimental setup

In the course of this thesis, the experimental apparatus had to be moved from one lab to another. After the move, different parts of the setup had to be rebuilt, these includes the laser system which had to be rebuilt to address the ^{87}Rb isotope instead of the previously used ^{85}Rb isotope. Also a new trapping and cooling scheme for the atoms was implemented. The aim of this chapter is to explain these new developments. Further details of the apparatus can be found in [109].

4.1. Laser system and cavity parameters

For the realization of the cavity EIT experiment described in the previous chapter, we decided to use the ^{87}Rb isotope because of its less complicated hyperfine structure of the D_2 line with less Zeeman substates compared to ^{85}Rb [147, 148]. Two diode lasers, addressing the D_2 line, are required for preparing and probing the atoms. We use two other diode lasers at 784 nm and 786 nm to trap atoms inside the cavity. Finally, a diode laser addressing the D_1 line of ^{87}Rb is used in some measurements as a repumper. The operation of a rubidium magneto-optical trap (MOT) and an atomic fountain requires two lasers running on two different hyperfine transitions of the D_2 line of ^{87}Rb as shown in Fig. 4.1. A laser beam generated by a commercial tapered amplifier (TA pro, Toptica) driving the closed $F = 2 \rightarrow F' = 3$ transition is used to laser-cool the atoms. To compensate for off-resonant scattering to the dark $F = 1$ hyperfine ground state, a repumping laser (DL 100 pro, Toptica) on resonance with the $F = 1 \rightarrow F' = 2$ transition of the D_2 line is applied to the atoms.

Those two lasers, the TA pro and the DL 100 pro, operate at a wavelength of 780 nm and are both locked to a commercial frequency comb reference (Menlo Systems, FC 1500-250) using a beat-lock scheme (linewidth ~ 200 kHz [149, 150]). The light from the two lasers is frequency-shifted and intensity-controlled using acousto-optic modulators (AOM) to address each transition of the ^{87}Rb D_2 line. In addition to the operating the MOT, the generated beams are used to probe the atoms inside the cavity either on the closed cycling transition or on the open $F = 1 \rightarrow F' = 2$ transition for the cavity EIT measurements (Fig. 4.1 c)). Moreover, some beams are used for repumping the atom inside the cavity. Further details about the configuration of those

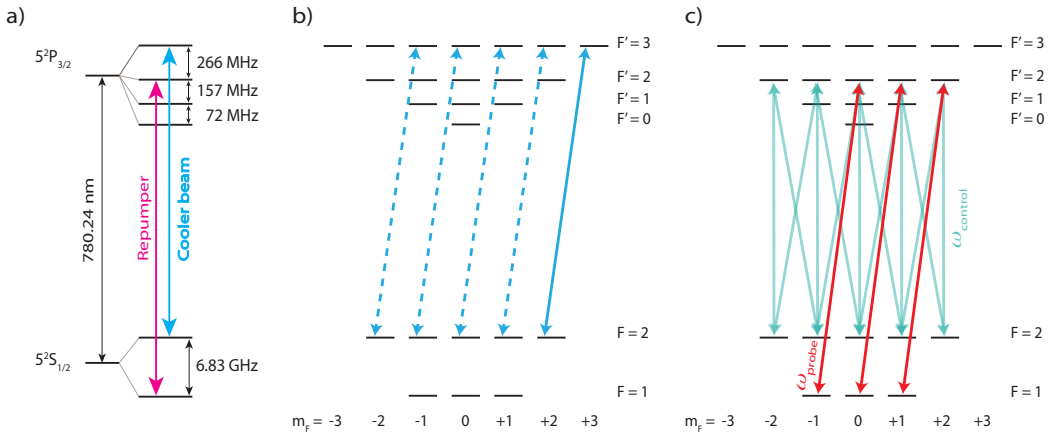

Figure 4.1.: a) Relevant hyperfine transitions of the D_2 line of ^{87}Rb. The transitions driven by the cooler and the repumper for the operation of the MOT are shown. b) For cavity QED experiments with two-level atoms, a circularly polarized probe laser coupled to the cavity drives the closed $F = 2, m_F = +2$ to $F = 3, m_F = +3$ transition justifying the two-level approximation of the atom. c) For cavity EIT experiments, the atomic level scheme used is shown. A circularly polarized probe laser (red color) with a frequency ω_{probe} is coupled to the cavity and drives the $F = 1 \rightarrow F' = 2$ transition of the D_2 line of ^{87}Rb. The control laser (light green), drives the atom resonantly with the $F = 2 \rightarrow F' = 2$ transition of the D_2 line of ^{87}Rb in a lin $\perp$ lin polarization configuration.

two lasers can be found in [151].

Trapping lasers

For trapping the atom and stabilizing the cavity length two other diode lasers are used. The light provided by a commercial grating stabilized diode laser (DL 100 pro, Toptica) at 786 nm is split into two parts. The first part passes through an AOM in double-pass configuration and is superimposed with a frequency comb in a fiber beamsplitter (BS). The beat signal is focused through a 785 nm interference filter onto a fast, AC-coupled photodiode (FDP510, Menlo systems) and is used for the cavity lock as described in reference [109]. The second part of the light also passes through an AOM double-pass configuration and is coupled into a fiber that guides the light to the cavity.
The other laser (TA100, Toptica) runs at 784 nm and serves as a transverse dipole trap. This laser is not frequency stabilized and delivers a single mode (spatial and frequency) beam at a power of 0.5 W, which is intensity controlled using an AOM. The transverse dipole trap is necessary for the implementation of the new cooling and trapping scheme which was developed in the course of this thesis and which will be briefly described in the next section.

Mirror curvatures	$R_1 = 20$ cm, $R_2 = 1$ cm
Mirror transmittances	$T_1 = 2.5 \pm 0.5$ ppm,
	$T_2 = 17.8 \pm 0.5$ ppm
Mirror losses	$L_1 + L_2 = 11.0 \pm 0.5$ ppm
Cavity length	$\mathrm{l} = 200$ μm
Cavity finesse	$F = 195000 \pm 2000$
Cavity decay rate	$\kappa/2\pi = 2$ MHz
Mode waist	$\omega_0 = 19$ μm
Coupling constant ($F = 2 \rightarrow F' = 3$)	$g_0/2\pi = 20$ MHz
Coupling constant ($F = 1 \rightarrow F' = 2$)	$g_0^{m_F=\{-1,0,1\}}/2\pi = \{5.8, 9.2, 14.3\}$ MHz

Table 4.1.: Summary of the most important cavity parameters.

Cavity parameters

At the heart of the experimental setup is a high-finesse optical cavity. We choose the cavity parameters such that the regime of strong atom-cavity coupling is achieved both when the cavity is resonant with the closed cycling $F = 2 \rightarrow F' = 3$ transition and when it is resonant with the open $F = 1 \rightarrow F' = 2$ transition. Table 4.1 summarizes the main cavity parameters used for the different measurements performed in this thesis.

4.2. Cooling and trapping single atoms in the cavity

In previous experiments with our setup [152, 43], we relied on feedback cooling [40, 44, 43] to trap single atoms inside the cavity. The implementation of feedback cooling requires constant observation of the atomic motion in real time in order to be able to react to it. This is possible with the usual two-level cavity QED system, where the probe laser drives a closed cycling transition. However, for a cavity EIT system one needs to drive an open transition where the excited state can decay to two possible ground states. Therefore, the requirement of feedback cooling to constantly "observe" the atom is no longer fulfilled with an open transition. If the atom decays to the ground state that is not coupled to the cavity, the light transmitted through the cavity will no longer carry information about the atom. Moreover, driving an open transition requires constant repumping of the atom to the right ground state, which induces large heating rates.

To solve this issue, we developed a new cooling and trapping scheme based on previous work [153, 154] which is independent on which of the atomic

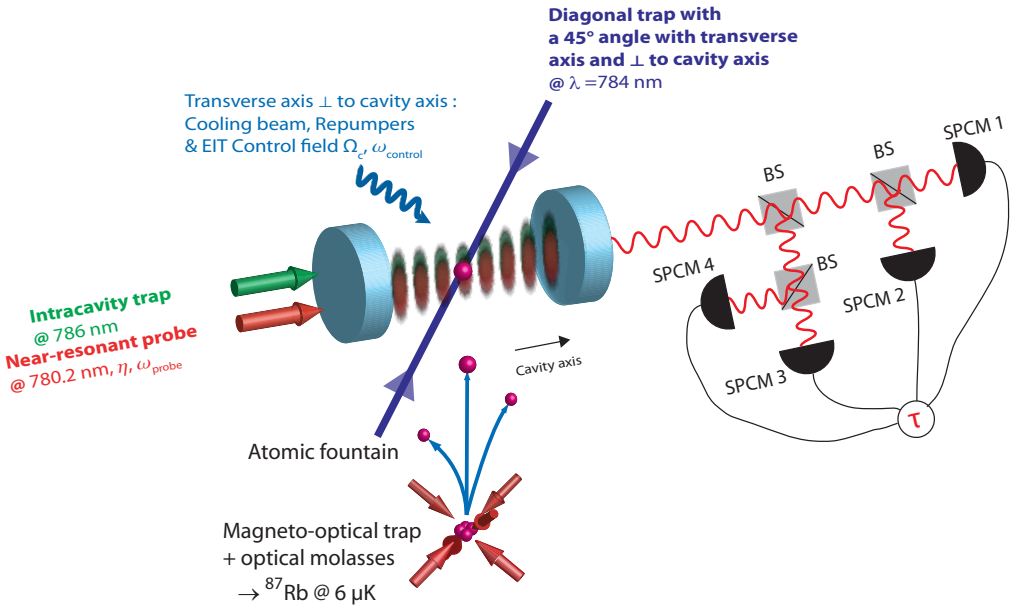

Figure 4.2.: Sketch of the experimental setup. A cloud of cold ^{87}Rb atoms is prepared in a MOT below the cavity. The cloud is later pushed towards the cavity by means of an atomic fountain. The presence of the atoms is detected by measuring the transmission of the near-resonant probe laser (red) via 4 single-photon counting modules (SPCM). A single ^{87}Rb atom (pink dot) is trapped inside the cavity within a TEM_{00} mode of the cavity, at the focus of a standing wave dipole trap (green) at 786 nm with a trap depth of 150 μK. A second standing wave dipole trap at 784 nm (violet) and with a trap depth of 1.4 mK, is applied at $+45°$ with respect to the cavity mode and perpendicular to the cavity axis. This *diagonal* trap serves as a second trap for the atom. Another diagonal beam path at $-45°$ is used to apply a resonant *push-out* beam (driving the $F = 2 \rightarrow F' = 3$ transition and not shown) few micrometers below the cavity mode to make sure that not more than a single atom is trapped. Finally, a transverse beam path on the same plane of the cavity axis and perpendicular to it, is used to apply the cooling beam (driving the $F = 2 \rightarrow F' = 3$ transition), the cooling beam repumper (driving the $F = 1 \rightarrow F' = 2$ transition), the EIT control field (driving the $F = 2 \rightarrow F' = 2$ transition) and the open transition repumper (driving the $F = 2 \rightarrow F' = 1$ transition) all in a lin $\perp$ lin polarization configuration. BS, beamsplitter.

transitions is coupled to the cavity mode. This cooling scheme requires two dipole traps to form a 2 dimensional lattice structure as shown in Fig. 4.2. The intracavity trap at 786 nm with a trap depth of 150 μK is constantly turned on. The diagonal trap at 784 nm with a trap depth of about 1.4 mK is perpendicular to the cavity axis and applied with a 45° angle with respect to the transverse axis of the cavity. This trap is only turned on upon a detection

of a transiting atom. A cooling beam with a power of about 4 μW, applied vertically to the cavity axis in a lin $\perp$ lin polarization configuration, drives the atom and is red detuned by 40 MHz from the $F = 2 \rightarrow F' = 3$ atomic transition of the D_2 line. In order to compensate for off-resonant scattering to the dark $F = 1$ hyperfine ground state, a repumping beam originating from a DL 100 pro laser and above the saturation intensity, drives the $F = 1 \rightarrow F' = 2$ transition of the D_1 line along the same beam axis. Trapping times of up to 10 s were within reach after optimization of all cooling parameters. We believe that the main cooling force which is responsible of the long observed storage times is a Sisyphus-like cooling force along the diagonal trap axis [153]. A more detailed description on the implemented cooling scheme can be found in [155].

4.3. Experimental implementation of cavity EIT

This section gives some details on the experimental realization of the cavity EIT experiment described theoretically in the previous chapter. Figure 4.1 (c) shows the atomic level scheme which was chosen for observing single-atom cavity EIT. The cavity was put at a frequency $\Delta_{ac}/2\pi = (\omega_{cavity} - \omega_{atom})/2\pi$ = 16 MHz from the bare atomic transition $F = 1 \rightarrow F' = 2$ transition of the D_2 line of ^{87}Rb to compensate for the AC-Stark shift due to the dipole traps for an atom at the center of the cavity mode. For the same reason, the control field is put 16 MHz to the blue of the $F = 2 \rightarrow F' = 2$ transition of the D_2 line and drives the atom in a lin $\perp$ lin polarization configuration (Fig. 4.2). The probe laser is circularly polarized and drives the atom-cavity system with a driving strength η.

From the atomic level scheme, we see that our experimental cavity EIT system is a multilevel one with three ground states $F = 1, m_F = \{-1, 0, 1\}$, giving rise to three different maximal coupling strengths for an atom at the center of the cavity mode $g_0^{m_F=\{-1,0,1\}}/2\pi = \{5.8, 9.2, 14.3\}$ MHz, respectively. Since the cavity field decay rate $\kappa/2\pi = 2$ MHz and the atomic polarization decay rate $\gamma/2\pi = 3$ MHz are much smaller than the coupling to the cavity mode ($g_0^{m_F=\{-1,0,1\}} > \kappa, \gamma$) fulfilling the strong coupling condition of cavity QED for all of the three ground states.
The spectral properties of the system are investigated by modifying the probe frequency and observing the transmitted field intensity versus the probe cavity detuning $\Delta_{pc} = \omega_{probe} - \omega_{cavity}$.
In order to guarantee that a fixed phase relationship exists between the control laser and the probe laser, which is a prerequisite for EIT, we derive both fields from the same laser (TA pro, Toptica). As mentioned before, this laser is locked to a frequency comb and is near resonant to the $F = 2 \rightarrow F' = 3$ transition. Part of this laser light goes through an AOM and is frequency-shifted

to the $F = 2 \rightarrow F' = 2$ transition to generate the control field. Another part of the light goes through a fiber coupled electro-optic modulator (NIR-MPX800, Photline technologies) through which we apply a microwave signal, from a signal generator (Rohde & Schwarz SMA100A), of about 6.8 GHz to generate sidebands on the light. We send this light through an optical fiber to the cavity. Since the cavity linewidth is $\kappa/2\pi = 2$ MHz, it acts as an efficient frequency filter for the carrier and for all other sidebands. Only the +1 order, which is near-resonant with the $F = 1 \rightarrow F' = 2$ transition, can enter the cavity. This is our probe field. For measuring slow light (Chapter 6), we use an arbitrary waveform generator to send in Gaussian electrical pulses to modify the amplitude of the microwave signal and generate Gaussian pulses of light. We characterize the system by performing transmission and correlation measurements using single-photon counting modules (SPCM). As shown in Fig. 4.2, our setup contains four SPCMs. For the correlation measurements, unlike in a Hanbury Brown and Twiss (HBT) configuration [156] where only two detectors are used with one providing the "start" signal and the other providing the "stop" signal, we cross-correlate the photon clicks measured on all SPCMs. Therefore, in our case $g^{(2)}(\tau) = g^{(2)}(-\tau)$ for all τ.

Experimental sequence

The measurements performed in the course of this thesis require a well-defined switching of a number of analog and digital channels in time. These channels typically control laser frequencies, intensities and magnetic fields. The experimental sequence is programmed in a home-made Labview program and is executed by an Adwin real-time system (Adwin Pro, T9). A measurement sequence starts by loading ^{87}Rb atoms in a magneto-optical trap similarly to reference [109]. Depending on the desired number of atoms, we load the MOT for 1-1.5 s. During the loading phase a current of 4 A runs through the MOT coils and causes a magnetic field gradient of 10 G/cm along the coil axis. Later, we start the molasses phase by ramping up the detuning of the cooling light to 40 MHz within 50 ms and decreasing its power to 6 mW. At the end of the ramp, the magnetic coils are switched off. After 5 ms of molasses cooling, a temperature of about 6 μK is reached. The current through the compensation coils is adjusted to minimize the temperature after the molasses. Later, the cooled atomic cloud is launched towards the cavity by detuning the upper MOT beams with respect to the lower beams within 5 ms. For a detuning of about -3 MHz, the turning point of the trajectory of the atomic cloud is approximately located on the cavity axis. We detect the presence of atoms in the cavity by monitoring the transmission of a resonant probe laser through the cavity. A passing atom induces a drop in the transmission signal of the probe laser through the cavity which is detected via the SPCMs behind the cavity. By adjusting the horizontal magnetic field during the acceleration phase, the

horizontal velocity of the atomic cloud can be fine tuned. During the time of flight of the atoms to the cavity, we change the current in the compensation coils to minimize the magnetic field in the science chamber. In order to ensure that only single atoms are being trapped a "push-out" beam, resonant with the $F = 2 \rightarrow F' = 3$ transition located few micrometers below the cavity mode, is constantly turned on at the beginning of the sequence to prevent the remaining atoms in the cloud from reaching the cavity. After detecting an atom in the cavity, the measurement sequence can be started. As shown in Fig. 4.3, the sequence is composed of four intervals which are continuously repeated in time until the atom is lost from the cavity. The first interval is the cooling interval in which the diagonal trap at 784 nm is turned on at its full power (trap depth of 1.4 mK) along with the cooling beam driving the $F = 2 \rightarrow F' = 3$ transition and its repumper driving the $F = 1 \rightarrow F' = 2$ as explained previously. The duration of the cooling interval was varying in our measurements from 10 ms to 25 ms depending on the experimental parameters.

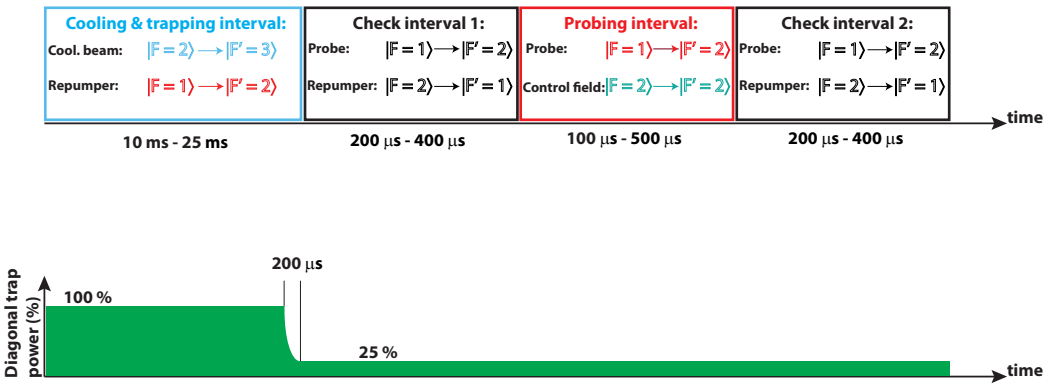

Figure 4.3.: The experimental sequence used for single-atom cavity EIT measurements. The sequence starts with a cooling and trapping interval where the atom is trapped for further processing, with the diagonal trap being at its full power (trap depth of 1.4 mK). The probe interval where the atom is in an EIT configuration lies between two check intervals where we check whether the atom is well localized in the center of the cavity while being probed. The trap depth is reduced to 340 μK within 200 μs before the first check interval to reduce the atomic stark shift and to bring the atom on resonance with the cavity. The sequence is continuously repeated in time as long as the atom is still trapped.

The cooling interval is followed by a check interval where the probe beam, resonant with the $F = 1 \rightarrow F' = 2$, transition drives the atom-cavity system

and where the diagonal trap power is reduced linearly to 25 % of its initial power within 200 μs. At the same time a repumper driving the atom on the $F = 2 \rightarrow F' = 1$ transition is applied perpendicular to the cavity axis in a lin $\perp$ lin polarization configuration. The check interval is used to check how well the atom is coupled to the cavity mode and typically lasts 200 μs to 400 μs. The lower the transmission of the probe beam through the cavity is, the better the atom is localized at the center of the cavity mode implying a higher coupling rate [157]. The first check interval is followed by a probing interval where the probe beam is kept on and where the repumper resonant with the $F = 2 \rightarrow F' = 1$ transition is exchanged by the control field resonant with $F = 2 \rightarrow F' = 2$ transition to be in an EIT configuration. Finally, another check interval similarly to the first one is applied after the probing interval, to ensure that the atom is still well coupled after it has been probed. For spectroscopy measurements, only atoms reducing the cavity transmission to 7 % of its empty cavity value and below, in both check intervals, were taken into account. For the second-order correlation measurements atoms reducing the cavity transmission to 40 % and below were taken into account to have enough statistics.

5. A cavity EIT-based photon blockade with memory

In this chapter, we present the experimental realization of the theoretical proposal described in Chapter 3. We start by making sure that the system is in the strong coupling regime of cavity QED by performing a normal-mode spectrum on the considered transition. Then, we show different transmission spectra of the single-atom cavity EIT system showing the optical control of the eigenstates of the system. Finally, results of the second-order intensity correlation function are presented. They show the optical control of the photon statistics of the emitted field and a photon blockade with a memory effect.

5.1. Spectroscopy results

5.1.1. Normal-mode spectroscopy of an open transition

The normal-mode splitting constitutes the benchmark of strong coupling in cavity QED. It is a manifestation of the avoided crossing of the cavity resonance and the atomic resonance. In the optical regime, first experiments investigating the normal-mode spectrum were with atoms from a thermal beam passing through the cavity [158, 18, 159]. Later, it was also measured using a cold atomic cloud transiting the cavity [160]. Finally, the normal-mode splitting was shown using single atoms [19, 20]. In the microwave regime, normal-mode splitting was also shown using artificial atoms [15, 17]. All those experiments were achieved using two-level atoms were the excited state can only decay to the ground state which is coupled to the cavity.
In contrast to this, the realization of the single-atom cavity EIT system described in Chapter 3 requires the cavity field to be strongly coupled to an open transition which can decay to two different ground states. Driving an open transition makes the normal-mode spectroscopy measurement more difficult to realize, since the constant repumping induces large heating rates which have to be compensated. We start by performing normal-mode spectroscopy on the $F = 1 \rightarrow F' = 2$ transition of the D_2 line of ^{87}Rb. This requires constant repumping of the atomic population decaying to the hyperfine ground state $F = 2$ back to the ground state $F = 1$. The repumper drives the $F = 2 \rightarrow F' = 1$ transition of the D_2 line of ^{87}Rb in a lin $\perp$ lin polarization configuration. The cavity was put blue with respect to the atomic transition

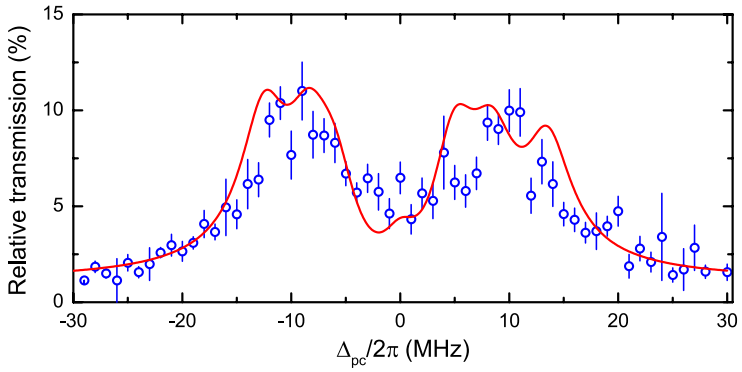

Figure 5.1.: Normal-mode spectroscopy of the open $(F = 1, m_F) \rightarrow (F' = 2, m_{F'} = m_F + 1)$ transition for a driving strength of $\eta = 0.16\ \kappa$. The observed normal-mode splitting is about $2g/2\pi = 2 \times 9.5$ MHz. The slight asymmetry is caused by a residual small atom-cavity detuning $\Delta_{ac}/2\pi$. The solid red line is a theoretical fit based on the steady-state solution of the master equation for each Zeeman sublevel involved in the considered transition (see text).

$\Delta_{ac}/2\pi = (\omega_{cavity} - \omega_{atom})/2\pi = 16$ MHz, so that the Stark shift induced by the 786 nm intracavity trap (5 MHz) and the 784 nm diagonal trap (11 MHz) compensates the initial atom-cavity detuning.

Similar to the cavity EIT experimental sequence shown in Fig. 4.3, the sequence used to measure the normal-mode spectrum on the open transition also contains a probe interval which is precedented and followed by a check interval, making sure that the probed atoms are strongly coupled to the cavity mode. The only difference here is that the control field is replaced by a repumper driving the $F = 2 \rightarrow F' = 1$ transition. The repumper ensures that the atomic population which has decayed to the $F = 2$ ground state is redistributed in all the three Zeeman sublevels of the $F = 1$ ground state. As explained in Chapter 4, these sublevels will result in different maximum coupling strengths for the atom due to the different Clebsch-Gordan coefficients with $g_0^{\{m_F=-1,0,1\}}/2\pi = \{5.8, 9.2, 14.3\}$ MHz depending on where the atomic population is.

In Fig. 5.1, the measured transmission spectrum (blue circles) with a driving strength of $\eta = 0.16\ \kappa$ is shown. It shows normal-mode splitting of about $2g/2\pi = 2 \times 9.5$ MHz, which we extract from a fit of a Voigt function to each normal mode. The measured coupling strength confirms that the system is in the single-atom strong-coupling regime of cavity QED. Since the atom can move axially and radially during the probing interval, it will see different polarizations of the repumper depending on its localization with respect to the repumper polarization pattern. This will lead to a changing atomic population in the $F = 1$ ground state Zeeman sublevels each time the atom is optically pumped. Moreover, there will be a nonzero probability for the atom to be

in a dark state if, for example, the atom is in a point in space where the repumper is σ^+-polarized and the atomic population is in the $F = 2, m_F = 2$ or vice versa. A full time-dependent model simulating the real experimental situation is beyond the scope of this thesis. However, in order to have a qualitative comparison with theory, we perform a theoretical calculation of the transmission spectra $T(g_0^{m_F})$ based on the steady-state solution of the master equation for each of the three $(F = 1, m_F) \rightarrow (F' = 2, m_{F'} = m_F + 1)$ transitions and their respective coupling strengths $g_0^{m_F}$. In the simulation we take only 80 % of the values of $g_0^{m_F}$ to account for te atomic motion. We assume an atom-cavity detuning of $\Delta_{ac}/2\pi = \pm 1$ MHz for the Zeeman sublevels $F = 1, m_F = \pm 1$, due to the differential Stark shift, and use the same driving strength used in the experiment $\eta = 0.16\ \kappa$. We then add the calculated spectra with a weighting coefficient as follows:

$$T(g_0^{m_F=-1,0,1}) = c_1 T(g_0^{m_F=-1}) + c_2 T(g_0^{m_F=0}) + c_3 T(g_0^{m_F=1}) + c_4 T_{EC} \qquad (5.1)$$

where $c_i, i = 1, 2, 3$ are the weighting coefficients for each transmission spectrum of the three Zeeman sublevels, and c_4 the weighting coefficient of the empty cavity spectrum T_{EC}, which would be the case if the atom is in a dark state for the repumper. We fit the data with the weighting coefficients as the only fit parameters. The solid red line in Fig. 5.1 shows the result with $(c_1, c_2, c_3, c_4) = (0.3, 0.3, 0.38, 0.02)$, which agrees pretty well with the measurement.

5.1.2. Single-atom cavity EIT in the strong coupling regime

So far, we have shown in the previous section that we achieved single-atom strong coupling in cavity QED using an open transition, a prerequisite for observing strongly coupled single-atom cavity EIT. Next, we demonstrate single-atom cavity EIT in the strong coupling regime and show how such a system can be used to optically tune the eigenstates of the system. To achieve this, we keep all experimental parameters the same as in the normal-mode spectroscopy measurement except of the repumper driving the $F = 2 \rightarrow F' = 1$ transition, which is replaced by a control field driving the $F = 2 \rightarrow F' = 2$ transition (see Fig. 4.1 (c)).

Figure 5.2 (a) shows the obtained cavity transmission spectra obtained for different control field Rabi frequencies Ω_c. Compared to the normal-mode spectrum shown in Fig. 5.1, we notice the appearance of an EIT transmission window at the empty cavity resonance. This window grows in amplitude to almost full transmission as the control field Rabi frequency is increased. Another remark concerns the normal-mode splitting which also grows as the control field Rabi frequency is enhanced as predicted by theory, with

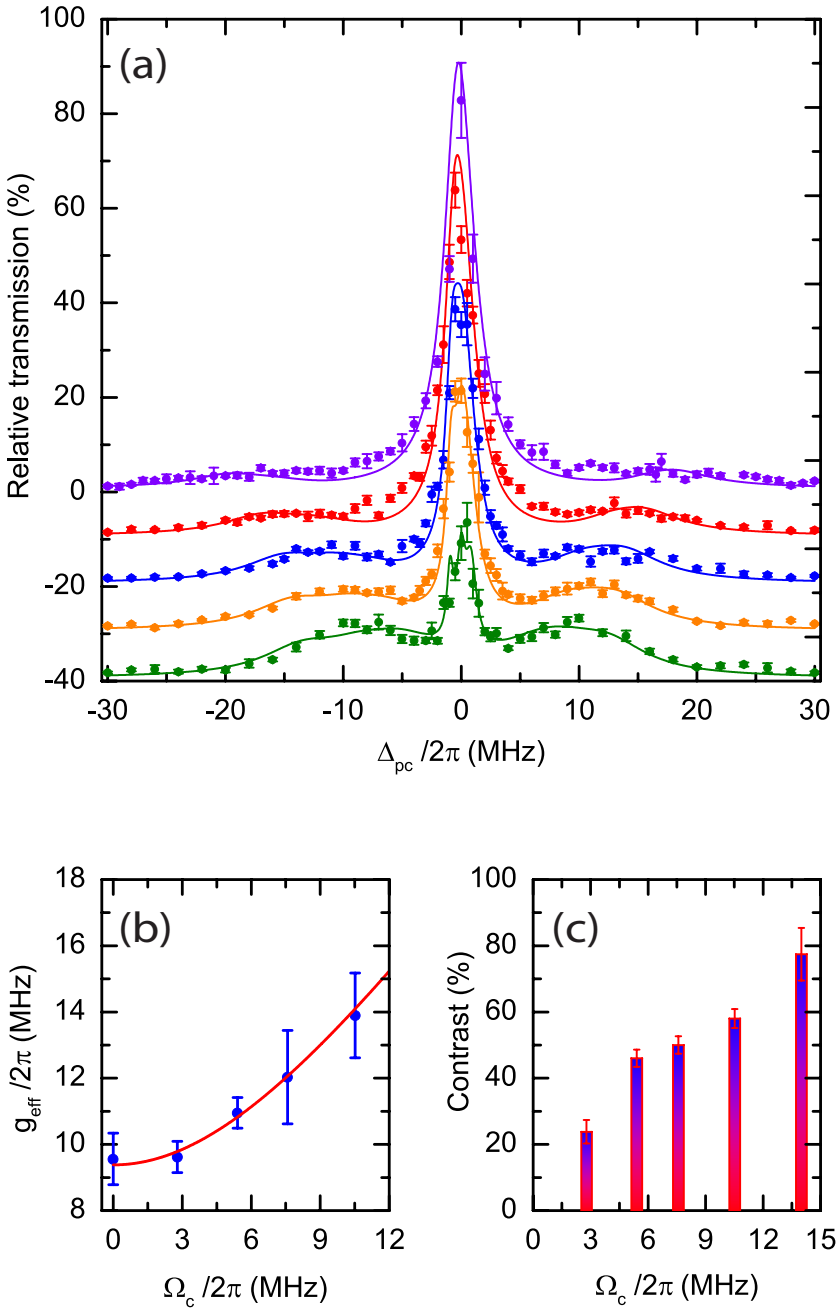

Figure 5.2.: (a) Single-atom cavity EIT transmission spectra for different control field Rabi frequencies (from top to bottom: $\Omega_c/2\pi$ =14 MHz, 10.5 MHz, 7.6 MHz, 5.4 MHz, 2.8 MHz with offsets of 0 %, -10%, -20 %, -30 %, -40% respectively for clarity) and for a driving strength of $\eta = 0.16\ \kappa$. The solid lines are theoretical fits based on the steady-state solution of the master equation for each Zeeman sublevel involved in the considered transition. Fit parameters are: $(c_1, c_2, c_3, c_4) = (0.3, 0.3, 0.4, 0)$ (see equation 5.1), Dephasing rate: $\gamma_{21}/2\pi = 0.2$ MHz. (b) The effective atom-cavity coupling $g_{eff}/2\pi$ is enhanced as the control Rabi frequency Ω_c/π is increased. (c) The on/off contrast of the single-atom transparency window at the empty cavity resonance increases with the control Rabi frequency to about 80 % for $\Omega_c/2\pi = 14$ MHz.

$2g^{(eff)} = 2\sqrt{g^2 + \Omega_c^2}$ (see Chapter 3). The theoretical simulations, showing excellent agreement with the data, are based on a similar model as the one used for the normal-mode spectroscopy in the previous section. However, here, it is based on the steady-state solution of the master equation of three single-atom cavity-EIT systems with three-level atoms with maximum coupling strengths $g_0^{\{m_F=-1,0,1\}}/2\pi = \{5.8, 9.2, 14.3\}$ MHz corresponding to the three Zeeman sublevels $F = 1, m_F = \{-1, 0, 1\}$. Also, the atomic motion will lead to fluctuations in the differential Stark shift of the ground states leading to a non negligible dephasing rate between the ground states estimated at: $\gamma_{21}/2\pi = 0.2$ MHz. Another source of dephasing is the magnetic field fluctuations observed by the atom.
Figure 5.2 (b) shows how the effective atom-cavity coupling $g_{eff}/2\pi$ follows a square root behavior with Ω_c^2 as predicted from theory: $g_{eff} = \sqrt{g^2 + \Omega_c}$ with $g/2\pi = 9.5$ MHz the atom-cavity coupling for $\Omega_c = 0$ (see Fig. 5.1). This confirms the optical control of the eigenstates of the system. The values of g_{eff} are again determined from a fit of a Voigt function to each of the normal modes for the respective control field Rabi frequency Ω_c. The error bars are standard errors obtained from the peak positions of the Voigt fit. g_{eff} for $\Omega_c/2\pi = 14$ MHz is not shown because for such a large value of the control Rabi frequency, the normal modes tend to vanish, leading to large error values in the fit. The dependence of the on/off contrast at the empty-cavity resonance on the control field is shown in Fig. 5.2 (c). It grows to about 80 % for a control field Rabi frequency of $\Omega_c/2\pi = 14$ MHz, which is unprecedented for a single emitter EIT medium [83, 82, 84].

5.2. Photon-photon correlations

In the previous section, we experimentally demonstrated that merging single-atom cavity QED with EIT in the strong coupling regime enables the optical control of the transmission of probe photons through the cavity and at the same time gives a possibility to tune the system resonances in the spectrum by simply varying the control field power. With these capabilities at hand, we show next the impact of these new features on the time-dependent second-order intensity correlation function $g^{(2)}(\tau)$ of the light transmitted through the single-atom cavity EIT system.

5.2.1. From photon blockade to two-photon gateway

For the measurements depicted in Fig. 5.3, the probe laser was detuned by $\Delta_{pc}/2\pi = -14$ MHz with respect to the cavity. This is to guarantee that it is red-detuned with respect to the normal mode even when the atom is at the Zeeman sublevel with the highest coupling strength $g_0^{m_F=1}/2\pi = 14.3$ MHz.

The driving strength was set to $\eta = 0.4\ \kappa$, which is still in the low driving regime but high enough to have relevant statistics. The measurements were performed in a similar way as in Fig. 4.3. Figure 5.3 (a) shows the result for a control Rabi frequency of $\Omega_c/2\pi = 4.3$ MHz, which results in an effective coupling strength of about $g_{eff}/2\pi = 10.5$ MHz.

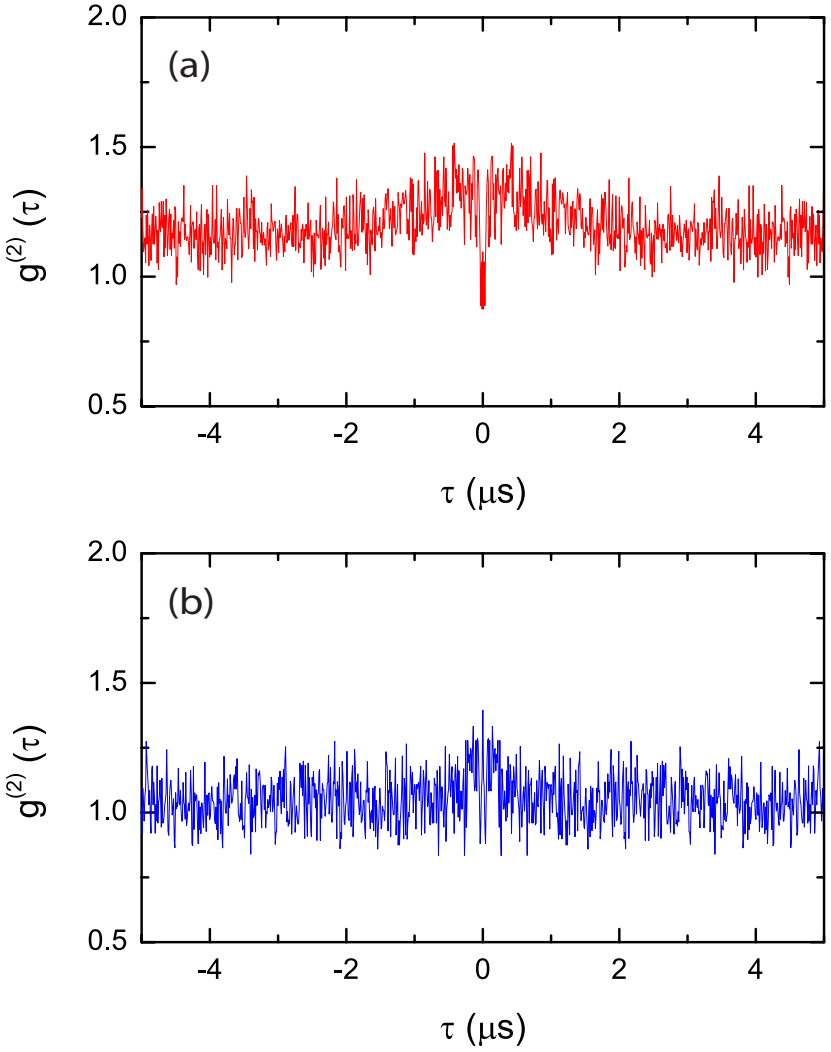

Figure 5.3.: (a) $g^{(2)}(\tau)$ over an interval of $\mid \tau \mid \leq 5\ \mu s$ for $\Omega_c/2\pi = 4.3$ MHz. The transmitted field exhibits photon anti-bunching and photon blockade. (b) $g^{(2)}(\tau)$ over an interval of $\mid \tau \mid \leq 5\ \mu s$ for $\Omega_c/2\pi = 12.3$ MHz. The transmitted field exhibits super-Poissonian photon statistics with $g^{(2)}(0) = (1.4 \pm 0.1) > 1$ due to a higher probability of photon pair emission. The binning time for both measurements is $\Delta t = 10$ ns.

We see that the second-order correlation function at $\tau = 0$ is smaller than its asymptotic values, which is an indication of a photon blockade effect and of

photon anti-bunching [85, 161, 162, 89, 22]. However, due to the atomic motion the photon distribution is super-Poissonian ($g^{(2)}(0) = (1.09 \pm 0.06) > 1$) and the asymptotic values are larger than 1 [163, 87, 89, 85, 164]. The values of $g^{(2)}(\tau)$ in the times $0.1\ \mu s \leq \mid \tau \mid \leq 2\ \mu s$ are larger than its values at later times due to the axial motion at a frequency of about $f_0 \simeq 125$ kHz (see Appendix A for details).
The observed photon anti-bunching in the $g^{(2)}(\tau)$ behavior is a result of the probe laser being near-resonant to the lower normal-mode thereby increasing the steady-state population in the $\left|\Psi_1^{(-)}\right\rangle$ state and thus the single photon emission probability (see Fig. 3.3), while suppressing the steady-state population in the $\left|\Psi_2^{(-)}\right\rangle$ state, much like the situation in a standard photon blockade from a Jaynes-Cummings system [85, 161].
Increasing the control field Rabi frequency to $\Omega_c/2\pi = 12.3$ MHz leads to an effective coupling strength of about $g_{eff}/2\pi = 15.5$ MHz. This would bring the probe laser frequency closer to the second manifold of the cavity EIT ladder and therefore increase the steady-state population in the eigenstate $\left|\Psi_2^{(-)}\right\rangle$, leading to a higher probability of photon pair emission in the transmitted field. Figure 5.3 (b) shows the resulting photon statistics, where we clearly see photon bunching with $g^{(2)}(0) = (1.4 \pm 0.1) > 1$ and $g^{(2)}(0) > g^{(2)}(\tau)$ for $\tau > 0$. The observed behavior is closely related to the two-photon gateway which was measured in our group with a standard two-level atom-cavity QED system [88].
A final remark concerning the measurements in Fig. 5.3, is that the steady-state value of $g^{(2)}(\tau)$ for $\tau > 2\ \mu s$ in Fig. 5.3 (a), with $g^{(2)}(\tau) \simeq 1.15$, is slightly larger than its counterpart in Fig. 5.3 (b), with $g^{(2)}(\tau) \simeq 1.05$. In fact by taking a closer look to the spectra shown in Fig. 5.2 (a), we see that the normal modes amplitude decreases for high control field Rabi frequencies. Therefore, a moving atom for small Ω_c values will induce larger intensity fluctuations than a moving atom for larger Ω_c. This explains why the steady-state value of $g^{(2)}(\tau)$ get closer to 1 for higher Ω_c.

5.2.2. A memory effect in the time-dependent second-order correlation function

We showed in the theoretical Chapter 3, that the time-dependent second-order correlation function $g^{(2)}(\tau)$ of a strongly coupled single-atom cavity EIT system can reveal a memory effect which is due to the long coherence times provided by EIT. This memory effect can lead to a quantum behavior of $g^{(2)}(\tau)$ which can last longer than the decay rates of the atom-cavity system, Γ_{31}, Γ_{32}, κ. Figure 5.4 (a) shows a measurement of $g^{(2)}(\tau)$ over an interval time of 500 ns with a probe-cavity detuning of $\Delta_{pc}/2\pi = -14$ MHz and for a control Rabi frequency of $\Omega_c/2\pi = 4$ MHz. We clearly see that the dynamics of the average photon number, $\langle a^\dagger a \rangle$, given by $g^{(2)}(\tau)$, is dominated by an

oscillation at exactly the probe-cavity detuning $\Delta_{pc}/2\pi$. This is a result of the new EIT field being generated at the empty cavity frequency beating with the impinging probe laser (see Chapter 3). The new field frequency is given by: $\omega_{newfield} = \omega_{probe} + \omega_{control} - (\omega_{control} + \Delta_{pc}) = \omega_{probe} - \Delta_{pc} = \omega_{cavity}$. To verify this, we perform a similar measurement at a different probe-cavity detuning Δ_{pc}. Figure 5.4 (b) depicts a $g^{(2)}(\tau)$ measurement with $\Delta_{pc}/2\pi = -12$ MHz over an interval time of 500 ns. It shows a beating pattern at 12 MHz confirming our understanding of the origin of this oscillatory behavior.

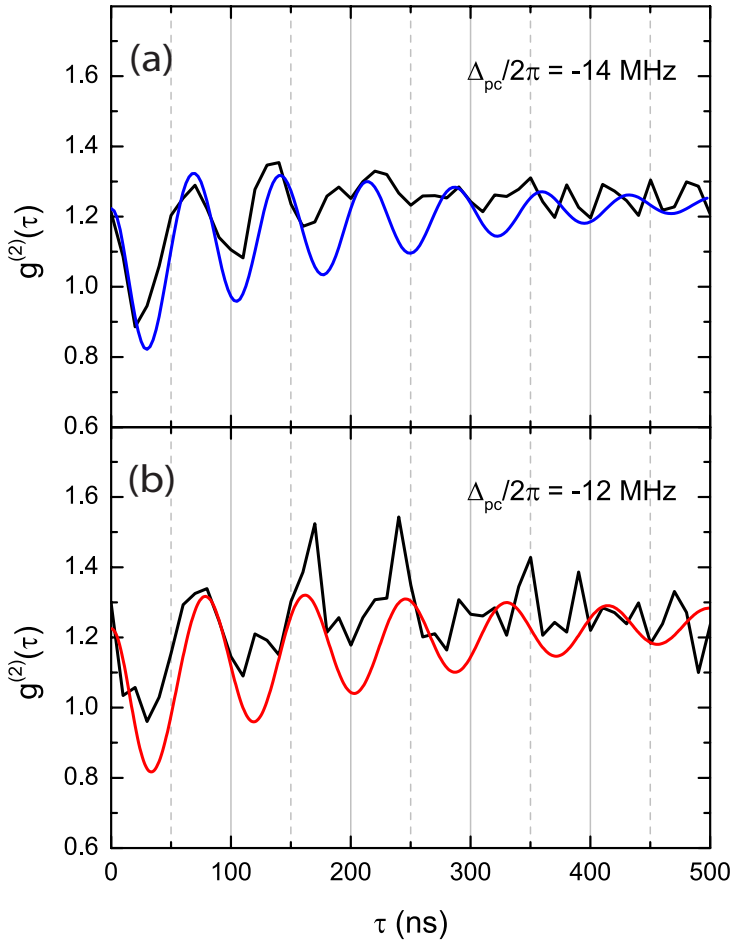

Figure 5.4.: (a) $g^{(2)}(\tau)$ at $\Delta_{pc}/2\pi = -14$ MHz and $\Omega_c/2\pi = 4$ MHz for the experiment (black solid line) and theory (blue solid line). (b) $g^{(2)}(\tau)$ at $\Delta_{pc}/2\pi = -12$ MHz and $\Omega_c/2\pi = 4.3$ MHz for the experiment (black solid line) and theory (red solid line). The theoretical fits have been scaled to match the asymptotic value of $g^{(2)}(\tau)$ in both measurements. The binning time for both measurements is $\Delta t = 10$ ns.

In both measurements we can directly notice that the observed oscillations have a longer coherence time than the dissipation rate of the system κ, Γ_{31} and

Γ_{32}. In fact by performing a Fourier transformation of the data, we find a width of $\delta = 0.8$ MHz corresponding to a decay time of 200 ns for the observed oscillations. This is more than a factor of 3 larger than the coherence time obtained with a usual two-level cavity QED system with similar parameters, where the relaxation time of the correlation function would be $2/(2\pi(\kappa+\gamma)) = 63$ ns. The observed decay time could in principle be enhanced by an order of magnitude by further cooling the atomic motion and reducing the dephasing between the ground states of the atom. The solid lines in Fig. 5.4 are theoretical calculations of the time-dependent second-order correlation function of a single-atom cavity EIT system with a three-level atom, with a dephasing between the ground states of $\gamma_{21}/2\pi = 0.2$ MHz and where the coupling strength g is a fit parameter via the weighting coefficients $(c_1, c_2, c_3, c_4) = (0.3, 0.55, 0.15, 0)$.
Unlike the results obtained in the numerical simulation in Fig. 3.8, where the non-classical behavior in the $g^{(2)}(\tau)$ could be prolonged in time by at least an order of magnitude beyond the dissipation rates of the system, we are limited in the experiment by our coupling strength $g/2\pi = 9.5$ MHz (see Fig. 5.1). Enhancing the coupling strength would in principle allow for the observation of a long lived photon blockade such as the one observed in Fig. 3.8 for $\Omega_c = 4\ \kappa$. Nevertheless, the observed oscillations in the $g^{(2)}(\tau)$ measurements, confirms that although we are limited by the coupling strength g and by the atomic motion, the coherence time of EIT is robust enough and lives beyond the decay times of both the cavity and the atom.

5.2.3. Time-dependent second-order correlations at the EIT resonance

Further insight into the quantum dynamics of the single-atom cavity EIT system can be gained by performing $g^{(2)}(\tau)$ measurements at the EIT resonance for different control field Rabi frequencies.

As mentioned before, since the dephasing rate of our cavity EIT system is non negligible ($\gamma_{21}/2\pi = 0.2$ MHz), the EIT window does not reach 100% of the empty cavity transmission (see Fig. 5.2), and the EIT amplitude will depend on the strength of the control field [115]. Moreover, the coherence of the EIT state depends on the dephasing γ_{21}. The higher the dephasing, the faster the decay of the EIT state. For a fixed dephasing rate, it is mainly the control field Rabi frequency Ω_c which determines how fast the system reaches the steady-state [165]. Larger values of Ω_c will lead the system to reach the steady-state faster. Fig. 5.5 shows measurements of $g^{(2)}(\tau)$ at the EIT resonance for different control field Rabi frequencies with $\Omega_c > \gamma_{21}$ for all measurements.
A first general remark for the three measurements is the disappearance of the oscillatory behavior observed in Fig. 5.4 which was due to the new EIT field beating with the probe field. The reason for this is that in Fig. 5.5, the probe field frequency is the same as the cavity frequency since we are sitting

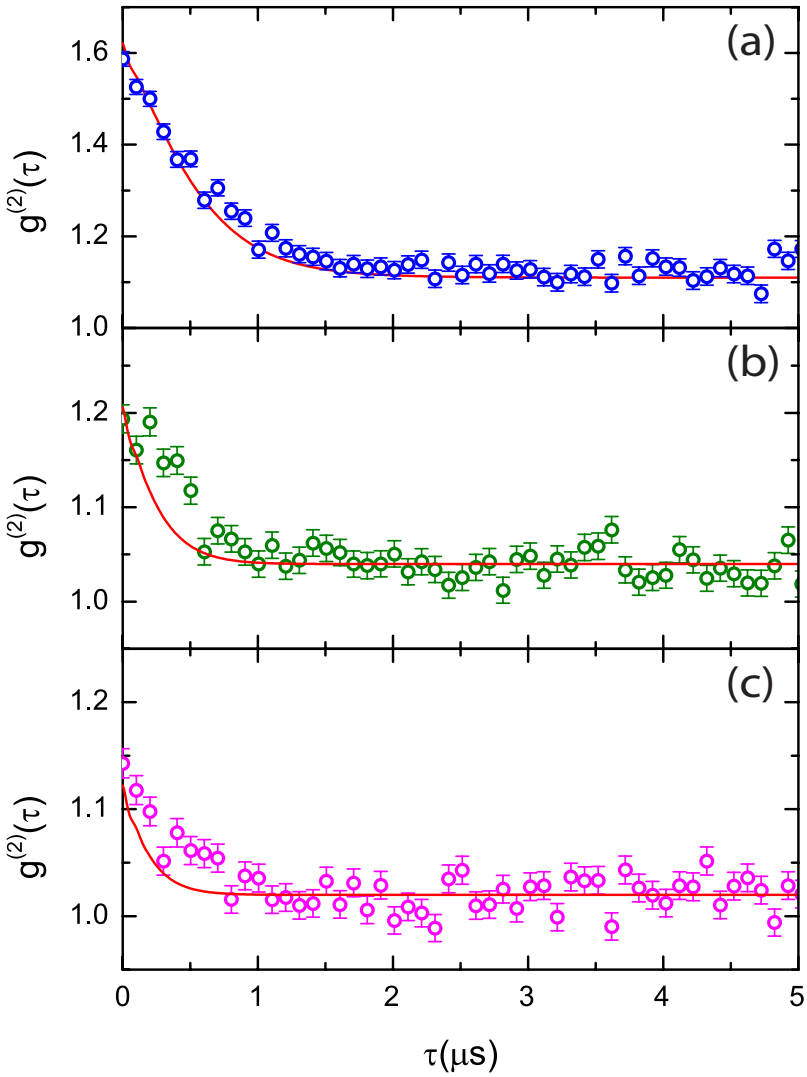

Figure 5.5.: $g^{(2)}(\tau)$ measurement at the EIT resonance ($\Delta_{pc} = 0$) with a driving strength of $\eta = 0.16\ \kappa$ and a control Rabi frequency of (a) $\Omega_c/2\pi = 3.3$ MHz (blue, ∘), (b) $\Omega_c/2\pi = 6$ MHz (green, ∘) and (c) $\Omega_c/2\pi = 7.5$ MHz (pink, ∘). The red solid lines are theoretical simulations where the coupling strength g via $(c_1, c_2, c_3, c_4) = (0.015, 0.96, 0.025, 0)$, the atom-cavity detuning $\Delta_{ac}/2\pi = 0.5$ MHz and the dephasing $\gamma_{21}/2\pi = 0.2$ MHz are the only fit parameters. The only parameter changed from one fit to the other is the corresponding control field Rabi frequency Ω_c. The binning time for all measurements is $\Delta t = 100$ ns.

at the EIT resonance. Moreover, all measurements show a value of $g^{(2)}(0) > 1$, whereas we know that EIT induces a coherent field to be transmitted through the cavity with $g^{(2)}(0) = 1$ as shown in Chapter 3. This can be explained by the non negligible dephasing rate γ_{21} which makes the system behave similarly to a cavity QED system with a two-level atom for short timescales and before

the control field enters into play.
We remind the reader that in a cavity QED system with a single two-level atom, $g^{(2)}(0)$ can reach very high values at the empty cavity frequency due to quantum interference between the probe field and the atomic polarization [138, 135]. Increasing the control field Rabi frequency Ω_c while keeping all other experimental parameters unchanged, brings the value of $g^{(2)}(0)$ closer to one, as large control field Rabi frequencies compensate for the dephasing γ_{21}. We can also notice that as Ω_c is increased, $g^{(2)}(\tau)$ reaches its steady-state faster. The steady-state value of $g^{(2)}(\tau)$ also depends on Ω_c. It gets closer to one for the highest value of Ω_c where the atom becomes more *transparent* to the probe field.

5.3. Conclusion and outlook

In conclusion, we experimentally demonstrated single-atom cavity EIT in the strong coupling regime. We showed that such system can be used to optically control the photon statistics of the transmitted field through the cavity. For the first time, we showed that a photon blockade behavior could be changed to a two-photon gateway behavior just by altering the control field power and this for the same input field frequency. The memory effect in the $g^{(2)}(\tau)$ which we theoretically predicted in Chapter 3 was experimentally observed, revealing the creation of a new field inside the cavity. Finally, the measurements of $g^{(2)}(\tau)$ at the EIT resonance show the dynamics of the EIT state. Our results represent a first step towards the realization of a cavity QED system based on an N-type level scheme where two atomic transitions are simultaneously strongly-coupled to two different cavity modes. Such a system, which requires EIT, would enable the optical control of the $g^{(2)}(\tau)$ behavior observed here, at the few photon level.

6. Slow Light with a Single Atom

So far, we showed in the previous chapters how EIT can be used to optically control the propagation of a cw laser field through an atom-cavity system. However, an EIT medium also provides the possibility of reducing the group velocity of a light pulse traveling through the medium. In this chapter we will show that by means of our single-atom cavity EIT system, light pulses can be delayed in time by about 200 ns. After an overview of slow light, we present briefly some theoretical aspects of slow light based on cavity EIT and later show the experimental results.

6.1. Overview of slow light

When going through a medium, a wave packet composed of different frequency components may travel at a different velocity than that of any of the individual waves making up the packet. Already at the beginning of the 20th century, Brillouin, in the context of his study of a periodic array of coupled harmonic oscillators, found solutions for the displacement of each oscillator in the form of waves propagating along the array [166]. Under the condition that the individual waves must not all propagate at the same speed, these waves could be added together to form solutions with a dramatically different propagation velocity, called group velocity. Since a pulse of light is a wave packet which is composed of an infinite number of monochromatic component waves, the group velocity gives the velocity at which light pulses propagate through a dispersive material. It is given by:

$$v_g = \frac{c}{n_g} = \frac{c}{n + \omega \frac{dn}{d\omega}} \tag{6.1}$$

where c is the speed of light in vacuum, n_g is the group index, ω the angular frequency of light and n is the refractive index of the material. One refers to light as being *slow* for $v_g << c$ or *fast* for $v_g > c$ or $v_g < 0$ [167]. By inspection of Eq. (6.1), we see that v_g may be largely reduced by finding a material with either a large refractive index n or a large derivative in the refractive index with respect to the optical frequency.
First experimental observations of slow light were performed in the context of the effect of self-induced transparency (SIT) in 1967 [168], where optical pulses were sent through cooled rods of ruby. Later, delayed pulses were measured in gases [169] and atomic vapors [170, 171] using the same effect. Later

experiments showed slow light based on the dispersion associated with electromagnetically induced transparency [124, 172, 73, 72, 77, 76, 173]. More recently, other resonances have been explored, including spectral hole burning [174], stimulated Raman scattering [175, 176], coherent population oscillations [177, 178, 179] and stimulated Brillouin scattering [180, 181, 182, 183].
All the aforementioned experiments were performed using highly dense atomic systems where a significantly large number of atoms interact with the optical pulse. To our knowledge, there has been no experiment where the delay induced by a single atom on a probe pulse is studied. We show next how our single-atom cavity EIT system can be used to enhance the dispersive properties of an individual atom resulting in a non negligible group delay on a propagating optical pulse.

6.2. Slow light in cavity EIT

The linear susceptibility $\chi^{(1)}(\omega_p)$ of a medium, describes its optical response when it is excited by a weak probe beam with an angular frequency ω_p. The imaginary part of the susceptibility, Im $\chi^{(1)}$, determines the absorption of the exciting probe beam, while the real part, Re $\chi^{(1)}$, determines the refractive index of the medium. Although considered as being intrinsically a macroscopic quantity, one may derive the linear susceptibility of a single-atom cavity EIT system using a semiclassical model [117, 184, 185]:

$$\chi^{(1)} = g^2 \frac{\Delta_{pc} - \Delta_{ac} + \Delta_{con} + i\gamma_{21}}{-(\Delta_{pc} - \Delta_{ac} + i\Gamma)(\Delta_{pc} - \Delta_{ac} + \Delta_{con} + i\gamma_{21}) + \frac{1}{4}\Omega_c^2} \tag{6.2}$$

where g is the coupling strength between the atom and the cavity field, Δ_{pc} is the probe-cavity detuning, Δ_{ac} is the atom-cavity detuning, Ω_c the control field Rabi frequency, Δ_{con} is the atom detuning from the control field, Γ is the decay rate of the atomic excited state to the two ground states and γ_{21} is the dephasing rate. Figure 6.1 shows the dependence of Im $\chi^{(1)}$ and Re $\chi^{(1)}$ on the probe cavity detuning Δ_{pc} for a single-atom cavity EIT system using a real set of parameters. We see that, at the EIT resonance, the narrow transparency window (Im $\chi^{(1)} = 0$) is accompanied by a very steep variation in Re $\chi^{(1)}$. This results in a large reduction of the group velocity v_g of light pulses traveling through the medium at the EIT resonance compared to vacuum speed of light c where:

$$v_g = \frac{c}{1 + \frac{g^2(\frac{\Omega_c^2}{4} - \gamma_{21}^2)}{2(\frac{\Omega_c^2}{4} + \Gamma\gamma_{21})^2}} \tag{6.3}$$

To have an idea about the expected delay in our system, we perform theoretical simulations following the Master equation approach for a time-dependent

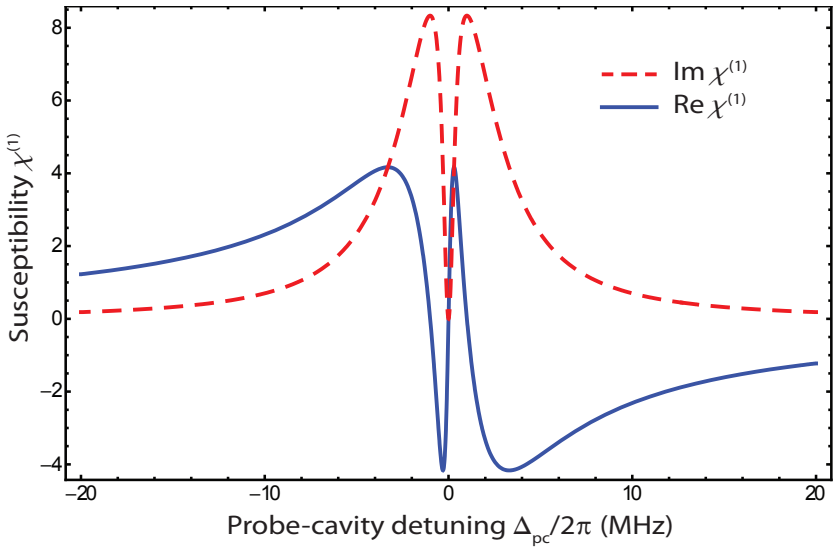

Figure 6.1.: Linear susceptibility $\chi^{(1)}$ of a three-level atom coupled with $g/2\pi = 5$ MHz to the mode of an optical cavity. Solid line: real part of $\chi^{(1)}$; dashed line: imaginary part of $\chi^{(1)}$. The control laser Rabi frequency and detuning are $\Omega_c/2\pi = 2$ MHz and $\Delta_{con} = 0$, respectively. The atom is put on resonance with the cavity: $\Delta_{ac} = 0$ and the dephasing rate is set to $\gamma_{21} = 0$. At $\Delta_{pc} = 0$, both Im $\chi^{(1)}$ and Re $\chi^{(1)}$ vanish due to EIT.

Hamiltonian. The difference now with respect to the method presented in Chapter 3 is that the driving field is time dependent $\eta(t)$ and corresponds to a Gaussian function with a variable width to simulate Gaussian laser pulses. Figure 6.2 shows numerical simulations for a pulse, containing on average 0.1 photons and of a duration of approximately 2 μs FWHM, traveling through a single-atom cavity EIT system for different values of the coupling strength g. The delay is defined as being the difference in time between the maximum of the input Gaussian pulse (empty cavity) and the maximum of the delayed pulse when the cavity contains a single atom. We notice that increasing g has mainly two consequences. First, it increases the delay as it reduces the group velocity v_g as can be predicted from Eq. 6.3. Second, it reduces the transmission intensity of the delayed pulse. This is due to the fact that increasing g, while keeping the control Rabi frequency constant, reduces the EIT linewidth (see Eq. 3.12 in Chapter 3). Therefore, the pulse duration would have to be increased in order to fit spectrally in the EIT window, otherwise only parts of it will be transmitted. It is also interesting to notice that although for the highest coupling strength, $g = 10\ \kappa$, the center of the pulse is delayed by about 450 ns, its back end is delayed by more than 1 μs. This is due to the increased EIT coherence time (or memory) for higher coupling strengths. A final remark is that the delayed pulse cannot be completely outside of the input pulse even for high values of g. Ideally, an optical delay line would delay optical pulses

by many pulse widths, however this is not possible when using a single atom as the delay medium. In fact, when a pulse enters the cavity, part of it will be instantaneously transmitted without interacting with the atom. This effect cannot be avoided even for high coupling strengths.

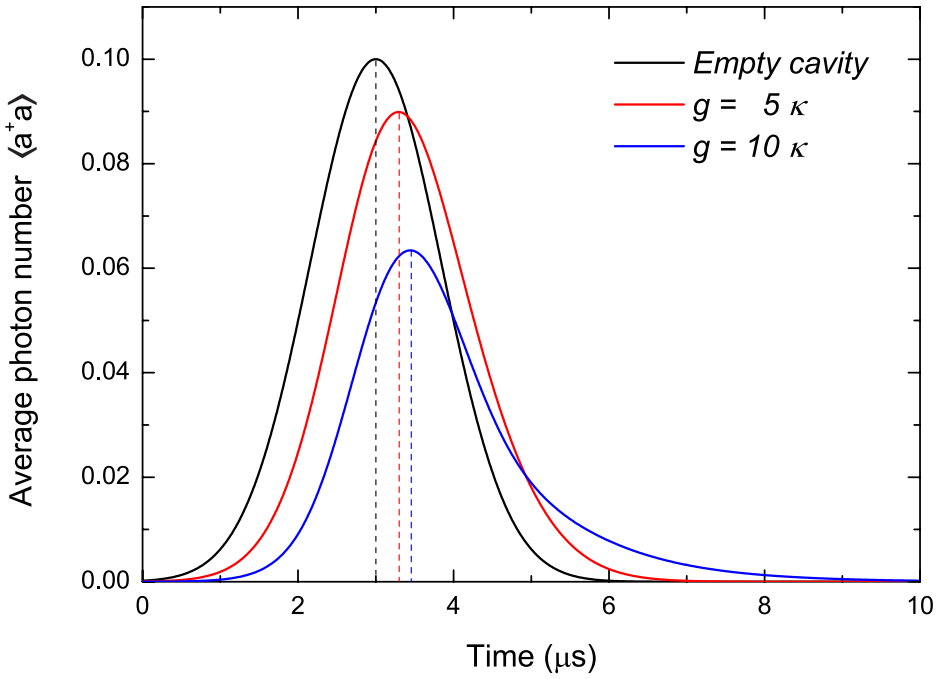

Figure 6.2.: Numerical simulations of delayed pulses traveling through a single-atom cavity EIT system for different values of the coupling strength g. The input pulse contains 0.1 photons on average and has a duration of approximately 2 μs FWHM. Control Rabi frequency $\Omega_c = 2\ \kappa$, dephasing $\gamma_{21} = 0$. The dashed lines indicate the maximum amplitude of the corresponding pulse.

As in the real experiment the dephasing rate γ_{21} cannot be neglected, we need to investigate its influence on the delayed pulses. Figure 6.3 shows numerical simulations with similar input pulse duration and photon number as in Fig. 6.2 and for different values of γ_{21}. We see that an increase in γ_{21} reduces both, the delay time and the transmitted intensity. Since increasing the dephasing reduces the coherence of the EIT state this is not unexpected. Moreover, we see that the dephasing has a strong influence on the back end of the delayed pulse. Even for values as small as $\gamma_{21} = 0.05\ \kappa$ (magenta curve in Fig 6.3) the back end of the pulse is almost within the input pulse (black curve) although the center of the pulse is delayed by about 250 ns. The reason for this is that since the EIT coherence time decreases for larger γ_{21}, the back end of the pulse will have smaller chances of being delayed. This also explains why the width of the delayed pulse is always smaller than the reference pulse except when $\gamma_{21} = 0$, where it is larger as explained by linear theory [186, 124], which

predicts that higher Fourier frequency components are attenuated, causing the probe pulse to lengthen.

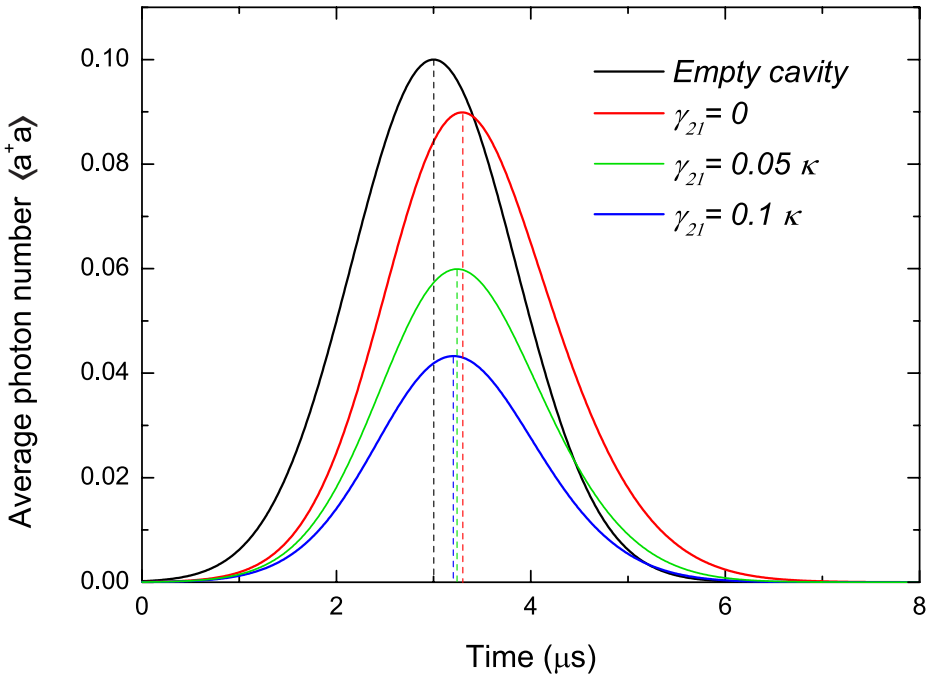

Figure 6.3.: Numerical simulations of delayed pulses traveling through a single-atom cavity EIT system for different values of the dephasing rate γ_{21}. The input pulse contains 0.1 photons on average and has a duration of approximately 2 μs FWHM. Control field Rabi frequency $\Omega_c = 2\ \kappa$, coupling strength $g = 5\ \kappa$. The dashed lines indicate the maximum amplitude of the corresponding pulse.

Next, we investigate the effect of the control field on the delayed pulses. Keeping the pulse duration and the photon number the same, we show in Fig. 6.4 numerical simulations for delayed pulses with different values of the control field Rabi frequency Ω_c. We see that increasing Ω_c induces a reduction in the delay as predicted from Eq. 6.3. Moreover, for $\Omega_c = 0.5\ \kappa$, the back end of the pulse is delayed by several microseconds due to the higher coherence of the EIT state. Finally, increasing Ω_c enhances the transmission intensity of the delayed pulses as it increases the width of the EIT window and therefore more Fourier components of the pulse can be transmitted.

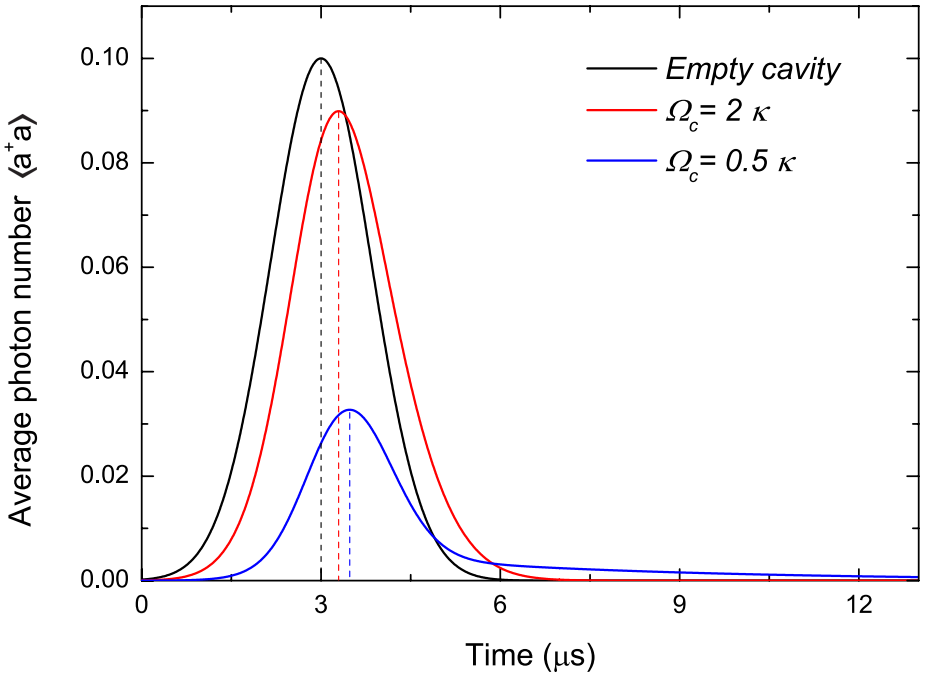

Figure 6.4.: Numerical simulations of delayed pulses traveling through a single-atom cavity EIT system for different values of the control field Rabi frequency Ω_c. The input pulse contains 0.1 photons on average and has a duration of approximately 2 μs FWHM. Coupling strength $g = 5\ \kappa$, dephasing $\gamma_{21} = 0$. The dashed lines indicate the maximum amplitude of the corresponding pulse.

Figure 6.5 shows a numerical simulation showing the expected delay for our system when optimizing the experimental parameters and for no dephasing ($\gamma_{21} = 0$). The average photon number in the pulse was decreased to 0.001 photons and the control field Rabi frequency to $\Omega_c = 0.65\ \kappa$. The pulse duration was increased to 10 μs FWHM in order to spectrally fit the EIT window. We see that the delay achieved is approximately 2 μs. If we consider our cavity length of $L_c = 200\ \mu$m, and our cavity finesse of $F = 195000$, the pulse should undergo $N = \frac{F}{2\pi}$ round trips in the cavity before leaving it [187]. However, the pulse length is too long (hundreds of meters) compared to the cavity length L_c. To estimate the delay predicted from Eq. 6.3, we consider that the EIT medium length is $L = \frac{F}{\pi} L_c$ as if the EIT medium is composed of a number of single-atom cavity EIT systems equal to two times the number of round trips of a pulse inside the cavity. With the experimental parameters used in Fig. 6.5 and from Eq. 6.3, we get $v_g \approx \frac{c}{107}$, resulting in a group delay of:

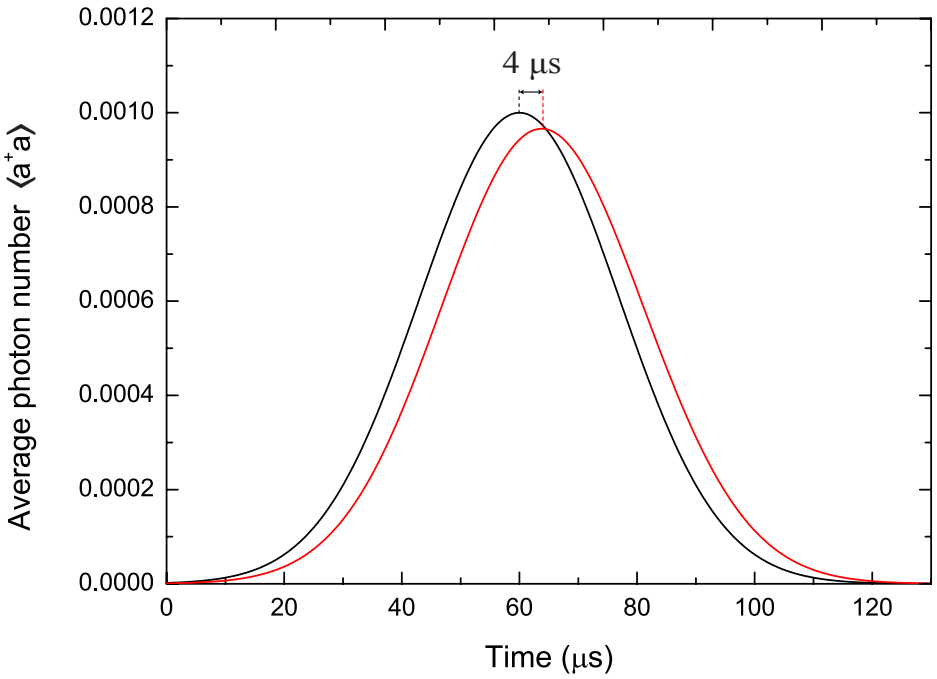

Figure 6.5.: A numerical simulations showing a delayed pulse traveling through a single-atom cavity EIT system for our best experimental parameters. The input pulse contains 0.001 photons on average and has a duration of 40 μs FWHM. Coupling strength $g = 4.75\ \kappa$, dephasing $\gamma_{21} = 0$, control field Rabi frequency $\Omega_c = 0.65\ \kappa$. The dashed lines indicate the maximum amplitude of the corresponding pulse.

$$\tau = (\frac{1}{v_g} - \frac{1}{c})\frac{F}{\pi}L_c \approx 4.3\ \mu s \tag{6.4}$$

which agrees pretty well with the delay observed in the numerical simulation shown in Fig. 6.5. Therefore, under weak excitation, the semiclassical model on which Eq. 6.3 is based, can predict the result of the full quantum model used in the simulation of Fig. 6.5.

6.3. Experimental results

The experiment is performed using the same experimental sequence as the one used for single-atom cavity EIT transmission spectra measurements (see Fig. 5.2) presented in Chapter 5, however, here, the probe beam is pulsed during the probing interval while the control field is constantly turned on. We use Gaussian light pulses with a duration of approximately 2 μs FWHM and measure the time delay by comparing the time arrival of the pulse when the cavity is empty with the time arrival of the pulse when the cavity contains a single atom which is strongly coupled to the cavity mode in EIT configuration. Figure 6.6 shows the measured light pulses versus time. The time delay of the

single-atom cavity EIT pulse relative to the reference pulse propagating in the empty cavity is determined by fitting the detected light pulses with a Gaussian function. We observe a probe pulse delay of 191 ± 5 ns and a transmission of $\sim 50\%$ of the incident pulse amplitude. The observed delay corresponds to a group velocity of approximately $v_g = \frac{c}{6}$ (see Equation 6.4). However, using our experimental parameters Eq. 6.3 gives $v_g \approx \frac{c}{24}$. This is due to the high photon number per pulse used in the experiment. Similar delay times have been observed in experiments involving many atoms in high-finesse cavities [188, 189], whereas here only a single atom is sufficient thanks to its strong coupling to the cavity mode. We find excellent agreement with theory, shown as solid lines in Fig. 6.6, when using real experimental parameters and a dephasing rate of $\gamma_{21}/2\pi = 0.1$ MHz. This is to our knowledge the first time that slow light is observed with a single emitter as the delaying medium.

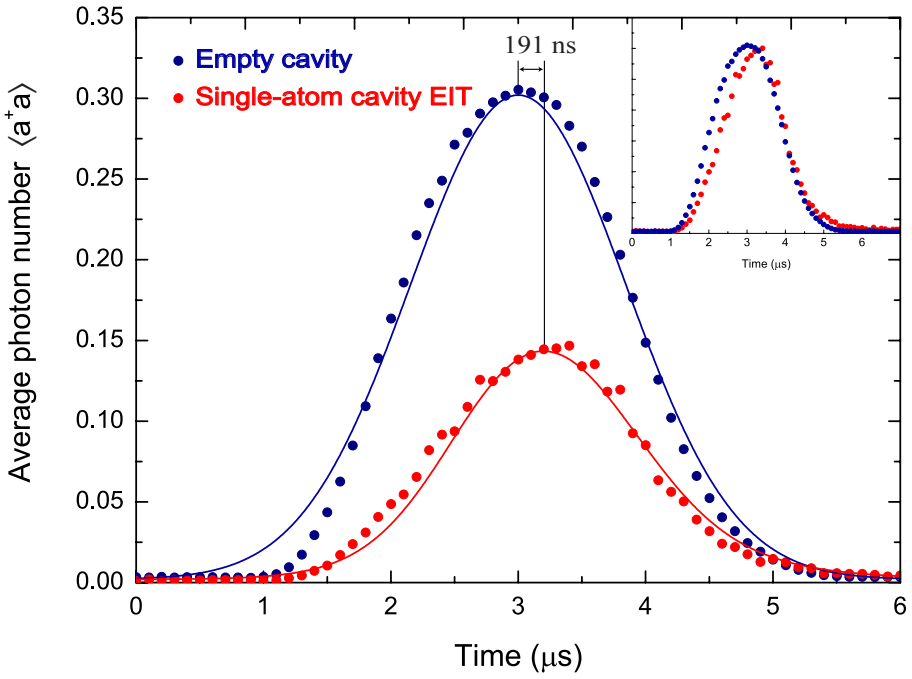

Figure 6.6.: Measurement of slow light with single-atom cavity EIT. A Gaussian probe pulse containing 0.3 photons on average with a duration of 2 μs FWHM, is delayed by 191 ± 5 ns with a transmitted intensity of about 50 % of the the incident pulse amplitude. The solid lines show theoretical simulations for a three-level atom in cavity EIT configuration using the following experimental parameters: $\Omega_c/2\pi = 2$ MHz, $g/2\pi = 9$ MHz, $\Delta_{pc} = \Delta_{ac} = \Delta_{con} = 0$, and $\gamma_{21}/2\pi = 100$ kHz. The inset shows the delayed pulse being rescaled by a factor of 2 for easier visualization of the group delay.

The dependence of the delayed pulses on the control field Rabi frequency Ω_c is shown in Fig. 6.7 which shows several measurements of delayed pulses with the same incident pulse duration and intensity and for different values of Ω_c. We notice that increasing Ω_c increases the transmitted pulse intensity at the expense of smaller delay times as expected from equation 6.3. The transmission increases from 30 % for $\Omega_c/2\pi = 2$ MHz to about 70 % for $\Omega_c/2\pi = 5.4$ MHz while the delay time is reduced from about 175 ns to 82 ns respectively. We find a good agreement between data and theory for all measurements. For the theoretical fits, all experimental parameters were kept constant and only Ω_c was varied from one measurement to the other as in the experiment.

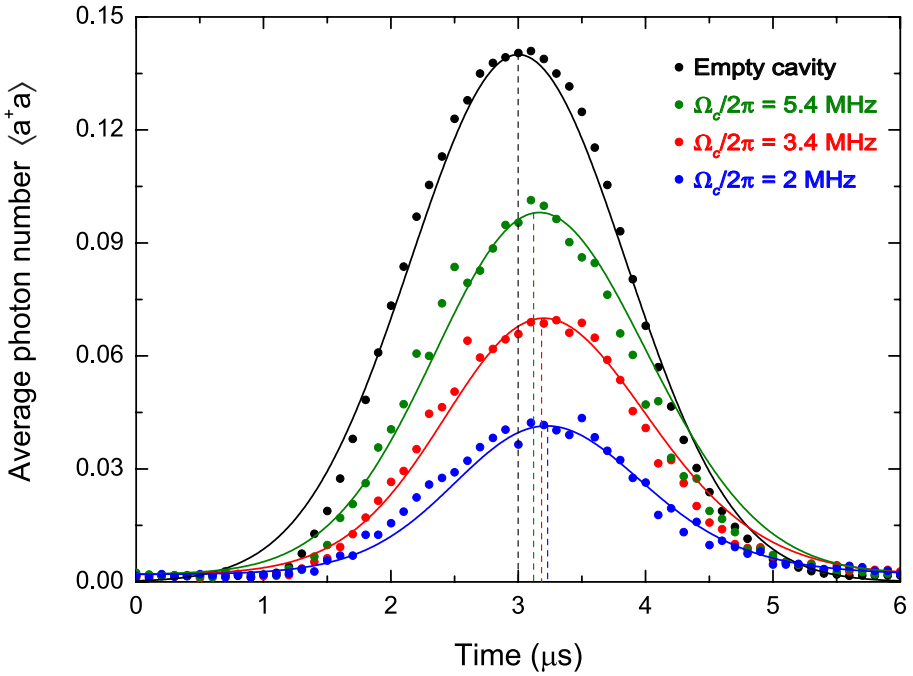

Figure 6.7.: Measurement of slow light with single-atom cavity EIT for different values of Ω_c. The impinging Gaussian probe pulse contains 0.14 photons on average with a duration of 2 μs FWHM. For $\Omega_c/2\pi = 2$ MHz (blue data points) the pulse is delayed by 175 ± 8 ns with a transmitted intensity of about 30 %. With $\Omega_c/2\pi = 3.4$ MHz (red data points) the pulse is delayed by 157 ± 6 ns with a transmitted intensity of about 50 %. Finally, $\Omega_c/2\pi = 5.4$ MHz (green data points) induces a delay of 82 ± 6 ns with a transmitted intensity of about 70 % The solid lines show theoretical simulations for a three-level atom in cavity EIT configuration using the following experimental parameters: $g/2\pi = 9$ MHz, $\Delta_{pc} = \Delta_{ac} = \Delta_{con} = 0$, and $\gamma_{21}/2\pi = 160$ kHz which were kept constant for all measurements. Only the corresponding control field Rabi frequency Ω_c was changed from one measurement to the other to fit the data.The dashed lines indicate the maximum amplitude of the corresponding pulse.

6.4. Conclusion and outlook

To conclude, we have shown both, theoretically and experimentally, that an optical pulse can be delayed using a single atom which is strongly coupled to a cavity mode in an EIT configuration. We discussed the main parameters which have a strong influence on the delay time. The observed group delay depends on the EIT resonance width, which depends mainly on the coupling strength g, the control field Rabi frequency Ω_c and the dephasing rate γ_{21}. In the experiment, the delay is limited by the large dephasing rate. In the future, this can be improved by cooling the atomic motion even further and by optically pumping the atom to the Zeeman sublevel $F = 1, m_F = 1$ with the highest coupling strength, before sending the probe pulse.

7. Conclusion and outlook

This thesis reported on the implementation of a strongly-coupled single-atom cavity EIT system. This system was investigated both theoretically and experimentally. All theoretical predictions were verified in the experiment. The successful combination of single-atom cavity QED in the strong-coupling regime with EIT enabled us to observe different new features. These include a record EIT on/off transmission contrast for a single emitter of 80 %, an optical tunability of the eigenstates of the system while still conserving the features of a standard cavity QED system with a two-level atom in the strong coupling regime, such as photon blockade and two-photon gateway. Furthermore, analyzing the time-dependent second order correlation function revealed the generation of a new field at the empty cavity frequency. The new field is an EIT-related field with a high coherence time. This results in a *memory* effect observed in the behavior of the correlation functions which can be used to extend the nonclassicality of the emitted fields from the cavity beyond the decay rates of the cavity EIT system. These findings pave the way towards the realization of a cavity QED system with a N-type level scheme where two atomic transitions are simultaneously strongly-coupled to two different longitudinal modes of the cavity. If realized, this system can exhibit large interactions between two optical beams at the level of individual photons [52, 111, 54], opening up a new regime in optics and in all-optical quantum information processing [113]. The high nonlinearity which would be provided at low light powers, where individual photons interact so strongly with one another, could improve the performance of classical nonlinear devices, enabling fast energy-efficient optical transistors that avoid Ohmic heating [190, 110], as well as other applications that rely on the generation and manipulation of non-classical light fields [191, 192]. Finally, the observed memory in the photon statistics of the emitted light fields could be used to engineer a quantum memory for nonclassical states [79, 145], or for quantum simulation with a cavity QED system [193].

In a second experiment, we demonstrated slow light using a single atom in the cavity as the EIT medium. We have used the fact that the atom is strongly coupled to the cavity mode to observe pulse delays of up to 200 ns. We saw that the decoherence of the EIT state, mainly characterized by the dephasing rate of the ground states, strongly limits the delay we observe in the experiment. A possible solution to this could be the implementation of a three-dimensional trapping scheme [194], which should reduce the atomic motion, the main cause

of dephasing in our measurements. In the future, we could implement a quantum state filter which can be employed to build a deterministic single-photon source [195]. The basic idea is that the group delay of the probe pulse is made quantum state dependent, using the fact that the observed group delays will be photon-number dependent. In such a scheme, the strong coupling of the atoms to the cavity mode in an EIT configuration achieved here, is a prerequisite.

A. Photon blockade with a two-level atom

We have shown theoretically in Chapter 3, and experimentally in Chapter 5 that a single-atom cavity EIT system in the strong coupling regime can be used to achieve photon blockade. However, the *standard* cavity QED system with a two-level atom strongly coupled to the cavity mode can also exhibit photon blockade as shown theoretically in Chapter 2.
To achieve this experimentally, we put our cavity on resonance with the $F = 2, m_F = +2 \rightarrow F = 3, m_F = +3$ transition of ^{87}Rb. We measure the time-dependent second-order correlation function $g^{(2)}(\tau)$ using the same experimental sequence as the one shown in Fig. 4.3. However, here, the probe laser is circularly polarized and is driving the closed $F = 2, m_F = +2$ to $F = 3, m_F = +3$ transition of ^{87}Rb. Moreover, a laser beam applied perpendicular to the cavity axis and driving the $F = 1 \rightarrow F' = 2$ transition serves as a repumper during the probing interval. In this configuration, a maximum coupling strength of $g_0/2\pi = 20$ MHz is expected for an atom placed at the center of the cavity mode, putting the system in the strong coupling regime.

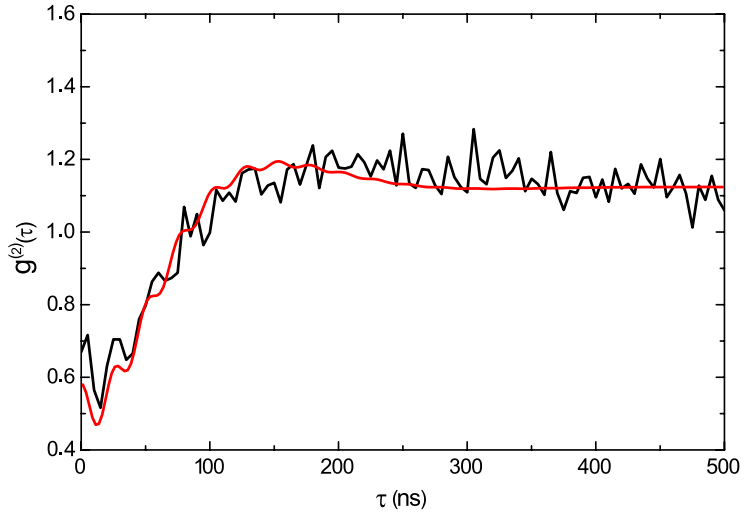

Figure A.1.: $g^{(2)}(\tau)$ at a probe-cavity detuning of $\Delta_{pc}/2\pi = -20$ MHz and a driving strength of $\eta = 0.4\ \kappa$ for the experiment (black solid line) and theory (red solid line). The fit parameters for the theoretical simulation are the coupling strength: $g/2\pi = 18$ MHz and the atom-cavity detuning: $\Delta_{ac}/2\pi = -2$ MHz. The binning time for the measurement is $\Delta t = 5$ ns.

Figure A.1 shows the experimental result of $g^{(2)}(\tau)$ for a probe-cavity detuning of $\Delta_{pc}/2\pi = -20$ MHz. We notice that $g^{(2)}(0) = 0.67 \pm 0.04$ is smaller than the asymptotic value of $g^{(2)}(\tau)$ of about 1.12 which indicates photon blockade. Since $g^{(2)}(0) < 1$, the transmitted field shows sub-Poissonian statistics. Moreover, the vacuum-Rabi oscillation with a period of about 25 ns is clearly visible. The theoretical simulation is scaled to match the asymptotic value of $g^{(2)}(\tau)$ which is larger than 1 due to the atomic motion.

Photon blockade using a strongly coupled cavity QED system with a two-level atom was already observed in the microwave regime [161], however, in the optical regime photon blockade was only measured using a multilevel atom [85]. Moreover, in our measurement of photon blockade, the incident probe field has the same polarization as the detected field contrary to the experiment in [85] where the two fields had orthogonal polarizations.

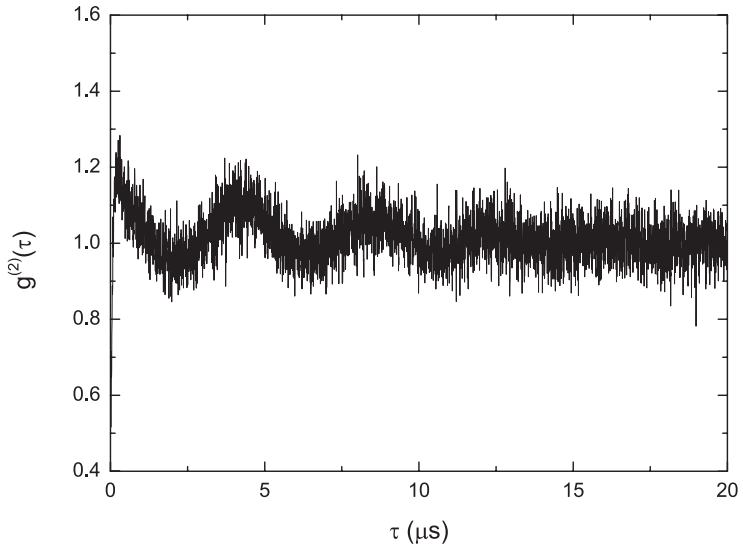

Figure A.2.: Zoom out of Fig. A.1 up to 20 μs. The axial motion of the atom inside the intracavity trap is clearly visible.

Figure A.2 shows a zoom out of Fig. A.1 up to 20 μs. It clearly shows a modulation of $g^{(2)}(\tau)$ at a period of about 4 μs. This modulation is due to the atomic motion along the cavity axis at half the oscillation frequency of $g^{(2)}(\tau)$, i.e. at a frequency of 125 kHz, which is in the same frequency range expected for the axial oscillation inside the intracavity trap depth of 150 μK used in the experiment.

Bibliography

[1] A. Ibn Al-Haytham, *Book of Optics*. Bagdad, 1021.

[2] M. Planck, "Über das Gesetz der Energieverteilung im Normalspectrum," *Annalen der Physik*, vol. 309, pp. 553–563, Jan. 1901.

[3] A. Einstein, "Über einen die Erzeugung und Verwandlung des Lichtes betreffenden heuristischen Gesichtspunkt," *Annalen der Physik*, vol. 322, pp. 132–148, Jan. 1905.

[4] E. Schrödinger, "Quantisierung als Eigenwertproblem," *Annalen der Physik*, vol. 386, pp. 109–139, Jan. 1926.

[5] S. S. Schweber, *QED and the Men who Made it: Dyson, Feynman, Schwinger, and Tomonaga*. Princeton University Press, 1994.

[6] V. Weisskopf and E. Wigner, "Berechnung der natürlichen Linienbreite auf Grund der Diracschen Lichttheorie," *Zeitschrift für Physik*, vol. 63, pp. 54–73, Jan. 1930.

[7] H. A. Bethe, "The Electromagnetic Shift of Energy Levels," *Physical Review*, vol. 72, pp. 339–341, Aug. 1947.

[8] W. E. Lamb and R. C. Retherford, "Fine Structure of the Hydrogen Atom by a Microwave Method," *Physical Review*, vol. 72, pp. 241–243, Aug. 1947.

[9] E. Jaynes and F. Cummings, "Comparison of quantum and semiclassical radiation theories with application to the beam maser," *Proceedings of the IEEE*, vol. 51, pp. 89–109, Jan. 1963.

[10] P. R. Berman, D. R. Bates, and B. Bederson, eds., *Cavity Quantum Electrodynamics*. Boston: Academic Press, 1st edition ed., Dec. 1993.

[11] G. Rempe, H. Walther, and N. Klein, "Observation of quantum collapse and revival in a one-atom maser," *Physical Review Letters*, vol. 58, pp. 353–356, Jan. 1987.

[12] M. Brune, F. Schmidt-Kaler, A. Maali, J. Dreyer, E. Hagley, J. M. Raimond, and S. Haroche, "Quantum Rabi Oscillation: A Direct Test of Field Quantization in a Cavity," *Physical Review Letters*, vol. 76, pp. 1800–1803, Mar. 1996.

[13] D. Meschede, H. Walther, and G. Mller, "One-Atom Maser," *Physical Review Letters*, vol. 54, pp. 551–554, Feb. 1985.

[14] K. B. Cooper, M. Steffen, R. McDermott, R. W. Simmonds, S. Oh, D. A. Hite, D. P. Pappas, and J. M. Martinis, "Observation of Quantum Oscillations between a Josephson Phase Qubit and a Microscopic Resonator Using Fast Readout," *Physical Review Letters*, vol. 93, p. 180401, Oct. 2004.

[15] A. Wallraff, D. I. Schuster, A. Blais, L. Frunzio, R.-S. Huang, J. Majer, S. Kumar, S. M. Girvin, and R. J. Schoelkopf, "Strong coupling of a single photon to a superconducting qubit using circuit quantum electrodynamics," *Nature*, vol. 431, pp. 162–167, Sept. 2004.

[16] I. Chiorescu, P. Bertet, K. Semba, Y. Nakamura, C. J. P. M. Harmans, and J. E. Mooij, "Coherent dynamics of a flux qubit coupled to a harmonic oscillator," *Nature*, vol. 431, pp. 159–162, Sept. 2004.

[17] F. Deppe, M. Mariantoni, E. P. Menzel, A. Marx, S. Saito, K. Kakuyanagi, H. Tanaka, T. Meno, K. Semba, H. Takayanagi, E. Solano, and R. Gross, "Two-photon probe of the JaynesCummings model and controlled symmetry breaking in circuit QED," *Nature Physics*, vol. 4, pp. 686–691, Sept. 2008.

[18] R. J. Thompson, G. Rempe, and H. J. Kimble, "Observation of normal-mode splitting for an atom in an optical cavity," *Physical Review Letters*, vol. 68, pp. 1132–1135, Feb. 1992.

[19] P. Maunz, T. Puppe, I. Schuster, N. Syassen, P. W. H. Pinkse, and G. Rempe, "Normal-Mode Spectroscopy of a Single-Bound-Atom-Cavity System," *Physical Review Letters*, vol. 94, p. 033002, Jan. 2005.

[20] A. Boca, R. Miller, K. M. Birnbaum, A. D. Boozer, J. McKeever, and H. J. Kimble, "Observation of the Vacuum Rabi Spectrum for One Trapped Atom," *Physical Review Letters*, vol. 93, p. 233603, Dec. 2004.

[21] R. Gehr, J. Volz, G. Dubois, T. Steinmetz, Y. Colombe, B. L. Lev, R. Long, J. Estève, and J. Reichel, "Cavity-Based Single Atom Preparation and High-Fidelity Hyperfine State Readout," *Physical Review Letters*, vol. 104, p. 203602, May 2010.

[22] D. J. Alton, N. P. Stern, T. Aoki, H. Lee, E. Ostby, K. J. Vahala, and H. J. Kimble, "Strong interactions of single atoms and photons near a dielectric boundary," *Nature Physics*, vol. 7, pp. 159–165, Feb. 2011.

[23] D. OShea, C. Junge, J. Volz, and A. Rauschenbeutel, "Fiber-Optical Switch Controlled by a Single Atom," *Physical Review Letters*, vol. 111, p. 193601, Nov. 2013.

[24] E. Peter, P. Senellart, D. Martrou, A. Lematre, J. Hours, J. M. Grard, and J. Bloch, "Exciton-Photon Strong-Coupling Regime for a Single Quantum Dot Embedded in a Microcavity," *Physical Review Letters*, vol. 95, p. 067401, Aug. 2005.

[25] J. P. Reithmaier, G. Sęk, A. Löffler, C. Hofmann, S. Kuhn, S. Reitzenstein, L. V. Keldysh, V. D. Kulakovskii, T. L. Reinecke, and A. Forchel, "Strong coupling in a single quantum dotsemiconductor microcavity system," *Nature*, vol. 432, pp. 197–200, Nov. 2004.

[26] A. Laucht, F. Hofbauer, N. Hauke, J. Angele, S. Stobbe, M. Kaniber, G. Bhm, P. Lodahl, M.-C. Amann, and J. J. Finley, "Electrical control of spontaneous emission and strong coupling for a single quantum dot," *New Journal of Physics*, vol. 11, no. 2, p. 023034, 2009.

[27] K. Hennessy, A. Badolato, M. Winger, D. Gerace, M. Atatüre, S. Gulde, S. Fält, E. L. Hu, and A. Imamoğlu, "Quantum nature of a strongly coupled single quantum dotcavity system," *Nature*, vol. 445, pp. 896–899, Feb. 2007.

[28] T. Yoshie, A. Scherer, J. Hendrickson, G. Khitrova, H. M. Gibbs, G. Rupper, C. Ell, O. B. Shchekin, and D. G. Deppe, "Vacuum Rabi splitting with a single quantum dot in a photonic crystal nanocavity," *Nature*, vol. 432, pp. 200–203, Nov. 2004.

[29] G. Nogues, A. Rauschenbeutel, S. Osnaghi, M. Brune, J. M. Raimond, and S. Haroche, "Seeing a single photon without destroying it," *Nature*, vol. 400, pp. 239–242, July 1999.

[30] C. Guerlin, J. Bernu, S. Deléglise, C. Sayrin, S. Gleyzes, S. Kuhr, M. Brune, J.-M. Raimond, and S. Haroche, "Progressive field-state collapse and quantum non-demolition photon counting," *Nature*, vol. 448, pp. 889–893, Aug. 2007.

[31] S. Gleyzes, S. Kuhr, C. Guerlin, J. Bernu, S. Deléglise, U. Busk Hoff, M. Brune, J.-M. Raimond, and S. Haroche, "Quantum jumps of light recording the birth and death of a photon in a cavity," *Nature*, vol. 446, pp. 297–300, Mar. 2007.

[32] J. Volz, R. Gehr, G. Dubois, J. Estève, and J. Reichel, "Measurement of the internal state of a single atom without energy exchange," *Nature*, vol. 475, pp. 210–213, July 2011.

[33] A. Reiserer, S. Ritter, and G. Rempe, "Nondestructive Detection of an Optical Photon," *Science*, vol. 342, pp. 1349–1351, Dec. 2013.

[34] W. P. Smith, J. E. Reiner, L. A. Orozco, S. Kuhr, and H. M. Wiseman, "Capture and Release of a Conditional State of a Cavity QED System by Quantum Feedback," *Physical Review Letters*, vol. 89, p. 133601, Sept. 2002.

[35] C. Sayrin, I. Dotsenko, X. Zhou, B. Peaudecerf, T. Rybarczyk, S. Gleyzes, P. Rouchon, M. Mirrahimi, H. Amini, M. Brune, J.-M. Raimond, and S. Haroche, "Real-time quantum feedback prepares and stabilizes photon number states," *Nature*, vol. 477, pp. 73–77, Sept. 2011.

[36] Q. A. Turchette, C. J. Hood, W. Lange, H. Mabuchi, and H. J. Kimble, "Measurement of Conditional Phase Shifts for Quantum Logic," *Physical Review Letters*, vol. 75, pp. 4710–4713, Dec. 1995.

[37] A. Reiserer, N. Kalb, G. Rempe, and S. Ritter, "A quantum gate between a flying optical photon and a single trapped atom," *Nature*, vol. 508, pp. 237–240, Apr. 2014.

[38] T. G. Tiecke, J. D. Thompson, N. P. de Leon, L. R. Liu, V. Vuletić, and M. D. Lukin, "Nanophotonic quantum phase switch with a single atom," *Nature*, vol. 508, pp. 241–244, Apr. 2014.

[39] A. Ourjoumtsev, A. Kubanek, M. Koch, C. Sames, P. W. H. Pinkse, G. Rempe, and K. Murr, "Observation of squeezed light from one atom excited with two photons," *Nature*, vol. 474, pp. 623–626, June 2011.

[40] T. Fischer, P. Maunz, P. W. H. Pinkse, T. Puppe, and G. Rempe, "Feedback on the Motion of a Single Atom in an Optical Cavity," *Physical Review Letters*, vol. 88, p. 163002, Apr. 2002.

[41] P. Maunz, T. Puppe, I. Schuster, N. Syassen, P. W. H. Pinkse, and G. Rempe, "Cavity cooling of a single atom," *Nature*, vol. 428, pp. 50–52, Mar. 2004.

[42] M. Wolke, J. Klinner, H. Keler, and A. Hemmerich, "Cavity Cooling Below the Recoil Limit," *Science*, vol. 337, pp. 75–78, July 2012.

[43] M. Koch, C. Sames, A. Kubanek, M. Apel, M. Balbach, A. Ourjoumtsev, P. W. H. Pinkse, and G. Rempe, "Feedback Cooling of a Single Neutral Atom," *Physical Review Letters*, vol. 105, p. 173003, Oct. 2010.

[44] A. Kubanek, M. Koch, C. Sames, A. Ourjoumtsev, P. W. H. Pinkse, K. Murr, and G. Rempe, "Photon-by-photon feedback control of a single-atom trajectory," *Nature*, vol. 462, pp. 898–901, Dec. 2009.

[45] S. E. Harris, "Electromagnetically Induced Transparency," *Physics Today*, vol. 50, pp. 36–42, July 1997.

[46] T. Hänsch, R. Keil, A. Schabert, C. Schmelzer, and P. Toschek, "Interaction of laser light waves by dynamic stark splitting," *Zeitschrift für Physik*, vol. 226, pp. 293–296, June 1969.

[47] G. Alzetta, A. Gozzini, L. Moi, and G. Orriols, "An experimental method for the observation of r.f. transitions and laser beat resonances in oriented Na vapour," *Il Nuovo Cimento B (1971-1996)*, vol. 36, pp. 5–20, Nov. 1976.

[48] E. Arimondo and G. Orriols, "Nonabsorbing atomic coherences by coherent two-photon transitions in a three-level optical pumping," *Lettere al Nuovo Cimento (1971-1985)*, vol. 17, pp. 333–338, Nov. 1976.

[49] K.-J. Boller, A. Imamoğlu, and S. E. Harris, "Observation of electromagnetically induced transparency," *Physical Review Letters*, vol. 66, pp. 2593–2596, May 1991.

[50] J. E. Field, K. H. Hahn, and S. E. Harris, "Observation of electromagnetically induced transparency in collisionally broadened lead vapor," *Physical Review Letters*, vol. 67, pp. 3062–3065, Nov. 1991.

[51] S. E. Harris, J. E. Field, and A. Imamolu, "Nonlinear optical processes using electromagnetically induced transparency," *Physical Review Letters*, vol. 64, pp. 1107–1110, Mar. 1990.

[52] H. Schmidt and A. Imamoglu, "Giant Kerr nonlinearities obtained by electromagnetically induced transparency," *Optics Letters*, vol. 21, pp. 1936–1938, Dec. 1996.

[53] A. Imamoğlu, H. Schmidt, G. Woods, and M. Deutsch, "Strongly Interacting Photons in a Nonlinear Cavity," *Physical Review Letters*, vol. 79, pp. 1467–1470, Aug. 1997.

[54] S. E. Harris and Y. Yamamoto, "Photon Switching by Quantum Interference," *Physical Review Letters*, vol. 81, pp. 3611–3614, Oct. 1998.

[55] S. Rebic, A. S. Parkins, and S. M. Tan, "Photon statistics of a single-atom intracavity system involving electromagnetically induced transparency," *Physical Review A*, vol. 65, p. 063804, May 2002.

[56] S. Rebic, S. M. Tan, A. S. Parkins, and D. F. Walls, "Large Kerr nonlinearity with a single atom," *Journal of Optics B: Quantum and Semiclassical Optics*, vol. 1, p. 490, Aug. 1999.

[57] M. D. Lukin and A. Imamoğlu, "Controlling photons using electromagnetically induced transparency," *Nature*, vol. 413, pp. 273–276, Sept. 2001.

[58] M. Bajcsy, S. Hofferberth, V. Balic, T. Peyronel, M. Hafezi, A. S. Zibrov, V. Vuletić, and M. D. Lukin, "Efficient All-Optical Switching Using Slow Light within a Hollow Fiber," *Physical Review Letters*, vol. 102, p. 203902, May 2009.

[59] W. Chen, K. M. Beck, R. Bücker, M. Gullans, M. D. Lukin, H. Tanji-Suzuki, and V. Vuletić, "All-Optical Switch and Transistor Gated by One Stored Photon," *Science*, vol. 341, pp. 768–770, Aug. 2013.

[60] M. D. Lukin, M. Fleischhauer, R. Cote, L. M. Duan, D. Jaksch, J. I. Cirac, and P. Zoller, "Dipole Blockade and Quantum Information Processing in Mesoscopic Atomic Ensembles," *Physical Review Letters*, vol. 87, p. 037901, June 2001.

[61] I. Friedler, D. Petrosyan, M. Fleischhauer, and G. Kurizki, "Long-range interactions and entanglement of slow single-photon pulses," *Physical Review A*, vol. 72, p. 043803, Oct. 2005.

[62] E. Shahmoon, G. Kurizki, M. Fleischhauer, and D. Petrosyan, "Strongly interacting photons in hollow-core waveguides," *Physical Review A*, vol. 83, p. 033806, Mar. 2011.

[63] A. V. Gorshkov, J. Otterbach, M. Fleischhauer, T. Pohl, and M. D. Lukin, "Photon-Photon Interactions via Rydberg Blockade," *Physical Review Letters*, vol. 107, p. 133602, Sept. 2011.

[64] D. Paredes-Barato and C. S. Adams, "All-Optical Quantum Information Processing Using Rydberg Gates," *Physical Review Letters*, vol. 112, p. 040501, Jan. 2014.

[65] J. Otterbach, M. Moos, D. Muth, and M. Fleischhauer, "Wigner Crystallization of Single Photons in Cold Rydberg Ensembles," *Physical Review Letters*, vol. 111, p. 113001, Sept. 2013.

[66] S. Sevinli, N. Henkel, C. Ates, and T. Pohl, "Nonlocal Nonlinear Optics in Cold Rydberg Gases," *Physical Review Letters*, vol. 107, p. 153001, Oct. 2011.

[67] G. Morigi, J. Eschner, and C. H. Keitel, "Ground State Laser Cooling Using Electromagnetically Induced Transparency," *Physical Review Letters*, vol. 85, pp. 4458–4461, Nov. 2000.

[68] G. Morigi, "Cooling atomic motion with quantum interference," *Physical Review A*, vol. 67, p. 033402, Mar. 2003.

[69] Y. Lin, J. P. Gaebler, T. R. Tan, R. Bowler, J. D. Jost, D. Leibfried, and D. J. Wineland, "Sympathetic Electromagnetically-Induced-Transparency Laser Cooling of Motional Modes in an Ion Chain," *Physical Review Letters*, vol. 110, p. 153002, Apr. 2013.

[70] T. Kampschulte, W. Alt, S. Manz, M. Martinez-Dorantes, R. Reimann, S. Yoon, D. Meschede, M. Bienert, and G. Morigi, "Electromagnetically-induced-transparency control of single-atom motion in an optical cavity," *Physical Review A*, vol. 89, p. 033404, Mar. 2014.

[71] E. Haller, J. Hudson, A. Kelly, D. A. Cotta, B. Peaudecerf, G. D. Bruce, and S. Kuhr, "Single-atom imaging of fermions in a quantum-gas microscope," *Nature Physics*, vol. 11, pp. 738–742, Sept. 2015.

[72] L. V. Hau, S. E. Harris, Z. Dutton, and C. H. Behroozi, "Light speed reduction to 17 metres per second in an ultracold atomic gas," *Nature*, vol. 397, pp. 594–598, Feb. 1999.

[73] D. Budker, D. F. Kimball, S. M. Rochester, and V. V. Yashchuk, "Nonlinear Magneto-optics and Reduced Group Velocity of Light in Atomic Vapor with Slow Ground State Relaxation," *Physical Review Letters*, vol. 83, pp. 1767–1770, Aug. 1999.

[74] A. H. Safavi-Naeini, T. P. M. Alegre, J. Chan, M. Eichenfield, M. Winger, Q. Lin, J. T. Hill, D. E. Chang, and O. Painter, "Electromagnetically induced transparency and slow light with optomechanics," *Nature*, vol. 472, pp. 69–73, Apr. 2011.

[75] X. Zhou, F. Hocke, A. Schliesser, A. Marx, H. Huebl, R. Gross, and T. J. Kippenberg, "Slowing, advancing and switching of microwave signals using circuit nanoelectromechanics," *Nature Physics*, vol. 9, pp. 179–184, Mar. 2013.

[76] C. Liu, Z. Dutton, C. H. Behroozi, and L. V. Hau, "Observation of coherent optical information storage in an atomic medium using halted light pulses," *Nature*, vol. 409, pp. 490–493, Jan. 2001.

[77] D. F. Phillips, A. Fleischhauer, A. Mair, R. L. Walsworth, and M. D. Lukin, "Storage of Light in Atomic Vapor," *Physical Review Letters*, vol. 86, pp. 783–786, Jan. 2001.

[78] D. Akamatsu, K. Akiba, and M. Kozuma, "Electromagnetically Induced Transparency with Squeezed Vacuum," *Physical Review Letters*, vol. 92, p. 203602, May 2004.

[79] J. Appel, E. Figueroa, D. Korystov, M. Lobino, and A. I. Lvovsky, "Quantum Memory for Squeezed Light," *Physical Review Letters*, vol. 100, p. 093602, Mar. 2008.

[80] K. Honda, D. Akamatsu, M. Arikawa, Y. Yokoi, K. Akiba, S. Nagatsuka, T. Tanimura, A. Furusawa, and M. Kozuma, "Storage and Retrieval of a Squeezed Vacuum," *Physical Review Letters*, vol. 100, p. 093601, Mar. 2008.

[81] M. Arikawa, K. Honda, D. Akamatsu, S. Nagatsuka, K. Akiba, A. Furusawa, and M. Kozuma, "Quantum memory of a squeezed vacuum for arbitrary frequency sidebands," *Physical Review A*, vol. 81, p. 021605, Feb. 2010.

[82] L. Slodička, G. Hétet, S. Gerber, M. Hennrich, and R. Blatt, "Electromagnetically Induced Transparency from a Single Atom in Free Space," *Physical Review Letters*, vol. 105, p. 153604, Oct. 2010.

[83] M. Mücke, E. Figueroa, J. Bochmann, C. Hahn, K. Murr, S. Ritter, C. J. Villas-Boas, and G. Rempe, "Electromagnetically induced transparency with single atoms in a cavity," *Nature*, vol. 465, pp. 755–758, June 2010.

[84] T. Kampschulte, W. Alt, S. Brakhane, M. Eckstein, R. Reimann, A. Widera, and D. Meschede, "Optical Control of the Refractive Index of a Single Atom," *Physical Review Letters*, vol. 105, p. 153603, Oct. 2010.

[85] K. M. Birnbaum, A. Boca, R. Miller, A. D. Boozer, T. E. Northup, and H. J. Kimble, "Photon blockade in an optical cavity with one trapped atom," *Nature*, vol. 436, pp. 87–90, July 2005.

[86] J. A. Souza, E. Figueroa, H. Chibani, C. J. Villas-Boas, and G. Rempe, "Coherent Control of Quantum Fluctuations Using Cavity Electromagnetically Induced Transparency," *Physical Review Letters*, vol. 111, p. 113602, Sept. 2013.

[87] G. Rempe, R. J. Thompson, R. J. Brecha, W. D. Lee, and H. J. Kimble, "Optical bistability and photon statistics in cavity quantum electrodynamics," *Physical Review Letters*, vol. 67, pp. 1727–1730, Sept. 1991.

[88] A. Kubanek, A. Ourjoumtsev, I. Schuster, M. Koch, P. W. H. Pinkse, K. Murr, and G. Rempe, "Two-Photon Gateway in One-Atom Cavity Quantum Electrodynamics," *Physical Review Letters*, vol. 101, p. 203602, Nov. 2008.

[89] B. Dayan, A. S. Parkins, T. Aoki, E. P. Ostby, K. J. Vahala, and H. J. Kimble, "A Photon Turnstile Dynamically Regulated by One Atom," *Science*, vol. 319, pp. 1062–1065, Feb. 2008.

[90] J. McKeever, A. Boca, A. D. Boozer, J. R. Buck, and H. J. Kimble, "Experimental realization of a one-atom laser in the regime of strong coupling," *Nature*, vol. 425, pp. 268–271, Sept. 2003.

[91] F. Dubin, C. Russo, H. G. Barros, A. Stute, C. Becher, P. O. Schmidt, and R. Blatt, "Quantum to classical transition in a single-ion laser," *Nature Physics*, vol. 6, pp. 350–353, May 2010.

[92] M. Koch, C. Sames, M. Balbach, H. Chibani, A. Kubanek, K. Murr, T. Wilk, and G. Rempe, "Three-Photon Correlations in a Strongly Driven Atom-Cavity System," *Physical Review Letters*, vol. 107, p. 023601, July 2011.

[93] H. Mabuchi and A. C. Doherty, "Cavity Quantum Electrodynamics: Coherence in Context," *Science*, vol. 298, pp. 1372–1377, Nov. 2002.

[94] J.-M. Raimond and J. Zinn-Justin, eds., *Fundamental Systems in Quantum Optics*. Amsterdam ; New York: North Holland, Jan. 1993.

[95] S. Ritter, C. Nölleke, C. Hahn, A. Reiserer, A. Neuzner, M. Uphoff, M. Mücke, E. Figueroa, J. Bochmann, and G. Rempe, "An elementary quantum network of single atoms in optical cavities," *Nature*, vol. 484, pp. 195–200, Apr. 2012.

[96] A. Reiserer and G. Rempe, "Cavity-based quantum networks with single atoms and optical photons," *arXiv:1412.2889 [quant-ph]*, Dec. 2014.

[97] H. Walther, B. T. H. Varcoe, B.-G. Englert, and T. Becker, "Cavity quantum electrodynamics," *Reports on Progress in Physics*, vol. 69, p. 1325, May 2006.

[98] D. F. Walls and G. J. Milburn, *Quantum Optics*. Berlin: Springer, 2nd ed. 2008 edition ed., Jan. 2008.

[99] H. J. Carmichael, *Statistical Methods in Quantum Optics*. Theoretical and Mathematical Physics, Berlin, Heidelberg: Springer, 2008.

[100] S. M. Dutra, *Cavity Quantum Electrodynamics: The Strange Theory of Light in a Box*. New York: Wiley-Interscience, 1 edition ed., Dec. 2004.

[101] S. Haroche and J.-M. Raimond, *Exploring the Quantum: Atoms, Cavities, and Photons*. Oxford University Press, 1 edition ed., Oct. 2006.

[102] P. Meystre and M. Sargent, eds., *Elements of Quantum Optics*. Springer Berlin Heidelberg, 2007.

[103] H. J. Carmichael, *An Open Systems Approach to Quantum Optics*, vol. 18 of *Lecture Notes in Physics Monographs*. Springer Berlin Heidelberg, 1993.

[104] C. Cohen-Tannoudji, J. Dupont-Roc, and G. Grynberg, *Atom-Photon Interactions: Basic Processes and Applications*. New York: Wiley-VCH, Mar. 1998.

[105] M. Lax, "Formal Theory of Quantum Fluctuations from a Driven State," *Physical Review*, vol. 129, pp. 2342–2348, Mar. 1963.

[106] R. J. Glauber, "Photon Correlations," *Physical Review Letters*, vol. 10, pp. 84–86, Feb. 1963.

[107] X. T. Zou and L. Mandel, "Photon-antibunching and sub-Poissonian photon statistics," *Physical Review A*, vol. 41, pp. 475–476, Jan. 1990.

[108] H. J. Kimble, M. Dagenais, and L. Mandel, "Photon Antibunching in Resonance Fluorescence," *Physical Review Letters*, vol. 39, pp. 691–695, Sept. 1977.

[109] M. Koch, *Classical and Quantum Dynamics of a Strongly Coupled Atom-Cavity System*. PhD thesis, Technische Universität München, 2011.

[110] D. E. Chang, V. Vuletić, and M. D. Lukin, "Quantum nonlinear optics photon by photon," *Nature Photonics*, vol. 8, pp. 685–694, Sept. 2014.

[111] S. E. Harris and L. V. Hau, "Nonlinear Optics at Low Light Levels," *Physical Review Letters*, vol. 82, pp. 4611–4614, June 1999.

[112] P. Grangier, D. F. Walls, and K. M. Gheri, "Comment on "Strongly Interacting Photons in a Nonlinear Cavity"," *Physical Review Letters*, vol. 81, pp. 2833–2833, Sept. 1998.

[113] H. J. Kimble, "The quantum internet," *Nature*, vol. 453, pp. 1023–1030, June 2008.

[114] S. E. Harris, "Electromagnetically Induced Transparency," *Physics Today*, vol. 50, pp. 36–42, Jan. 2008.

[115] M. Fleischhauer, A. Imamoğlu, and J. P. Marangos, "Electromagnetically induced transparency: Optics in coherent media," *Reviews of Modern Physics*, vol. 77, pp. 633–673, July 2005.

[116] M. Albert, A. Dantan, and M. Drewsen, "Cavity electromagnetically induced transparency and all-optical switching using ion Coulomb crystals," *Nature Photonics*, vol. 5, pp. 633–636, Oct. 2011.

[117] M. D. Lukin, "*Colloquium*: Trapping and manipulating photon states in atomic ensembles," *Reviews of Modern Physics*, vol. 75, pp. 457–472, Apr. 2003.

[118] E. Arimondo, *Progress in Optics*, vol. 35. Elsevier, Amsterdam, 1996.

[119] B. Julsgaard, J. Sherson, J. I. Cirac, J. Fiurášek, and E. S. Polzik, "Experimental demonstration of quantum memory for light," *Nature*, vol. 432, pp. 482–486, Nov. 2004.

[120] H. P. Specht, C. Nölleke, A. Reiserer, M. Uphoff, E. Figueroa, S. Ritter, and G. Rempe, "A single-atom quantum memory," *Nature*, vol. 473, pp. 190–193, May 2011.

[121] T. Chanelière, D. N. Matsukevich, S. D. Jenkins, S.-Y. Lan, T. a. B. Kennedy, and A. Kuzmich, "Storage and retrieval of single photons transmitted between remote quantum memories," *Nature*, vol. 438, pp. 833–836, Dec. 2005.

[122] K. Hammerer, K. Mølmer, E. S. Polzik, and J. I. Cirac, "Light-matter quantum interface," *Physical Review A*, vol. 70, p. 044304, Oct. 2004.

[123] M. Fleischhauer and M. D. Lukin, "Dark-State Polaritons in Electromagnetically Induced Transparency," *Physical Review Letters*, vol. 84, pp. 5094–5097, May 2000.

[124] A. Kasapi, M. Jain, G. Y. Yin, and S. E. Harris, "Electromagnetically Induced Transparency: Propagation Dynamics," *Physical Review Letters*, vol. 74, pp. 2447–2450, Mar. 1995.

[125] S. Baur, D. Tiarks, G. Rempe, and S. Dürr, "Single-Photon Switch Based on Rydberg Blockade," *Physical Review Letters*, vol. 112, p. 073901, Feb. 2014.

[126] D. A. Cardimona, P. M. Alsing, H. Mozer, and C. Rhodes, "Interference effects in a three-level atom in a cavity beyond the weak-field approximation," *Physical Review A*, vol. 79, p. 063817, June 2009.

[127] P. Bermel, A. Rodriguez, S. G. Johnson, J. D. Joannopoulos, and M. Soljačić, "Single-photon all-optical switching using waveguide-cavity quantum electrodynamics," *Physical Review A*, vol. 74, p. 043818, Oct. 2006.

[128] M. J. Werner and A. Imamoḡlu, "Photon-photon interactions in cavity electromagnetically induced transparency," *Physical Review A*, vol. 61, p. 011801, Dec. 1999.

[129] M. D. Lukin, M. Fleischhauer, M. O. Scully, and V. L. Velichansky, "Intracavity electromagnetically induced transparency," *Optics Letters*, vol. 23, p. 295, Feb. 1998.

[130] G. Hernandez, J. Zhang, and Y. Zhu, "Vacuum Rabi splitting and intracavity dark state in a cavity-atom system," *Physical Review A*, vol. 76, p. 053814, Nov. 2007.

[131] H. Wu, J. Gea-Banacloche, and M. Xiao, "Observation of Intracavity Electromagnetically Induced Transparency and Polariton Resonances in a Doppler-Broadened Medium," *Physical Review Letters*, vol. 100, p. 173602, May 2008.

[132] S. M. Tan, "A computational toolbox for quantum and atomic optics," *Journal of Optics B: Quantum and Semiclassical Optics*, vol. 1, p. 424, Aug. 1999.

[133] I. Schuster, A. Kubanek, A. Fuhrmanek, T. Puppe, P. W. H. Pinkse, K. Murr, and G. Rempe, "Nonlinear spectroscopy of photons bound to one atom," *Nature Physics*, vol. 4, pp. 382–385, May 2008.

[134] L. Tian and H. J. Carmichael, "Quantum trajectory simulations of two-state behavior in an optical cavity containing one atom," *Physical Review A*, vol. 46, pp. R6801–R6804, Dec. 1992.

[135] H. J. Carmichael, R. J. Brecha, and P. R. Rice, "Quantum interference and collapse of the wavefunction in cavity QED," *Optics Communications*, vol. 82, pp. 73–79, Apr. 1991.

[136] Y. Li and M. Xiao, "Enhancement of nondegenerate four-wave mixing based on electromagnetically induced transparency in rubidium atoms," *Optics Letters*, vol. 21, p. 1064, July 1996.

[137] M. D. Lukin, M. Fleischhauer, A. S. Zibrov, H. G. Robinson, V. L. Velichansky, L. Hollberg, and M. O. Scully, "Spectroscopy in Dense Coherent Media: Line Narrowing and Interference Effects," *Physical Review Letters*, vol. 79, pp. 2959–2962, Oct. 1997.

[138] R. J. Brecha, P. R. Rice, and M. Xiao, "N two-level atoms in a driven optical cavity: Quantum dynamics of forward photon scattering for weak incident fields," *Physical Review A*, vol. 59, pp. 2392–2417, Mar. 1999.

[139] J. P. Clemens and P. R. Rice, "Nonclassical effects of a driven atoms-cavity system in the presence of an arbitrary driving field and dephasing," *Physical Review A*, vol. 61, p. 063810, May 2000.

[140] S. L. Mielke, G. T. Foster, and L. A. Orozco, "Nonclassical Intensity Correlations in Cavity QED," *Physical Review Letters*, vol. 80, pp. 3948–3951, May 1998.

[141] M. J. Hartmann, F. G. S. L. Brando, and M. B. Plenio, "Strongly interacting polaritons in coupled arrays of cavities," *Nature Physics*, vol. 2, pp. 849–855, Dec. 2006.

[142] D. G. Angelakis, M. F. Santos, and S. Bose, "Photon-blockade-induced Mott transitions and XY spin models in coupled cavity arrays," *Physical Review A*, vol. 76, p. 031805, Sept. 2007.

[143] A. D. Greentree, C. Tahan, J. H. Cole, and L. C. L. Hollenberg, "Quantum phase transitions of light," *Nature Physics*, vol. 2, pp. 856–861, Dec. 2006.

[144] M. Schubert, I. Siemers, R. Blatt, W. Neuhauser, and P. E. Toschek, "Photon antibunching and non-Poissonian fluorescence of a single three-level ion," *Physical Review Letters*, vol. 68, pp. 3016–3019, May 1992.

[145] A. I. Lvovsky, B. C. Sanders, and W. Tittel, "Optical quantum memory," *Nature Photonics*, vol. 3, pp. 706–714, Dec. 2009.

[146] M. Lobino, C. Kupchak, E. Figueroa, and A. I. Lvovsky, "Memory for Light as a Quantum Process," *Physical Review Letters*, vol. 102, p. 203601, May 2009.

[147] D. A. Steck, *Rubidium-85 D-Line Data*. Los Alamos National Laboratory, 2010.

[148] D. A. Steck, *Rubidium-87 D-Line Data*. Los Alamos National Laboratory, 2010.

[149] C. Vo, *Ein kohrentes Logikgatter fr Lichtpulse basierend auf atomarer Vierwellenmischung in einem Bose-Einstein-Kondensat*. PhD thesis, Technische Universitt Mnchen, 2012.

[150] S. E. Baur, *A Single-Photon Switch and Transistor based on Rydberg Blockade*. PhD thesis, Technische Universitt Mnchen, 2015.

[151] G. Braunbeck, "Aufbau und charakterisierung eines phasen-stabilisierten laserpaars," Bachelor thesis, Technische Universität München, 2012.

[152] C. Sames, H. Chibani, C. Hamsen, P. Altin, T. Wilk, and G. Rempe, "Antiresonance Phase Shift in Strongly Coupled Cavity QED," *Physical Review Letters*, vol. 112, p. 043601, Jan. 2014.

[153] S. Nußmann, K. Murr, M. Hijlkema, B. Weber, A. Kuhn, and G. Rempe, "Vacuum-stimulated cooling of single atoms in three dimensions," *Nature Physics*, vol. 1, pp. 122–125, Nov. 2005.

[154] K. Murr, S. Nußmann, T. Puppe, M. Hijlkema, B. Weber, S. C. Webster, A. Kuhn, and G. Rempe, "Three-dimensional cavity cooling and trapping in an optical lattice," *Physical Review A*, vol. 73, p. 063415, June 2006.

[155] I. C. Tietje, "Localisation of a single atom inside an optical cavity," Master thesis, Technische Universität Berlin, 2014.

[156] R. Hanbury Brown and R. Q. Twiss, "Correlation between Photons in two Coherent Beams of Light," *Nature*, vol. 177, pp. 27–29, Jan. 1956.

[157] P. Maunz, *Cavity cooling and spectroscopy of a bound atom-cavity system.* PhD thesis, Technische Universität München, 2004.

[158] Y. Zhu, D. J. Gauthier, S. E. Morin, Q. Wu, H. J. Carmichael, and T. W. Mossberg, "Vacuum Rabi splitting as a feature of linear-dispersion theory: Analysis and experimental observations," *Physical Review Letters*, vol. 64, pp. 2499–2502, May 1990.

[159] J. J. Childs, K. An, M. S. Otteson, R. R. Dasari, and M. S. Feld, "Normal-Mode Line Shapes for Atoms in Standing-Wave Optical Resonators," *Physical Review Letters*, vol. 77, pp. 2901–2904, Sept. 1996.

[160] P. Münstermann, T. Fischer, P. Maunz, P. W. H. Pinkse, and G. Rempe, "Observation of Cavity-Mediated Long-Range Light Forces between Strongly Coupled Atoms," *Physical Review Letters*, vol. 84, pp. 4068–4071, May 2000.

[161] C. Lang, D. Bozyigit, C. Eichler, L. Steffen, J. M. Fink, A. A. Abdumalikov, M. Baur, S. Filipp, M. P. da Silva, A. Blais, and A. Wallraff, "Observation of Resonant Photon Blockade at Microwave Frequencies Using Correlation Function Measurements," *Physical Review Letters*, vol. 106, p. 243601, June 2011.

[162] A. Faraon, I. Fushman, D. Englund, N. Stoltz, P. Petroff, and J. Vučković, "Coherent generation of non-classical light on a chip via photon-induced tunnelling and blockade," *Nature Physics*, vol. 4, pp. 859–863, Nov. 2008.

[163] P. Münstermann, T. Fischer, P. W. H. Pinkse, and G. Rempe, "Single slow atoms from an atomic fountain observed in a high-finesse optical cavity," *Optics Communications*, vol. 159, pp. 63–67, Jan. 1999.

[164] M. B. Plenio and P. L. Knight, "The quantum-jump approach to dissipative dynamics in quantum optics," *Reviews of Modern Physics*, vol. 70, pp. 101–144, Jan. 1998.

[165] Y.-q. Li and M. Xiao, "Transient properties of an electromagnetically induced transparency in three-level atoms," *Optics Letters*, vol. 20, p. 1489, July 1995.

[166] L. Brillouin, *Wave Propagation and Group Velocity*. Academic Press, Jan. 1960.

[167] R. W. Boyd and D. J. Gauthier, "Controlling the Velocity of Light Pulses," *Science*, vol. 326, pp. 1074–1077, Nov. 2009.

[168] S. L. McCall and E. L. Hahn, "Self-Induced Transparency by Pulsed Coherent Light," *Physical Review Letters*, vol. 18, pp. 908–911, May 1967.

[169] C. K. N. Patel and R. E. Slusher, "Self-Induced Transparency in Gases," *Physical Review Letters*, vol. 19, pp. 1019–1022, Oct. 1967.

[170] D. J. Bradley, G. M. Gale, and P. D. Smith, "Self-induced Transparency and Dispersion Delays in Potassium Vapour," *Nature*, vol. 225, pp. 719–721, Feb. 1970.

[171] R. E. Slusher and H. M. Gibbs, "Self-Induced Transparency in Atomic Rubidium," *Physical Review A*, vol. 5, pp. 1634–1659, Apr. 1972.

[172] M. M. Kash, V. A. Sautenkov, A. S. Zibrov, L. Hollberg, G. R. Welch, M. D. Lukin, Y. Rostovtsev, E. S. Fry, and M. O. Scully, "Ultraslow Group Velocity and Enhanced Nonlinear Optical Effects in a Coherently Driven Hot Atomic Gas," *Physical Review Letters*, vol. 82, pp. 5229–5232, June 1999.

[173] A. V. Turukhin, V. S. Sudarshanam, M. S. Shahriar, J. A. Musser, B. S. Ham, and P. R. Hemmer, "Observation of Ultraslow and Stored Light Pulses in a Solid," *Physical Review Letters*, vol. 88, p. 023602, Dec. 2001.

[174] R. M. Camacho, M. V. Pack, and J. C. Howell, "Slow light with large fractional delays by spectral hole-burning in rubidium vapor," *Physical Review A*, vol. 74, p. 033801, Sept. 2006.

[175] J. E. Sharping, Y. Okawachi, and A. L. Gaeta, "Wide bandwidth slow light using a Raman fiber amplifier," *Optics Express*, vol. 13, no. 16, p. 6092, 2005.

[176] D. Dahan and G. Eisenstein, "Tunable all optical delay via slow and fast light propagation in a Raman assisted fiber optical parametric amplifier: a route to all optical buffering," *Optics Express*, vol. 13, no. 16, p. 6234, 2005.

[177] M. S. Bigelow, N. N. Lepeshkin, and R. W. Boyd, "Superluminal and Slow Light Propagation in a Room-Temperature Solid," *Science*, vol. 301, pp. 200–202, July 2003.

[178] X. Zhao, P. Palinginis, B. Pesala, C. J. Chang-Hasnain, and P. Hemmer, "Tunable ultraslow light in vertical-cavity surface-emitting laser amplifier," *Optics Express*, vol. 13, no. 20, p. 7899, 2005.

[179] P. Palinginis, F. Sedgwick, S. Crankshaw, M. Moewe, and C. J. Chang-Hasnain, "Room temperature slow light in a quantum-well waveguide via coherent population oscillation," *Optics Express*, vol. 13, no. 24, p. 9909, 2005.

[180] K. Y. Song, M. G. Herrez, and L. Thévenaz, "Long optically controlled delays in optical fibers," *Optics Letters*, vol. 30, p. 1782, July 2005.

[181] Y. Okawachi, M. S. Bigelow, J. E. Sharping, Z. Zhu, A. Schweinsberg, D. J. Gauthier, R. W. Boyd, and A. L. Gaeta, "Tunable All-Optical Delays via Brillouin Slow Light in an Optical Fiber," *Physical Review Letters*, vol. 94, p. 153902, Apr. 2005.

[182] M. González-Herráez, K.-Y. Song, and L. Thévenaz, "Optically controlled slow and fast light in optical fibers using stimulated Brillouin scattering," *Applied Physics Letters*, vol. 87, p. 081113, Aug. 2005.

[183] M. González Herráez, K. Y. Song, and L. Thévenaz, "Arbitrary-bandwidth Brillouin slow light in optical fibers," *Optics Express*, vol. 14, no. 4, p. 1395, 2006.

[184] M. Mücke, *Elektromagnetisch induzierte Transparenz mit einem einzelnen Atom*. PhD thesis, Technische Universität München, 2011.

[185] T. Kampschulte, *Coherently driven three-level atoms in an optical cavity*. PhD thesis, Universität Bonn, 2011.

[186] S. E. Harris, J. E. Field, and A. Kasapi, "Dispersive properties of electromagnetically induced transparency," *Physical Review A*, vol. 46, pp. R29–R32, July 1992.

[187] D. Kleckner, W. Marshall, M. J. A. de Dood, K. N. Dinyari, B.-J. Pors, W. T. M. Irvine, and D. Bouwmeester, "High Finesse Opto-Mechanical Cavity with a Movable Thirty-Micron-Size Mirror," *Physical Review Letters*, vol. 96, p. 173901, May 2006.

[188] J. Zhang, G. Hernandez, and Y. Zhu, "Slow light with cavity electromagnetically induced transparency," *Optics Letters*, vol. 33, no. 1, p. 46, 2008.

[189] Y. Shimizu, N. Shiokawa, N. Yamamoto, M. Kozuma, T. Kuga, L. Deng, and E. W. Hagley, "Control of Light Pulse Propagation with Only a Few Cold Atoms in a High-Finesse Microcavity," *Physical Review Letters*, vol. 89, p. 233001, Nov. 2002.

[190] D. A. B. Miller, "Are optical transistors the logical next step?," *Nature Photonics*, vol. 4, pp. 3–5, Jan. 2010.

[191] A. Muthukrishnan, M. O. Scully, and M. S. Zubairy, "Quantum microscopy using photon correlations," *Journal of Optics B: Quantum and Semiclassical Optics*, vol. 6, no. 6, p. S575, 2004.

[192] V. Giovannetti, S. Lloyd, and L. Maccone, "Advances in quantum metrology," *Nature Photonics*, vol. 5, pp. 222–229, Apr. 2011.

[193] S. Barrett, K. Hammerer, S. Harrison, T. E. Northup, and T. J. Osborne, "Simulating Quantum Fields with Cavity QED," *Physical Review Letters*, vol. 110, p. 090501, Feb. 2013.

[194] A. Reiserer, C. Nölleke, S. Ritter, and G. Rempe, "Ground-State Cooling of a Single Atom at the Center of an Optical Cavity," *Physical Review Letters*, vol. 110, p. 223003, May 2013.

[195] G. Nikoghosyan and M. Fleischhauer, "Photon-Number Selective Group Delay in Cavity Induced Transparency," *Physical Review Letters*, vol. 105, p. 013601, June 2010.

Acknowledgments

First and foremost, all praise is due to Allah for his assistance and help, without him the work performed in this thesis would have been impossible. To my parents, your support was vital and essential during my whole academic career. I would also like to thank you for helping me make the right decisions at the right time and I hope that you are satisfied with the results of your education. To my brother and sister, I thank you for your support, encouragement and for your precious advice. To my wife, thank you for being all the time optimistic and supportive even in quiet difficult situations.

For my academic development, I am deeply thankful to my advisor Gerhard Rempe for his constant support during all the years I spent at MPQ. I really appreciated the discussions I had with Gerhard during my whole thesis and I would also like to thank him for the confidence he had in giving me the freedom to choose which experiment to perform. I thank Tatjana Wilk for being the supervisor of the *Cavies* experiments and for carefully proof-reading my thesis.

I would like to thank my predecessors Markus Koch and Christian Sames for introducing me to the field of cavity QED and to the experimental apparatus. Despite being quiet short, I greatly appreciated the time I spent with Markus in the lab in which I learned considerably from his way of performing the experiments and analyzing the results. I want to thank my lab partner Christoph Hamsen for his constant efforts and in particular for his great help with the data evaluation and analysis. During the move of the experiment, the help of Paul Altin was extremely beneficial, I also enjoyed discussing different experimental ideas with him. I thank all the students, who made their Master, Bachelor or HiWi projects in the *Cavies* lab for their contributions: Georg Braunbeck, Anna Caroline Eckl, Ingmari Tietje, Matthias Redies thanks to all of you. I thank Eden Figueroa and Celso Villas-Boas for introducing me to cavity EIT during the beginning of my thesis and Maria Bernard-Schwarz for programming an efficient well designed sequence program.

Running such a complicated experiment was made possible with the help of a team of skillful technicians. I would like to thank Thomas Wiesmeier, Tobias Urban, Helmut Stehbeck, Franz Denk, Sepp Bayerl for their great support specially during the move. Thank you Thomas for the nice discussions we had during our usual daily walk.

Finally, I would like to thank all the members of Gerhard Rempe's group for the excellent cooperation and for the nice atmosphere.